Modeling and Control of Hemoglobin for Anemia Management in Chronic Kidney Disease

by

Jayson McAllister

A thesis submitted in partial fulfillment of the requirements for the degree of

Master of Science

in

Process Control

Department of Chemical and Materials Engineering

University of Alberta

Abstract

Chronic Kidney Disease (CKD) affects millions of people throughout the world today. One of the major side effects of this disease is the inability to regulate the body's red blood cell production, and subsequently the mass of the protein called hemoglobin within the body. The health of these patients deteriorates and they become anemic. Recently, erythropoietin stimulating agents have become the standard for treating anemia in chronic kidney disease. The medication works extremely well for what it is designed to do. The problem with this scenario is the inability of the physician's to be able to choose an appropriate dose for each patient. The dosing protocols are not standardized across hospitals, and many of the dosing regimens are poorly designed. As such, many patients' hemoglobin levels are poorly controlled. The poor control of hemoglobin in CKD patients is well documented through peer reviewed research. The focus of this thesis is to present an individualized epoetin-alfa dosing regimen, through the use of well known model predictive control technologies. Due to the absence of a proper setpoint, zone model predictive control becomes the focus of the controller methods.

The foundation of any model predictive controller is the system model. This thesis presents several different hemoglobin response modeling techniques including classical ARX, pharmacokinetic and pharmacodynamic (PKPD) delayed differential equation modeling and a novel new nonlinear constrained ARX modeling (C-ARX) method. The hemoglobin response modeling methods are compared on a clinical data set of 167 patients. It will be shown that the new modeling method offers similar modeling results to the previously developed PKPD model, with the added benefit of being linear and easily estimated through nonlinear programming. The nonlinear C-ARX method is also converted to a weighted linear C-ARX, which improves the robustness of estimation even further, without a large loss in estimation performance.

Different model predictive controllers were tested against the current anemia management protocol (AMP) from a participating hospital. The first set of tests were performed using the identified models as the simulated patient and represent a more nominal case for controller testing. Using these results, some of the controllers were eliminated from further testing. The second set of simulations were performed on a patient simulator that was designed based on the PKPD models. The simulator uses random integrating process noise to represent a slowly changing dose over time. The designed simulator also incorporates random step and ramp disturbances to simulate blood loss, infections and other acute anomalies observed in the clinical data. The remaining controller types were tested on the designed patient simulator and represent a realistic and rigorous test scenario for the modeling and control methods. The final controller recommended for use is a weighted recursive least squares zone model predictive controller that uses a funnel shaped control zone.

Acknowledgements

First and foremost, I'd like to thank my supervisors Dr. Jinfeng Liu and Dr. Zukui Li of the Chemical and Material Engineering Department at the University of Alberta. Without their guidance, this thesis would not have been possible. Both Dr. Liu and Dr. Li contributed unique aspects of their knowledge to aid in guiding me on the creation of this thesis. Without Dr. Li, the constrained optimization ARX method would not be a reality. I value his infinite wisdom in the field of optimization and taking the time to share his knowledge with me as I used complex optimization techniques in both the modeling and control aspects of the project. I thank Dr. Liu for providing a great deal of support in regards to the entire hemoglobin control project. His broad and detailed knowledge of control theory was extremely useful, and he seemed to always have new and better ideas when I came upon roadblocks in my research. I have learned so much in these two short years as a result of both of their hard work and dedication to me, and I will be forever grateful to them.

I also owe a great deal of thanks to the individuals and organizations that provided funding to allow me to research this project. This includes the University of Alberta Faculty of Graduate Studies and Research and the Graduate Student's Association for the contribution of travel assistance to allow me to present my research at the American Institute of Chemical Engineers conference in San Francisco, USA. I thank the Natural Sciences and Engineering Research Council of Canada for funding for this research. I thank Cybernius Medical Ltd. for their monetary contribution, as well as their knowledge and clinical data used on this project. I must also thank the International Society of Automation for the generous scholarship I received from them.

I'd like to thank Dr. Li, Dr. Liu and Dr. Stevan Dubljevic for the opportunity to become a teaching assistant in their classes. They say you do not truly know

something until you can teach it to someone else. Being a TA allowed me to refresh on some important control courses and also allowed me to teach and meet many of the bright future leaders of tomorrow.

Last but not least, I must thank the other graduate students who have contributed significantly to my progress. These include Su Liu, Tianrui An, Kevin Arulmaran, Xunyuan Yin and Jannatun Nahar. I wish them all the best in their future endeavors

Contents

List of Tables

List of Figures

Chapter 1

Introduction

1.1 Motivation

Chronic Kidney Disease (CKD) is estimated to affect nearly 10% of the world's population (A. Levey and Coresh, 2007). There are several stages of CKD that patients can be categorized into, with the most severe stage being classified as End Stage Renal Disease (ESRD). Millions of people worldwide are classified as ESRD patients and many undergo dialysis treatment or kidney transplants as a result (W. Couser *et al.*, 2011). Over 80 % of chronic kidney disease patients that receive treatment are in wealthy countries that have access to universal healthcare and have large elderly populations (V. Jha and Iseki, 2013). The elderly population is increasing at a quick rate in developing countires such as China and India and the number of chronic kidney disease patients is expected to increase drastically over the coming years (V. Jha and Iseki, 2013).

One of the major side effects of CKD is the inability to produce endogenous erythropoietin, which is a hormone used to regulate the production of red blood cells in the body. Red blood cells contain a protein called hemoglobin which is vital to the survival of a human. Hemoglobin is responsible for binding to oxygen and delivering it around the body to the tissues and organs. Without oxygen, the organs and tissues will die. When the natural production of erythropoietin drops significantly, these patients suffer from a condition called anemia, which is characterized as a reduced mass of red blood cells and hemoglobin within the body. In the 1980s, recombinant human erythropoietin (rHuEPO) was shown to help regulate the production of red blood cells and hemoglobin. It was in this time period that CKD patients suffering from anemia started to undergo erythropoietin stimulating agent (ESA) treatment. Since the initial discovery of rHuEPO, several drugs have been invented to stimulate the production of red blood cells and hemoglobin including darbepoetin-alfa, epoetin-alfa (EPO), epoetin-beta and methoxy polyethylene glycol-epoetin beta.

It has been recognized by the clinical community that while low hemoglobin levels lead to anemia, hemoglobin values above 13.0 g/dL can increase the risk of mortality for the patient (M. Rosner, 2008; Z. Jing *et al.*, 2012; A. Singh *et al.*, 2006). Hence, effective methods are needed to determine the appropriate dose of ESA to maintain the target hemoglobin level. Many conventional methods for guiding ESA and iron dosing used by clinicians, rely on a set of rules based on past experiences or retrospective studies. Those methods for ESA administration are generally imprecise, and as a result, the patient's hemoglobin levels are often poorly controlled. The hemoglobin often moves through the target range with large oscillations and overshoots. Of the 167 clinical patients studied, approximately 56% of the patients depict some varying degree of oscillatory behaviour that lasts for months or years. This phenomena is shown for several patients in Figure 1.1, where the control zone is from 9.5 to 11 g/dL. New effective anemia management methods are needed to avoid the adverse effects associated with increased hemoglobin levels, while minimizing the effects of anemia. It is estimated that CKD costs the United States 48 billion dollars per year (National Kidney Foundation, 2017), and utilizes approximately 6.7% of Medicare's annual budget to treat a small fraction (< 1%) of the population (P. Damien *et al.*, 2016). It becomes clear that major treatment cost savings could be possible, while also improving the health of CKD patients.

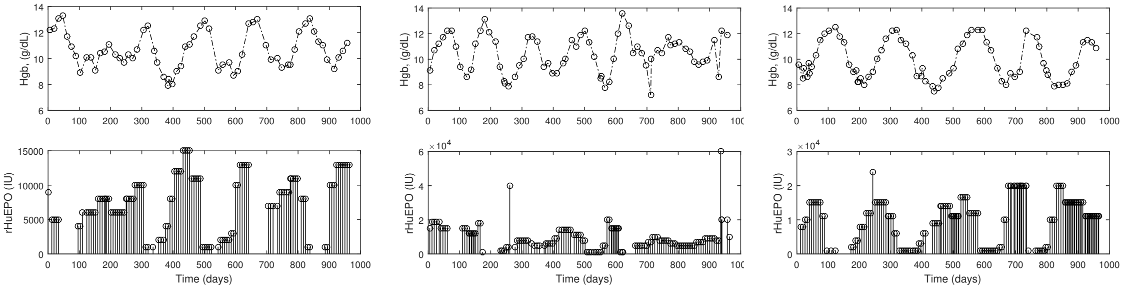

(a) Patient 1 **(b)** Patient 2 **(c)** Patient 3

Figure 1.1: Actual clinical patients that undergo hemoglobin cycling

1.2 Thesis Outline and Contributions

Chapter 2 begins with a method of data preprocessing that is introduced to resample the patient data into discrete weekly measurements. Three modeling methods are then introduced in detail including ARX modeling, Pharmacokinetic and Pharmacodynamic (PK/PD) modeling and nonlinear Constrained ARX modeling. The modeling methods are performed on the clinical data and the results are presented. This chapter shows that the new method of Hemoglobin Response modeling developed through Constrained ARX modeling is the most effective method in predicting patient hemoglobin. The nonlinear constrained ARX is also simplified into a weighted linear quadratic program making the optimization of the parameters more robust, without losing a great deal of model performance as compared to the nonlinear programming problem. The new linear C-ARX method is used on the clinical data to test the effectiveness of the model algorithm to recursively estimate models at each sampling instant. The model performance is based on the 8-step ahead prediction residuals.

Chapter 3 begins with an example of one of the current Anemia Management Protocols from a participating hospital. Then, a short description of the model structure used within the model predictive control algorithms is presented. Many different types of deterministic model predictive controllers are introduced, and subsequently reformulated in quadratic programs which are quickly and efficiently solved by conventional optimization methods. The next section of this chapter focuses on stochastic model predictive controllers which take in to account the best known uncertainties for additive process noise disturbance and measurement noise. This section explores the theory behind chance constraints and conditional value at risk constraints. The problems are reformulated into standard quadratic or linear programs. Three controller algorithms are then presented for dealing with time-varying disturbances. The chapter ends with some concluding remarks about the controller designs explored.

In Chapter 4, controller tuning is discussed in detail for the controllers to be tested through computer simulations and the results are presented. Simulation results are presented for the clinical patient models, and the current AMP is compared to several of the controller options. The controllers were tested using a combination of additive process noise and measurement noise while using the linear ARX model as the patient simulator. Some of the controllers were then tested on a Patient Simulator that was designed based on the PKPD clinical models. The Patient Simulator uses a non-stationary integrating disturbance, measurement noise and random step and ramp disturbances. Simulated input and output data was collected by controlling the clinical PKPD models with the AMP while several small disturbances entered the system. From this data, constrained ARX models were estimated to match the clinical PKPD models and used to begin simulations to test the controller set. The most promising controllers were tested on the patient simulator, and different tuning parameters and features for both the modeling and control algorithm are used for comparisons. The results were analyzed and a controller was chosen as the appropriate solution for clinical trials.

Chapter 5 presents some future work and considerations. Most notably among them, would be the design of a better patient simulator that was built based on the biological systems, rather than random noise.

The objective of this thesis was to explore several technologies for the implementation of a computerized dose optimizer for management of anemia in chronic renal disease. The application could be implemented in software programs to automatically gather measurements from the computer database, attain an individualized patient model, and calculate and offer improved epoetin-alfa (EPO) dosing regimens to the many patients suffering from chronic renal disease. As it has been shown, there exists many cases of extremely poor control in actual clinical data, and a large portion of economic waste on dosing excess recombinant human erythropoietin. This thesis aims to reduce these economic deficiencies and increase the quality of life for CKD patients through improved hemoglobin management.

Chapter 2

System Identification for Hemoglobin Response Models

2.1 Introduction

The aim of this chapter is establish a good mathematical model structure to describe the hemoglobin (Output) response to the administered ESA (Input), epoetin-alfa (EPO). 1-3 years of clinical data for 167 different patients was gathered from a participating hospital, along with their proprietary ESA protocol. Hemoglobin values were typically taken approximately 2 weeks apart, while ESA dosing was done typically once per week. Using this data several empirical modeling methods were explored including Classical ARX, Constrained ARX (C-ARX) and Pharmacokinetic and Pharmacodynamic (PK/PD) modeling. Hemoglobin response models vary drastically between patients. It has been recognized that due to the large variance in patient weight, drug sensitivity and stage of the disease, it may not be possible to attain a population model. Regardless of the ability to attain a population model, data-driven individualized hemoglobin response models should provide the best possible predictions for use in a model based controller.

2.2 Data Preprocessing for ARX Modeling

For the purpose of the simulation results in later chapters, it is assumed that weekly Hgb measurements are available. The clinically optimal Hgb sampling frequency for CKD is 4 times per month (A. Gaweda *et al.*, 2010). The available clinical data does not contain weekly hemoglobin measurements and must be re-sampled.

One of the difficulties in modeling the hemoglobin response models is that each patients' historical data contains inputs and outputs that have been sampled at different frequencies. Generally, the hemoglobin measurements occurred every 2 weeks but the sampling time could vary greatly over the course of a patients' historical data. The ESA dosing times also varied. Typically, the dosing was done every week, but it was not uncommon to see a patient not receive a dose for many weeks, or receive multiple doses in the same week. It has been recognized that the hemoglobin concentration responds very slowly and the system gain remains very small. The patient data used had each total drug dose in international units administered in multiples of thousands. The weekly sum of doses ranged from 0 IU to as high as 45 000 IU.

With such a small gain and large time constant, it was proposed to re-sample the patient data into weekly sampling intervals to perform ARX modeling. Figure 2.1 contains a pictorial example where the original data is shown in blue and the re-sampled data points are shown in red. For the hemoglobin measurements, the first measurement was taken to be the first day of the sampling time and corresponds to day 0. The next hemoglobin measurement would occur approximately 2 weeks later, for example at day 16. A linear interpolation was performed between these two measurements to attain an approximated measurement for the hemoglobin value on day 7. The next necessary measurement would be the day 14 measurement, where again a linear interpolation would be used between the day 0 and day 16 measurement. The rest of the hemoglobin measurements were re-sampled into weekly measurements in this fashion. The EPO doses were re-sampled into a weekly value by taking the sum of the current days EPO dose and the previous 6 days of doses.

2.3 Modeling Techniques

All three modeling methods described in this section are empirical modeling methods, that is, they are arrived at by using input and output data. Both the classical ARX and Constrained ARX modeling methods require the re-sampled weekly input/output data. The PK/PD modeling method is a continuous time modeling method, and it requires an accurate delayed differential equation solver which will be introduced in this section. Due to the medical communities affinity for a more

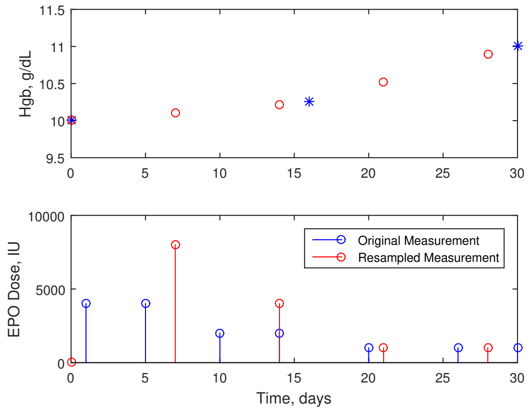

Figure 2.1: Patient Data Resampling Example

scientific approach, the PK/PD model may be more meaningful but it will be shown that a new Constrained ARX modeling technique can provide better modeling results. The original C-ARX method is nonlinear, and a simplification of this problem is introduced to facilitate the use of quadratic programming instead of nonlinear programming.

2.3.1 Autoregressive with Exogenous Inputs Modeling

Classical ARX modeling was the first method used to obtain a model. The model is derived through the well known solution to least squares regression. ARX models take the form of

$$y_{k+1} = a_1\ y_k + \cdots + a_n\ y_{k-n} + b_1 u_{k-d} + \cdots + b_m u_{k-m-d} \tag{2.1}$$

which can be described as an ARX model of order [n m d]. The letter n refers to the order of the output polynomial, m to the order of the input polynomial, and the letter d refers to the delay used on the inputs.

System identification techniques to attain an ARX model have many requirements in the data to be able to estimate an appropriate model. It is necessary to have sufficient process excitation. Normally, a proper input sequence would be designed, known as a Random Binary Sequence (RBS), but due to the actual system being a patient, such an input may not be ethical and could compromise the health of the patient. Without a properly designed input sequence, the results of this method are at the mercy of past doses chosen by the hemodialysis unit within the hospital. If the system data exhibits very little process excitation, this method will fail to obtain a proper model. It should also be noted that ARX modeling is highly sensitive to data corrupted by noise. The measurement noise when measuring the hemoglobin values in a lab setting is quite large compared to our target range of 9.5 to 11 g/dL.

ARX modeling was performed for many different model orders and delays. One of the first things that was noticed is that models with a large number of past output measurements (higher order n) resulted in very small b_k parameters making the input parameters insignificant in the resulting model. To improve the modeling results, the order of the output parameters was fixed at $n = 1$, meaning only the current hemoglobin and past doses are used for prediction. It is hypothesized that red blood cells have a lifespan of 3-4 months (Elliot, 2008), which means there is a possibility that the predicted hemoglobin is reliant on many of the past of doses. Figure 2.2 shows the results of the average b_k parameters, along with their respective standard error of every identified [1 20 1] patient model.

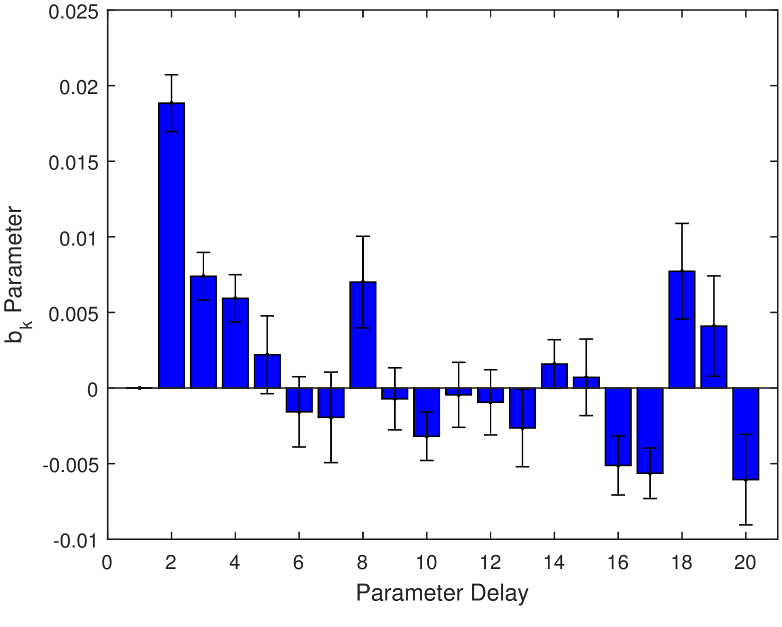

Figure 2.2: b_k Parameters for a [1 20 1] Population ARX Model, along with one standard error

The only significant pattern throughout the models was that many of the models displayed more positive b_k coefficients in the lower delays as seen by the average in Figure 2.2. Using the clinical data, the impulse response of the group of patients was estimated. Matlab's *cra* function was used to perform this analysis. Figure 2.3 shows the average impulse response (IR) for all the patients with whitening of the input and output, along with the Standard Error of the Mean (SEM), for lags up to 50 weeks. The prewhitening filter filters the input and output data through the same filter and computes the covariance functions. Positive values at each lag suggest that the output is influenced positively by the input, and the magnitude estimates the degree of influence. This figure has a similar trend as Figure 2.2.

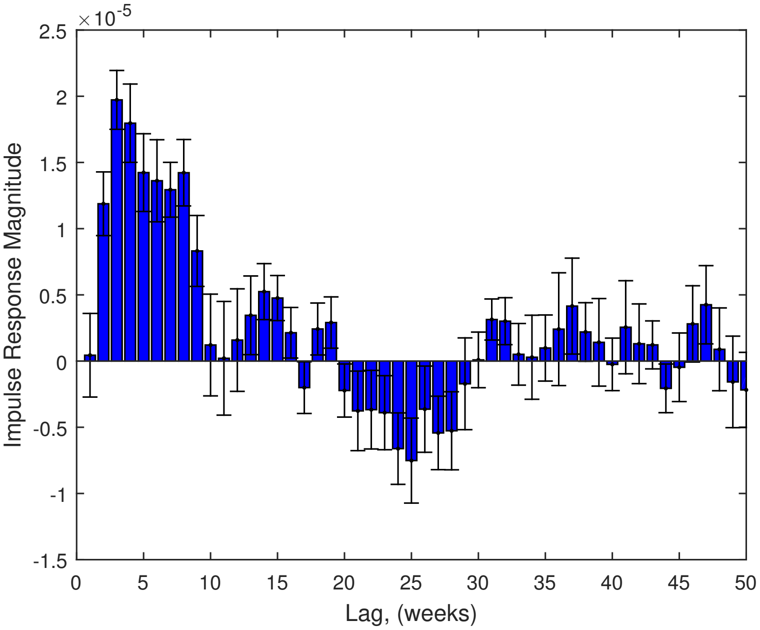

Figure 2.3: Average Impulse Response for the Filtered and Resampled Clinical Data with SEM, using a Pre-whitening filter

This observation is also reinforced by looking at the cross correlation of the resampled data at different lags. Before the cross correlation was calculated, the resampled data first had a weak filter applied to the input and output to help to alleviate some of the noise, as well as the input doses that happened to be very large/small due to timing in the resampling (ie. a one week total may contain two doses and the next week total could contain no doses even though the doses were spread out by 6 days). The filter was designed in Matlab using the *designfilt* function. The filter designed was a low pass finite impulse response filter, with a filter order of 4 and a cuttoff frequency of 0.2 hz and used a hamming window. Figure 2.4 shows the average cross correlation results of all the patients for lags up to 50 weeks. The oscillations in the figure suggest the system is of a very high order. The values of the cross correlation function suggest a strong influence of the input on the first 10-15 weeks of the output. This observation aligns with the hypothesis of red blood cells living for 3-4 months as previously suggested in the works by Elliot.

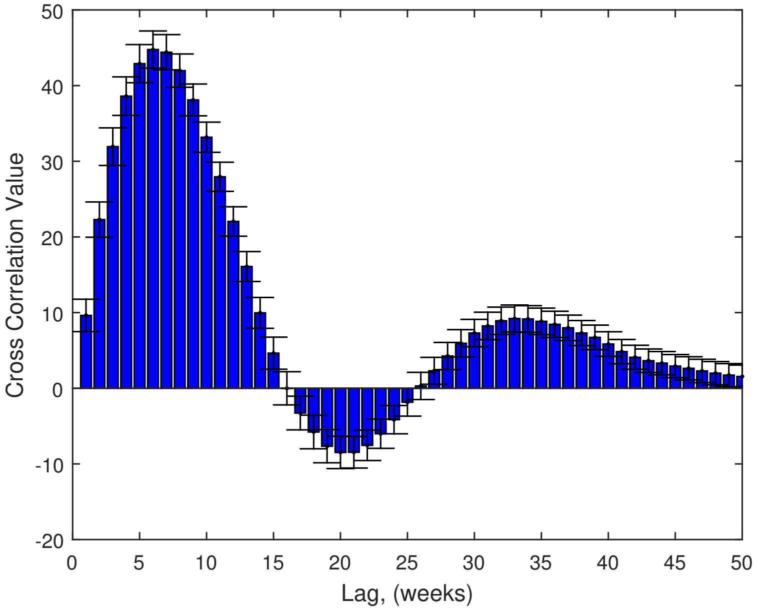

Figure 2.4: Cross Correlation Values for the filtered and resampled data, shown with the SEM

These results turn out to align with other observations in the PK/PD modeling method, and are a major contributor to the design of the Constrained ARX modeling method.

2.3.2 Pharmacokinetic and Pharmacodynamic Modeling

The grey box model type outlined in this section is based on pharmacokinetics and pharmacodynamics from a paper written by Chait et al in 2014. Pharmarcokinetics is the study of the movement of drugs within the body, while pharmacodynamics is the study of the effects that drugs have on the mechanisms within the body. This method is a continuous time model of delayed differential equations containing 8 unique parameters that are estimated for an individual patient through nonlinear least squares regression. The estimated parameters are represented in the Table 2.1. The system of delayed differential equations can be simplified into a continuous

Parameter	Description
H_{en}	Hemoglobin Level due to Endogenous Erythropoietin
μ	Mean RBC life span
V	Maximal clearance rate
K_m	Exogenous Erythropoietin level that produces half maximal clearance rate
α	Linear clearance constant
S	Maximal RBC production rate stimulated by E_P
C	Amount of E_P that produces half maximal RBC production rate
D	Time required for EPO-stimulated RBCs to start forming

Table 2.1: Estimated parameters and descriptions for the PK/PD Model

delayed nonlinear state space represented in Equation 2.2

$$E_{en} = \frac{C H_{en}}{\mu \; K_H \; S - H_{en}} \tag{2.2a}$$

$$\frac{dE(t)}{dt} = \frac{-V \; E(t)}{K_m + E(t)} - \alpha \; E(t) \; + \; dose(t) \tag{2.2b}$$

$$\frac{dR(t)}{dt} = \frac{S \; (E_{en} + E(t-D))}{(C + E_{en} + E(t-D))} - 4 \; \frac{x_1(t)}{\mu^2} \tag{2.2c}$$

$$\frac{dx_1(t)}{dt} = x_2(t) \tag{2.2d}$$

$$\frac{dx_2(t)}{dt} = \frac{S \; (E_{en} + E(t-D))}{(C + E_{en} + E(t-D))} - 4 \; \frac{x_1(t)}{\mu^2} - 4 \; \frac{x_2(t)}{\mu} \tag{2.2e}$$

where the states $E(t)$, $R(t)$ represent the pool of exogenous erythropoietin and the population of RBCs within the body. E_p is the summation of the endogenous and exogenous erythropoietin. K_H is the average amount of hemoglobin per RBC (also known as the mean corpuscular hemoglobin, MCH). The value used here is fixed at 29.5 pg/cell, which is within the reference range of 27-33 pg/cell (Y. Chait *et al.*, 2014). The hemoglobin value is directly proportionate to the RBC population; the hemoglobin value can be attained by multiplying the RBC population estimate by the MCH value. The function $dose(t)$ is a train of impulses, representing the EPO injections, which are estimated to occur on the exact day they were administered. The model has an initial condition as represented in Equations 2.3 and requires two measurements of hemoglobin (hgb_1 & hgb_2) and the time in between those measurements

(t_1 & t_2) to estimate.

$$\dot{R}_0 = \frac{(hgb_2 - hgb_1)}{K_H(t_2 - t_1)} \tag{2.3a}$$

$$E(0) = 0 \tag{2.3b}$$

$$R(0) = \frac{hgb_1}{K_H} \tag{2.3c}$$

$$x_1(0) = \frac{\mu(H_{en} - \mu\ K_H\ \dot{R}_0)}{4K_H} \tag{2.3d}$$

$$x_2(0) = R(0)\ - \ \frac{4\ x_1(0)}{\mu} \tag{2.3e}$$

It should be relatively obvious, the difficulties this model structure presents in estimating the model parameters by numerical computation methods. Firstly, the model includes the impulse function in the first state's derivative, $\frac{dE(t)}{dt}$, which introduces some discontinuities into the solution. Secondly, the model includes a delayed term, $E(t - D)$, in two of the state equations. This presents a very difficult problem because the state, $E(t)$, contains discontinuities and the delayed term allows the discontinuities to propagate throughout the system (Christopher, 2000). In order to effectively simulate this system, the discontinuities must be tracked and dealt with appropriately by the careful selection of the step size. Thirdly, unless the step size of the algorithm is fixed, the value for the delayed solution that is necessary for the current estimate of the derivatives may not be available. An estimate for the past solution must be used based on some sort of interpolation of the solution history. These problems invite a short segue into the design of an efficient solver to estimate these models.

Delayed Differential Equation Solver Design

As mentioned previously, it is desired to develop an efficient algorithm to simulate the system mentioned in Equations 2.2 and 2.3. It would be easy to use a fixed step size, first or second order method developed for ODEs and modify it to use the delayed terms. This certainly works, but is incredibly inefficient. The desire here, is to create an *efficient* solver, which naturally leads to a variable step size solver. Variable step solvers are capable of modifying their step size, and producing some minimum amount of taylor series truncation error when solving each point. The idea behind variable step solvers is that they estimate each point using two different methods, such as a first and second order Euler method, and then estimate the truncation error from the difference in the solutions between the two methods. The algorithm will check to make sure the error is within the desired user set tolerance. If it is acceptable, the highest order value (usually the most accurate) is kept and the step size is adjusted larger for the next iteration. If the point fails the error tolerances, the step size is reduced and the iteration is re-run. Larger step sizes allow the solver to skip over many calculations and the step size is desired to be as large as possible without compromising the accuracy of the solution. Efficiency is also lost within the solver for every failed iteration, so it is important to make appropriate adjustments to the step size.

The algorithm that was chosen here was a modified version of the explicit Bogacki-Shampine (2,3) variable step size algorithm (P. Bogacki, 1989) for ODEs which uses both a second order and a third order solution to estimate the truncation error and adjust the step size. The local error estimate achieved is for the lower order solution. The integration is advanced with the higher order solution because it is believed to be more accurate (Shampine, 2005). Four coefficients must be estimated using the current step size and second and third order estimates for the solution are then given by Equations 2.4

$$k_1 = f(t_n, y_n) \tag{2.4a}$$

$$k_2 = (t_n + \frac{h}{2}, y_n + \frac{h\ k_1}{2}) \tag{2.4b}$$

$$k_3 = f(t_n + \frac{3\ h}{4}, y_n + \frac{3\ h\ k_1}{4}) \tag{2.4c}$$

$$y_{n+1} = y_n + \frac{2\ h\ k_1}{9} + \frac{h\ k_2}{3} + \frac{4\ h\ k_3}{9} \tag{2.4d}$$

$$k_4 = f(t_n + h, y_{n+1}) \tag{2.4e}$$

$$z_{n+1} = y_n + \frac{7\ h\ k_1}{24} + \frac{h\ k_2}{4} + \frac{h\ k_3}{3} + \frac{h\ k_4}{8} \tag{2.4f}$$

where y_{n+1} represents the third order solution, and z_{n+1} represents the second order solution. It should be noted that k_4 for one iteration is the same estimate used for k_1 of the next iteration. This is a First Same As Last (FSAL) algorithm designed to aid in reducing the computational burden. The local error estimate is computed by $E_{est} = E_{local} + h.o.t.$ where $h.o.t.$ are the higher order taylor expansion terms. The error estimate must satisfy the following equation.

$$||E_{est}|| \leq R_{tol} \tag{2.5}$$

where R_{tol} is the relative error tolerance set by the user, and $||E_{est}||$ is a suitable weighted norm (Shampine, 2005). For this algorithm, we achieve an estimate for $||E_{est}||$ by using Equation 2.6 (L. Shampine, 2001).

$$||E_{est}|| = h * ||\frac{[k_1\ k_2\ k_3\ k_4][\frac{-5}{72}\ \frac{1}{12}\ \frac{1}{9}\ \frac{-1}{8}]^T}{max(|y_{n+1}|\ ,\ 0.1)}||_\infty \tag{2.6}$$

If the error estimate is lower than the relative tolerance, the iteration is successful and the step size is adjusted by one of two ways. If the following equation is satisfied

$$1.20 * (E_{est}/R_{tol})^{\frac{1}{3}} > 0.2 \tag{2.7}$$

then the new step size, h_{n+1} will be

$$h_{n+1} = \frac{h_n}{1.20 * (E_{est}/R_{tol})^{\frac{1}{3}}} \tag{2.8}$$

Which adjusts the step size only a small amount. If the error is mall then and Equation 2.7 is not satisfied, then the step size is increased at a faster rate using the following

$$h_{n+1} = 4 * h_n \tag{2.9}$$

One of the requirements of the algorithm is that the solution, y_{n+1}, to the problem, must be smooth. It is necessary to carefully choose the step sizes so that discontinuities become mesh points, which will allow the algorithm to compute the proper estimates for the solutions and the local error estimate (L. Shampine, 2001). To accomplish this, the discontinuities along with their propagations are tracked and the step size is appropriately adjusted. For example, take the system delay, D, to be 7 days. If the patient is given a dose on day 8, their will be a discontinuity in the derivative and solution for the first state, $E(t)$, on day 8. The history of $E(t)$ is used in the second ($R(t)$) and fourth state ($x_2(t)$) which means that on day 15, these states and derivatives will cross the day 8 discontinuity in $E(t)$ and create a discontinuity in the solutions for these states. A discontinuity will propagate through the solution D days after every dose. The location of these discontinuities are known and this solver pre-calculates them before the integration starts. If the step size is to step over a discontinuity, the step size is adjusted to be equal to the distance to the next discontinuity. The next point evaluated is immediately to the right of the discontinuity. An example of a simulation using the DDE solver for one of the attained models is shown in Figure 2.5.

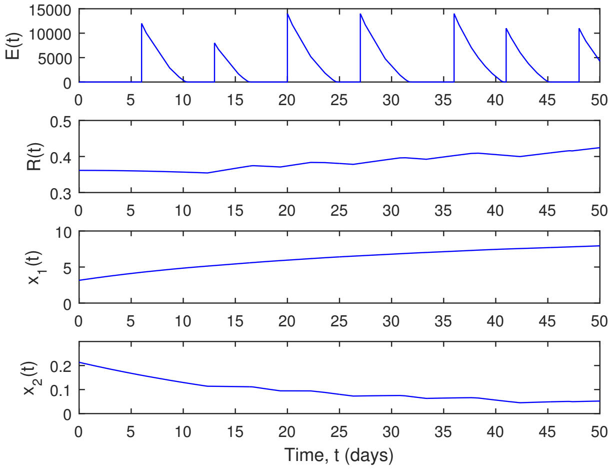

Figure 2.5: Example of the State Evolution when simulated with the designed DDE Solver

ARX Approximations of PK/PD Model

The nonlinear state space presented is difficult and slow to use within an MPC routine. A nonlinear model predictive controller could certainly be built using functions such as fmincon or IPOPT and will be introduced in the next chapter. The nonlinear controller does present a few challenges though. Firstly, the DDE solver is highly sensitive to inaccuracies in the initial condition, and there does not exist an accurate way of calculating the initial derivative $\dot{R}_0$ needed for the initial condition. Secondly, there are no guarantees that the DDE solver described above finds the proper solution. Due to the fact that the numerical method is an explicit method, the solver still runs a risk of becoming unstable which will greatly impact the optimization problem within the MPC controller. In the design of an MPC controller, the prediction horizon has been chosen to be 8 weeks. To start the DDE solver, it requires a history of the solution up to D days previous to the solution to become the most accurate. This is never available. For the first D days of the simulation, $E(t)$ is considered to be constant at zero, due to the lack of history data. This assumption does not impact the model training algorithm significantly, but can certainly affect the controller optimization problem over such a short prediction horizon.

It is desired to obtain a more convenient model, to avoid some of these problems. One proposed approach is to design a random binary sequence (RBS) based on a step test of the nonlinear model, and then subsequently filter it through the nonlinear model and use the resulting simulated data to obtain an ARX model. This method was used for its simplicity, but also for exploring the structure of the ARX models obtained, to aid in the design of the Constrained ARX method. Due to the small control zone and minimal nonlinearities, the linearization of the models in this manner does not introduce significant error. An example of an infinite step ahead prediction comparison is shown in Figure 2.6. The fit of the PK/PD nonlinear model is shown along with the ARX approximation and the actual data. It can be seen that the ARX model provides a relatively good estimate of the nonlinear model as long as the hemoglobin remains relatively close to the control zone. From looking at the past patient history, it can be seen that the hemoglobin of the patients rarely exits a zone of 8-13 g/dL.

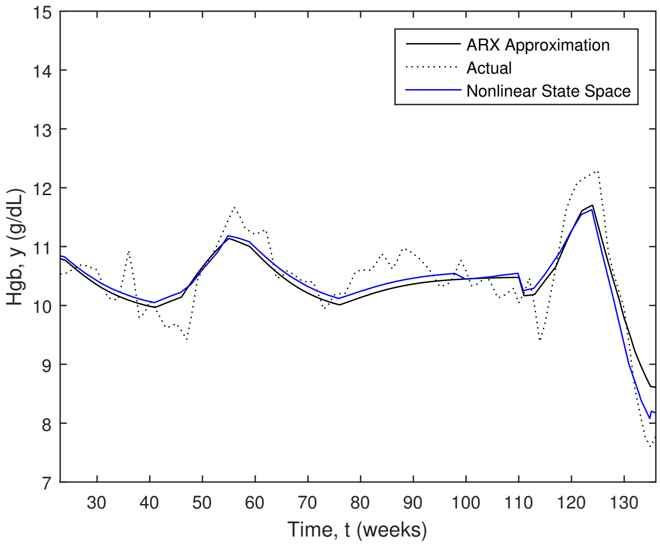

Figure 2.6: Example of the ARX approximation for the Nonlinear state space for an infinite step ahead prediction

An example of the structure of the b_k parameters is shown in Figure 2.7 for a patient. Here the ARX model has an order of [1 13 2]. The system is described by the following Equation.

$$\begin{aligned} Hgb_{t+1} - Hgb_{ss} = & - a_1 \left(Hgb_t - Hgb_{ss}\right) \ldots \\ & + \sum_{k=1}^{13} b_k \left(EPO_{t-k+1} - EPO_{ss}\right) + e_t \end{aligned} \tag{2.10}$$

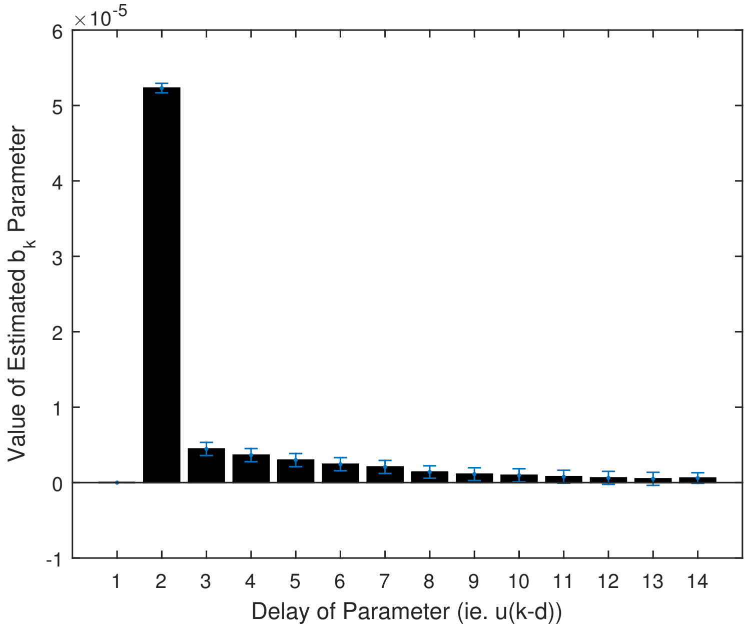

Figure 2.7: Example of the b_k parameter structure for the PK/PD ARX approximation

After analyzing the obtained models, it was found that every identified ARX model contained this same structure. That is, they all contained larger peak parameters at the delay of two weeks, and then slowly decreased towards zero, usually in some exponential decaying pattern. The majority of all the models contained only positive b_k parameters.

Using the PKPD-ARX models and matlabs *deconv* function, the impulse response (IR) of a model can be estimated. *deconv* works by performing long division of the $B(z^{-1})$ polynomial by the $A(z^{-1})$ polynomial, converting the ARX model directly to an impulse response model. The IR models can be represented by equation

$$y_{t+1} = \sum_{k=1}^{\infty} b_k u_{t-k+1} \tag{2.11}$$

Figure 2.8 shows the average values for the coefficients in the IR models for all the patients. Again, it can be seen that there exists a greater dependence on the models on the first few weeks of past inputs, and the effect decays exponentially overtime.

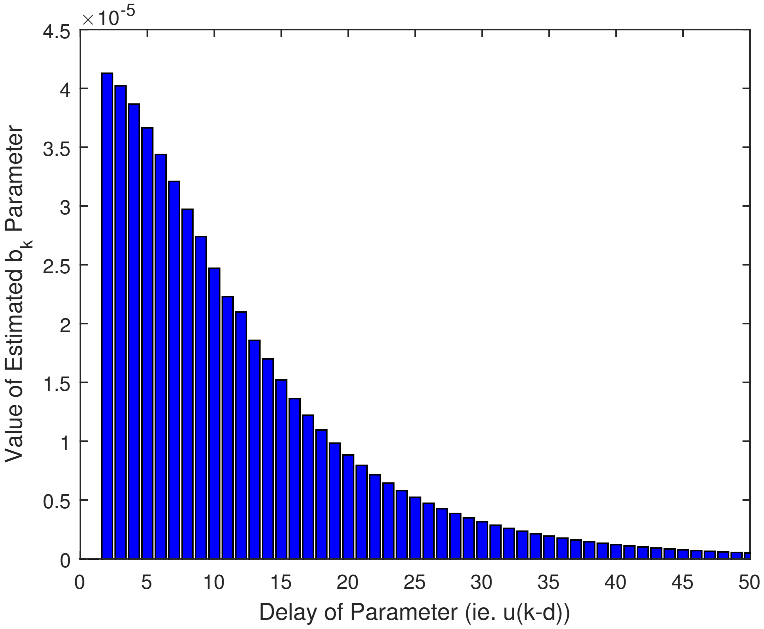

Figure 2.8: Average values of the b_k parameters in the IR models of all the estimated PKPD-ARX models over 50 lags

A combination of the observations in the ARX models and the PK/PD models, along with the medical background knowledge, aided in the development of the Constrained ARX modeling method which will be introduced next.

2.3.3 Constrained Autoregressive with Exogenous Inputs (C-ARX) Modeling

Inspired in part by the previous observations, a method of Constrained ARX modeling was designed as outlined in detail in a conference paper written by Dr. Jia Ren (J. Ren *et al.*, 2017). This method again uses the re-sampled one week data. The basic premise of the design is that the structure of the model is similar to the ARX model mentioned earlier, but has the b_k parameters constrained to be similar to the ARX models identified from the PKPD models. The resulting model takes a similar form as the PKPD-ARX, but it is much less restrictive on the location of the peak b_k parameter. The peak time parameter is allowed to float from a delay of 2 to a delay of 4. Another major benefit of this design is that the hemoglobin and EPO value that is used as the pseudo-steady state of the system is not the average value of the data, but rather it is also optimized within the problem. This results in an extra 2 degrees of freedom in the estimation problem.

The ARX model explored again contained a single a parameter, and 20 b_k parameters. It should be noted that some of the b_k parameters could take on a value of zero; there is not necessarily always 20 non-zero parameters. The model takes the form of Equation 2.12, with a one week sampling time.

$$\begin{aligned} Hgb_{t+1} - Hgb_{ss} =& a_1 \left(Hgb_t - Hgb_{ss}\right) \dots \\ &+ \sum_{k=1}^{20} b_k \left(EPO_{t-k+1} - EPO_{ss}\right) + e_t \end{aligned} \tag{2.12}$$

The optimization problem was originally designed as a mixed integer nonlinear programming problem (MINLP). The MINLP is outlined in Equation 2.13.

$$\min \sum_{t=1}^{tf} [Hgb_t - Hgb_{t,actual}]^2 \tag{2.13a}$$

$$s.t. - Kz_k + 0.001 \leq k - t_{peak} \leq K(1 - z_k) \qquad \forall k = 1, \dots, K \tag{2.13b}$$

$$- M(1 - z_k) \leq \alpha(k - 1) - b_k(t_{peak} - 1) \leq M(1 - z_k) \qquad \forall k = 1, \dots, K \tag{2.13c}$$

$$- Mz_k \leq \alpha \exp^{-\beta(k-t_{peak})} - b_k \leq Mz_k \qquad \forall k = 1, \dots, K \tag{2.13d}$$

$$7.0 \leq Hgb_t \leq 15.0 \ \ \forall t \qquad 7.0 \leq Hgb_{ss} \leq 11.0 \ \ \forall t \tag{2.13e}$$

$$0.7 \leq a_1 \leq 0.99 \qquad 0 \leq EPO_{ss} \tag{2.13f}$$

$$b_1 = 0 \qquad b_k \geq 0 \ \ \forall k = 2, \dots, K \tag{2.13g}$$

$$b_k \geq 0.1 \ \ k = k_{peak} \qquad 1.1 \leq t_{peak} \leq 3.9 \tag{2.13h}$$

$$\alpha \geq 0.1 \qquad \beta \geq 0.05 \qquad z_k \ \in \{0, 1\} \tag{2.13i}$$

The cost function is simply the sum of squared errors between the model and the actual measurements. The integers in the problem are contained in each z_k variable. z_k holds a value of 1 if time instance k is before the peak time, or 0 if it is after the peak time. Constraint 2.13b enforces this. The b_k parameters take on a linearly increasing pattern before the peak parameter, which is enforced by Equation 2.13c and the variable α.

$$b_k = \frac{\alpha(k-1)}{t_{peak}-1} \tag{2.14}$$

It should be noted that t_{peak} is a continuous variable, meaning the peak time can exist anywhere from 1.1 to 3.9 and α is the value of the parameter at that peak time. The b_k parameters take on an exponentially decreasing pattern after the peak parameter, which is enforced by Equation 2.13d, and the variable β, which is the decay rate. Equation 2.13d reduces to the following Equation for b_k parameters after the peak time.

$$b_k = \alpha \exp^{-\beta(k-t_{peak})} \tag{2.15}$$

Equations 2.13e,f help to enforce physically realizable solutions. The constraints on a_1 ensure the resulting model is open-loop stable. Another important equation is Equation 1 of line 2.13h. It is important to constrain the first b_k parameter after the peak time parameter for k_{peak} to be above 0.1. This ensures the model reliance on the past doses and overcomes the issues arising from the small gain of the inputs as mentioned in Section 2.3.1.

MINLP problems are relatively difficult to solve. There are commercially available solvers such as DICOPT in GAMS mentioned in the paper that are capable of finding this solution, efficiently. To reduce the computational complexity, the MINLP was converted to a series of nonlinear programming (NLP) problems. That is, instead of solving the integer variables for z_k in the optimization problem, the values are fixed at a specific value and then an NLP problem can be solved. This can be performed for all the combinations of z_k because there are only 3 different combinations that can occur for the chosen constraint on t_{peak}. The constraint $b_k \geq 0.1$ for $k = k_{peak}$ will also have to be modified for each case. The values of the cost functions are compared, and the model corresponding to the lowest cost function solution will be chosen as the best model. This iterative NLP problem is solved using both an IPOPT interface for Matlab as well as Matlab's native fmincon function. It is desired to have a complete Matlab solution for on-line implementation. It has been recognized that IPOPT is more robust than fmincon in some situations, and this will be explored in the next section.

Using the C-ARX models and Matlab's *deconv* function, the IR of a model can be estimated. Figure 2.9 shows the average values for the coefficients in the IR models for all the patients. The IRs again take on a similar shape as the cross correlation function figure and the IR of the PKPD-ARX models.

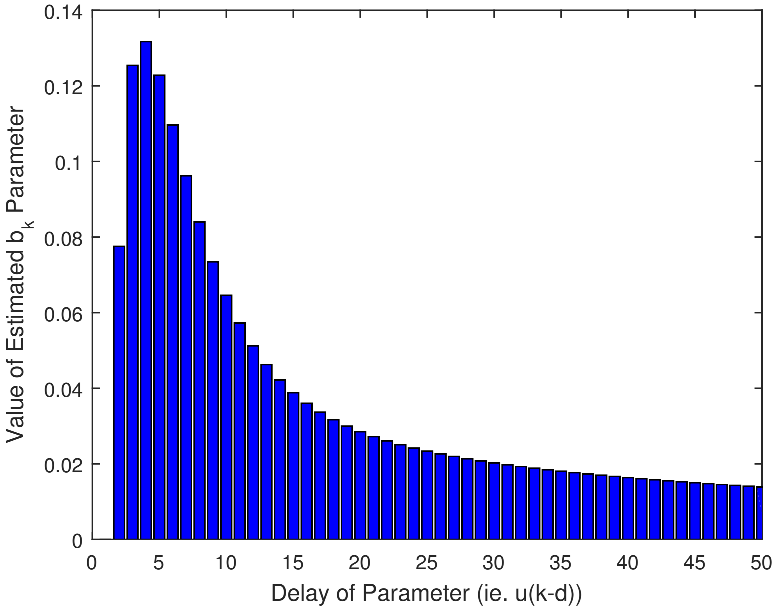

Figure 2.9: Average values of the b_k parameters in the IR models of all the estimated C-ARX models over 50 lags

2.3.4 Linear C-ARX Modeling

A conversion of the original nonlinear C-ARX modeling method was also explored. In the next Chapter, recursive modeling will be introduced for a control algorithm, where a new model is obtained after each new updated hemoglobin measurement. This requires a robust modeling method, which naturally leads to a conversion of the nonlinear problem to a linear problem. The only nonlinearities in the method are built into the shape of the b_k parameters and the steady state values. The steady state values can be taken as the average Hgb and EPO dose from the data used for the model estimation. The b_k parameter shape can be replaced by making each successive b_k parameter a certain percentage lower/higher depending on whether the parameter is before or after the peak time parameter. The model order was also reduced to a [1 8 1] ARX model. Three optimization problems are still solved for each peak time location, and again the best solution can be chosen. With this alteration, the problem can be formulated as the well known Quadratic Program. The derivation for the QP problem starts with the following equation.

$$\begin{bmatrix} y_{k+1} \\ y_{k+2} \\ \vdots \\ y_{k+tf} \end{bmatrix} = \begin{bmatrix} u_k & u_{k-1} & u_{k-2} & \dots & u_{k-7} & y_{k,actual} \\ u_{k+1} & u_k & u_{k-1} & \dots & u_{k-6} & y_{k+1,actual} \\ \vdots & & & & & \vdots \\ u_{k+tf-1} & u_{k+tf-2} & u_{k+tf-3} & \dots & u_{k+tf-8} & y_{k+tf,actual} \end{bmatrix} \begin{bmatrix} b_1 \\ b_2 \\ \vdots \\ b_8 \\ a_1 \end{bmatrix} \tag{2.16}$$

which can be represented by the following

$$\hat{y} = X\hat{\theta} \tag{2.17}$$

The cost function of the QP problem remains the same as before and is represented by the sum of squared errors between the model and actual measurements. y represents a vector of the actual measurements (Hgb_1 to Hgb_{tf}).

$$\min \;\; (y - \hat{y})^T (y - \hat{y}) \tag{2.18}$$

which can be easily reduced to the standard QP form.

$$\min \hat{\theta}^T H \hat{\theta} + 2\hat{\theta}^T f + c \tag{2.19}$$

where

$$\begin{aligned} H &= X^T X \\ f &= -X^T y \\ c &= y^T \; y \end{aligned}$$

along with the following constraints, which would correspond to a peak time b_k parameter at b_2. The other two configurations (peak time at 3 and 4 weeks) can be written in a similar manner by replacing Equations 2.21e-l with the appropriate constraints.

$$7.0 \leq y_k \leq 15.0 \;\; \forall k \tag{2.21a}$$

$$0.7 \leq a_1 \leq 0.99 \tag{2.21b}$$

$$b_1 = 0 \tag{2.21c}$$

$$b_k \geq 0 \;\; \forall k = 2, \dots, K \tag{2.21d}$$

$$b_2 \geq 0.1 \tag{2.21e}$$

$$b_3 < 0.8\ b_2 \tag{2.21f}$$

$$b_4 < 0.8\ b_3 \tag{2.21g}$$

$$b_5 < 0.8\ b_4 \tag{2.21h}$$

$$b_6 < 0.8\ b_5 \tag{2.21i}$$

$$b_7 < 0.8\ b_6 \tag{2.21j}$$

$$b_8 < 0.8\ b_7 \tag{2.21k}$$

$$b_8 < 0.005 \tag{2.21l}$$

Another alteration explored, was weighted least squares for the linear C-ARX method. This involves minimal alterations to the above formulation. The constraints remain the same, only the cost function is altered by adding in a weighting matrix (Q). The weighting matrix uses a chosen value of $\lambda \in \{\Re^n : 0 < \lambda \leq 1\}$ to weight the more recent measurements more heavily than the older measurements.

$$\min\ \ (y - \hat{y})^T Q (y - \hat{y}) \tag{2.22}$$

which can be reduced again to the standard QP form.

$$\min \hat{\theta}^T H \hat{\theta} + 2\hat{\theta}^T f + c \tag{2.23}$$

where

$$\begin{aligned} H &= X^T Q X \\ f &= -X^T Q y \\ c &= y^T\ Q\ y \end{aligned}$$

and

$$Q = \begin{bmatrix} \lambda^{tf} & 0 & \dots & 0 \\ 0 & \lambda^{tf-1} & \dots & 0 \\ \vdots & & \ddots & \vdots \\ 0 & \dots & & \lambda^1 \end{bmatrix} \tag{2.25}$$

2.4 Modeling Results on Clinical Data

This section outlines the results of performing the modeling methods on the available clinical data. The clinical data statistics are outlined in Table 2.2. It should be noted that there was no pre-screening of patients completed before attempting the modeling methods. For instance, there exists some patients that have no dose for the first half of the data. It is well known, this cannot possibly lead to a proper model. Similar situations exist for some other patients that may cause some of the modeling methods to fail. The cases where the modeling method fails will be filtered out after all models are obtained and tested. The filtration method will be discussed later in this section. The first 50% of the data was used as training data sets, and the models were validated on the last 50% of the data. The figures shown in this section start from the first actual hgb measurement that occurs at a time just after the initial condition. Due to the number of b_k coefficients, the simulation data for the training set do not start until 21 weeks after the initial point. Also, as the sampling time does not fall directly on these measurement days, a linear interpolation was used between the closest points for each modeling type. For the validation portion of the data, the simulation was reset to an initial condition matching the first actual hgb data point in that data range.

Statistic	Value
Number of Patients	168
Hemoglobin (Mean ± std)	10.48 ±0.57
EPO dose, IU/week (Mean ± std)	3167.2 ± 2484.4
Hgb Measurement Frequency (approximate)	2 weeks
Average Patient Data Length (Mean ± std)	126.4 ±19.7 (weeks)

Table 2.2: Statistics describing the clinical data used in the modeling methods

The results of the different modeling types on the clinical data are shown in Table 2.3. The results for the C-ARX are done using three different optimization solvers. The MINLP problem is solved directly in GAMS using DICOPTS. The NLP problem is solved using fmincon and also against a third party matlab interface for IPOPT. A couple initial conclusions can be made from these unfiltered results. It can be seen that the ARX modeling method (all types) tend to model more of the system noise. This can be inferred by the fact that the mean training RMSE is much better than the PKPD modeling method, yet the mean validation RMSE is significantly larger proportionally when compared to that of the PKPD modeling method. An example of this is shown in Figure 2.10. The NLP model in the figure represents the solution obtained from Matlab's fmincon.

	Mean RMSE		Std RMSE		Models
Modeling Method	Training	Validation	Training	Validation	Included
Classical ARX	1.12	5.06	3.24	21.18	168
Constrained ARX - MINLP	0.70	1.87	0.33	5.14	158
Constrained ARX - NLP (fmincon)	0.76	1.66	0.50	1.42	168
Constrained ARX - NLP (IPOPT)	0.76	1.66	0.50	1.43	168
PKPD	0.94	1.61	0.68	2.59	167
PKPD-ARX Approximations	1.47	2.72	3.54	11.26	158

Table 2.3: Modeling Results of the unfiltered models for the various modeling methods explored along with the number of models included in the resulting statistics

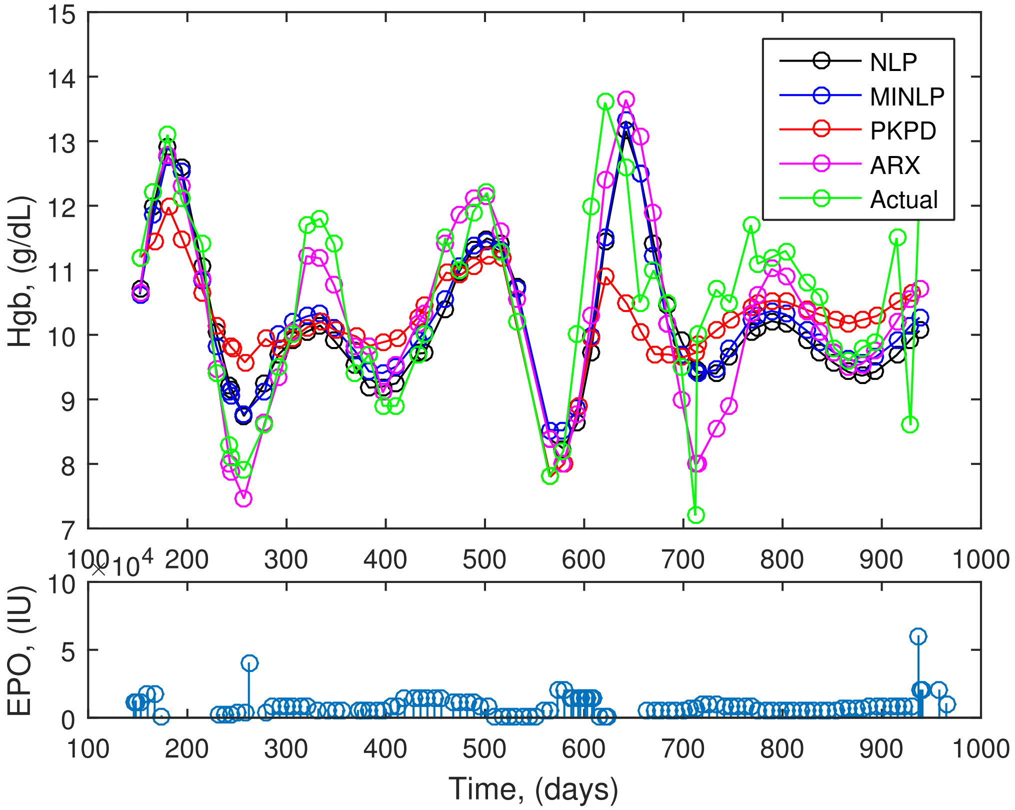

Figure 2.10: Example that shows the ARX modeling methods capturing the peaks of the data, where as the PKPD model does not capture the sharpness of the data peaks

The validation statistics for the Classical ARX method are very poor. From the filtered results, it will be shown that there are a few patients that skew these statistics greatly. This phenomenon is a result of an ill-conditioned X matrix in some of the patients when estimating the parameter set, $\hat{\theta}$, using the formula $\hat{\theta} = (X^T X)^{-1} X^T Y$.

This situation occurs when two rows or columns of the matrix X are the same or similar. Mathematically, this means the regressors are colinear or close to colinear (T. Soderstrom, 1989). An example of this can be seen in Figure 2.11.

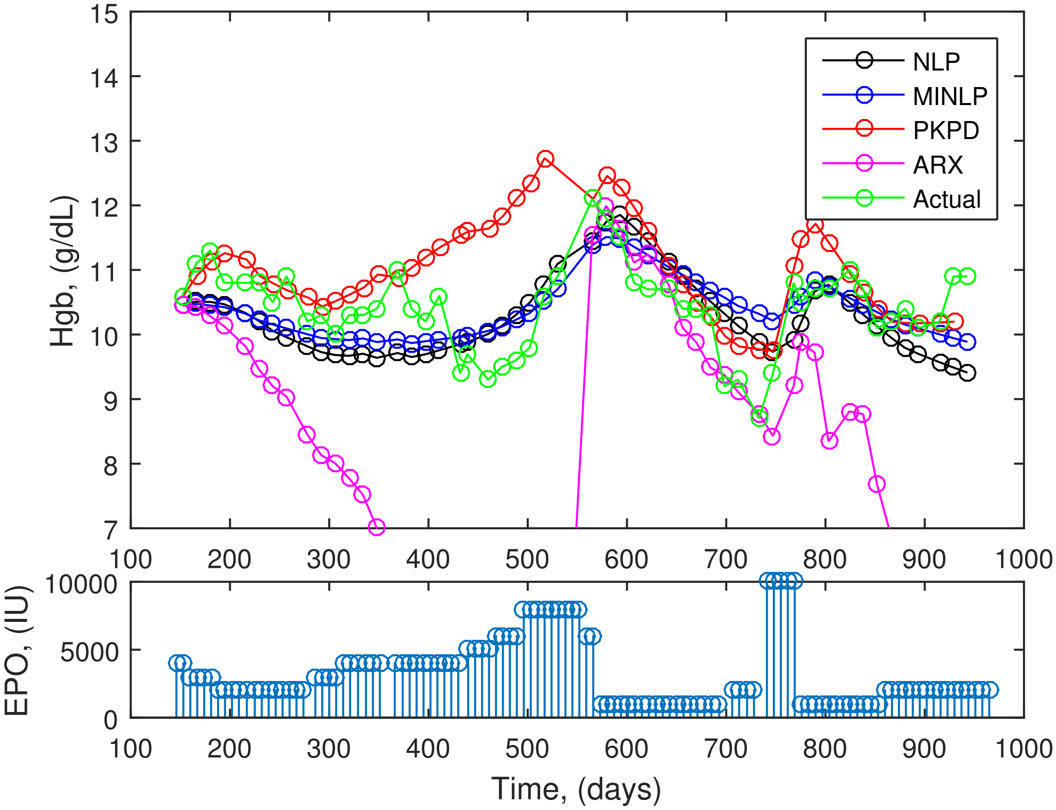

Figure 2.11: ARX modeling Algorithm fails to estimate a proper model. Modeling results for both training and validation data for all modeling methods

Another thing that can be seen in this data, is that both the NLP versions of the constrained ARX modeling using IPOPT and fmincon result in almost identical statistics. Due to the extra complexity, it is not worth using IPOPT over fmincon in a practical application, as it does not offer a substantial benefit.

Table 2.4 shows the filtered modeling results. Firstly, the filtered results confirm the fact that some patients skew the results in the Classical ARX modeling. The results are as expected for Classical ARX modeling because the training error is very close to the C-ARX modeling methods. The C-ARX method has two extra degrees of freedom allowing it have lower training error on some patients, even with the modeling structure constrained. Both the C-ARX methods using the MINLP and the NLP problem yield very similar results. On average, these results show that the C-ARX modeling method works better than Classical ARX and the PKPD modeling methods. The C-ARX is certainly better than Classical ARX as it provides lower validation RMSE on a larger number of models than the Classical ARX method. As will be discussed later, it is not overly desired to have a nonlinear modeling method for control purposes. On average, the C-ARX provides better results than the PKPD modeling method with the added benefit that the C-ARX models are linear, and estimated more easily and efficiently in Matlab. The algorithm for converting the PKPD models to PKPD-ARX approximations is based on performing successive step tests on the attained models using a bisection optimization algorithm to find corresponding EPO levels of the system that center the step test around the control zone of 9.5-11.0 g/dL. Using these results, an RBS was designed and the models can be converted to linear ARX models. It can be seen that the algorithm in its present form fails to identify a good linear model for some of the patients, which may be a result of the PKPD modeling method not achieving a proper model in the first place, or a failure in the conversion algorithm. When some of the worse models are filtered out of the PKPD-ARX models, it can be seen that these approximations result in relatively close performance to their nonlinear counterparts.

	Mean RMSE		Std RMSE		Models
Modeling Method	Training	Validation	Training	Validation	Included
Classical ARX	0.70	1.28	0.62	0.66	136
Constrained ARX - MINLP	0.70	1.21	0.34	0.58	145
Constrained ARX - NLP (fmincon)	0.69	1.18	0.35	0.60	144
PKPD	0.83	1.23	0.37	0.62	153
PKPD-ARX Approximations	1.09	1.26	0.62	0.60	133

Table 2.4: Modeling Results for the various modeling methods where patients with validation RMSE ≥ 3 removed from corresponding model type

Figure 2.13 shows the modeling techniques exhibit a degree of robustness against acute step disturbances, such as infections or blood losses. These scenarios present difficulty in determining dosing and how the patient's hemoglobin will respond to the ESA treatment.

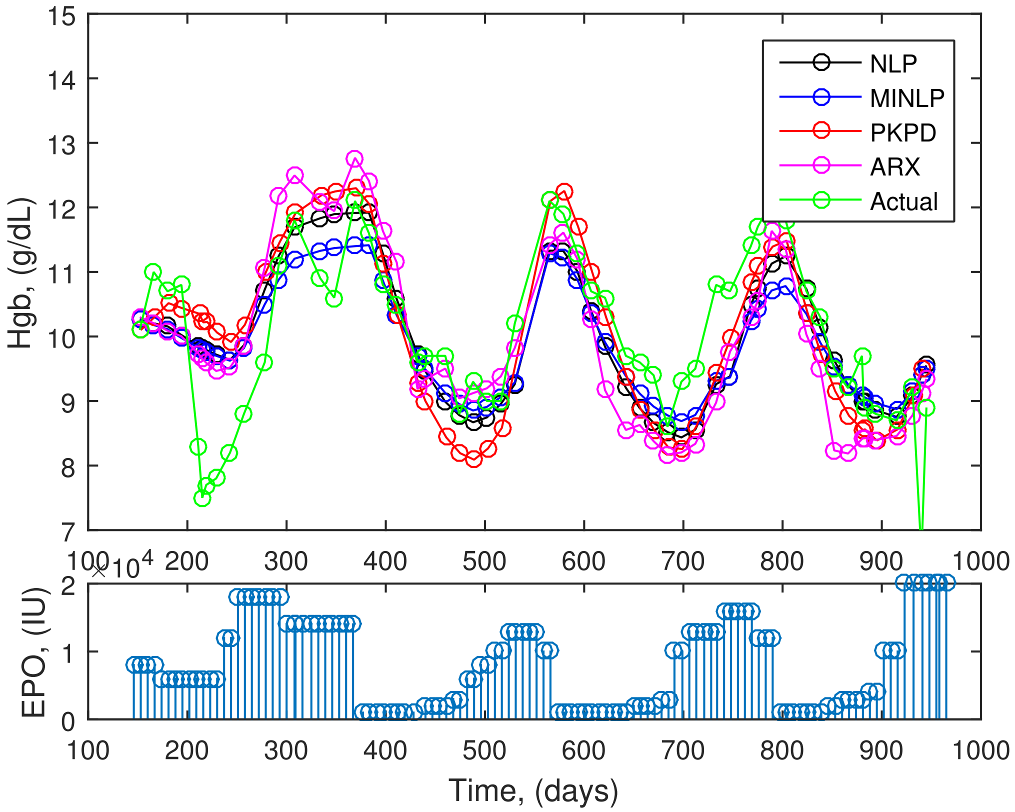

Figure 2.12: Example patient showing the modeling methods robustness for rejecting disturbances in the training data

Figure 2.12 shows an example where the patient model significantly changes over the course of the patients history. The patient's health deteriorates and the patient continually needs a higher degree of ESAs to manage their anemia. All modeling types validate poorly on this patient. As all patients will generally become more sick over time, this brings about the need to recursively attain new models for each patient to be able to capture the time-varying nature of the model parameters. Recursive modeling results will be obtained for the clinical data and presented later in this chapter.

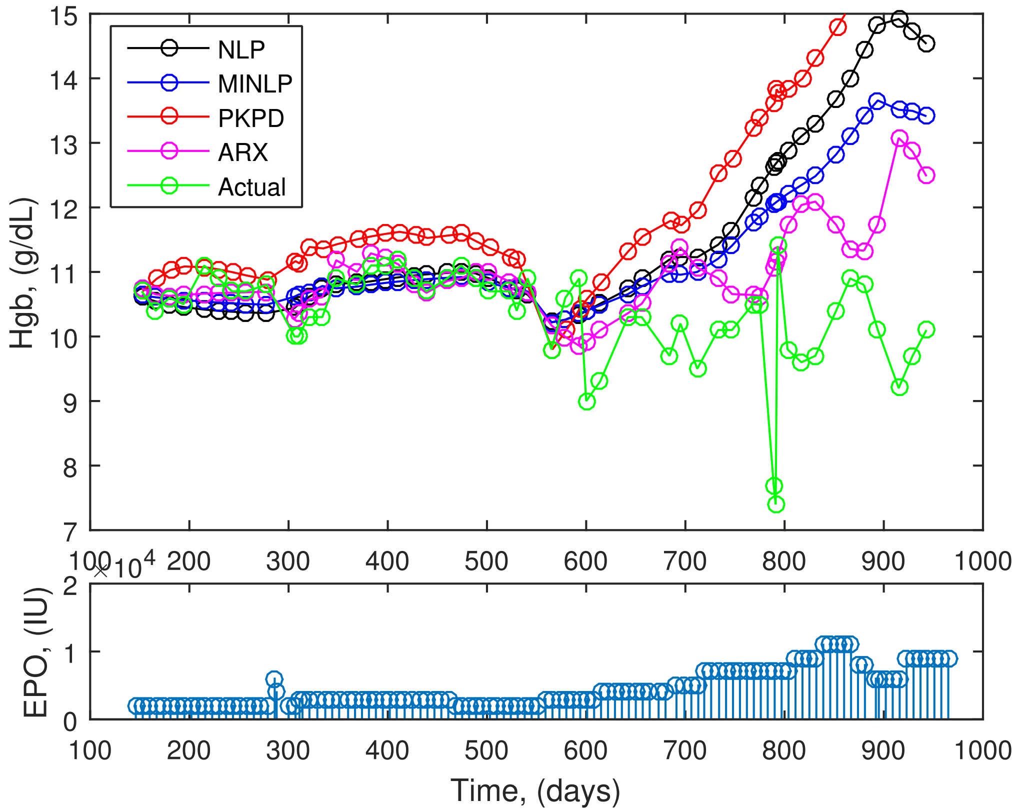

Figure 2.13: Example of a patient where the health continually deteriorates over the length of the patient history.

2.4.1 Model Order Reduction

It is desired to reduce the model order of the [1 20 1] nonlinear C-ARX models. A reduction in model order should yield a positive impact on the model estimation due to the fact that, in practice, more data points are available to perform the estimation. Another reason it should offer improvements, is that a large number of parameters often result in the modeling of noise in the system, which is undesirable. To perform the system identification with the new model orders, the same number of data points were used in each case, even though there would be extra data points for the C-ARX models with lower orders. This was done to be able to more accurately compare the model orders. Another small change from the original C-ARX conference paper is the addition of a constraint on the final b_k parameter. This was done to avoid large system gains seen in models that have low training RMSE values, but poor validation RMSE which is a result of the b_k parameters not decaying to zero by the final parameter. The new constraint applied is $b_{end} \leq 0.005$, which will ensure the b_k parameters decay towards zero by the final b_k parameter.

Different orders of the C-ARX models were identified for each of the 167 patients, and the unfiltered results are shown in Table 2.5. It can be seen that the validation RMSE for both [1 8 1] and [1 10 1] orders are better than the other model orders tested. The standard deviation of the RMSE is also much lower for these two model orders than the others, coming in at 0.80 and 0.78 versus 1.39 and 1.42. The training RMSE and standard deviation remain very comparable between all the methods.

	Mean RMSE		Std RMSE		Models
Model Order	Training	Validation	Training	Validation	Included
[1 5 1]	0.78	1.60	0.50	1.39	167
[1 8 1]	0.80	1.39	0.58	0.80	167
[1 10 1]	0.79	1.38	0.53	0.78	167
[1 20 1]	0.76	1.66	0.50	1.42	167

Table 2.5: Modeling Results without filtering for the various model orders of Constrained ARX models

Filtering the results by removing all the models with a validation RMSE greater than 3 yields the results in Table 2.6. It is very important to note that the model orders [1 8 1] and [1 10 1] both contain more models than the other orders, even though their the validation RMSE comes in a bit higher. This suggests that the [1 8 1] and [1 10 1] model orders are a bit more robust than the other model orders.

	Mean RMSE		Std RMSE		Models
Model Order	Training	Validation	Training	Validation	Included
[1 5 1]	0.72	1.21	0.36	0.65	149
[1 8 1]	0.76	1.29	0.51	0.67	161
[1 10 1]	0.77	1.33	0.52	0.70	164
[1 20 1]	0.71	1.19	0.40	0.61	145

Table 2.6: Constrained ARX Modeling Results with filtering out all models with Validation RMSE ≥ 3

Further filtering of the results in the statistics are shown in Table 2.7. This filtering shows that all 4 model orders remove a similar amount of the models from the statistics, leaving 73-75 models for each model order with Validation RMSE equal to 1 or less. These results show that for the better data sets, all four model orders seem acceptable for use.

	Mean RMSE		Std RMSE		Models
Model Order	Training	Validation	Training	Validation	Included
[1 5 1]	0.59	0.69	0.19	0.18	74
[1 8 1]	0.58	0.73	0.21	0.17	75
[1 10 1]	0.57	0.72	0.19	0.17	75
[1 20 1]	0.57	0.70	0.19	0.17	73

Table 2.7: Constrained ARX Modeling Results with filtering out all models with Validation RMSE ≥ 1

Considering all these results, it is recommended to use the model order of [1 8 1]. This model order offers similar validation RMSEs, while providing a certain degree of robustness with a smaller model order. In practice, it will allow the modelling method to have an extra 8 data points to perform the optimization problem versus the [1 20 1] C-ARX models.

2.4.2 Recursive Linear ARX Modeling Results

Recursive modeling results were also obtained on the clinical data to test the modeling accuracy of the 8-step residuals. An Exponentially Weighted Moving Average (EWMA) filter was designed and used to aid in removing some of the measurement noise from the clinical data. The EWMA filter uses a filter value, α, and takes the form of Equation 2.26.

$$y_{f,k} = \alpha y_k + (1 - \alpha) y_{f,k-1} \tag{2.26}$$

The linear constrained ARX modeling method was chosen for the recursive modeling algorithms due to the robustness and simplicity of the QP solver as compared to the NLP solver. Comparisons of the performance of the linear and nonlinear C-ARX method for modeling results using a 50/50 training/validation split are shown in Table 2.8. The weighted C-ARX method uses a λ value of 0.98.

	Mean RMSE		Std RMSE		Models
Modeling Method	Training	Validation	Training	Validation	Included
Constrained ARX - NLP	0.76	1.29	0.51	0.67	161
Constrained ARX - QP	0.70	1.26	0.35	0.63	150
Weighted Constrained ARX - QP	0.70	1.25	0.35	0.63	149

Table 2.8: Modeling Results for the 3 C-ARX methods where patients with validation Mean RMSE ≥ 3 removed from corresponding model type

Various settings were used to filter the data, and different estimation window lengths were explored when comparing the 8-step residuals obtained from recursively estimating a model at each sampling instant. The highlights of these results are presented in Table 2.9. It should be noted that the accuracy of the 8-step prediction is highly dependent on the initial condition, and the hemoglobin has very slow dynamics. This means the measurement noise of the clinical data may significantly effect the accuracy of the 8-step predictions. The highlights presented here show that the modeling accuracy improves as the window estimation size increases. It also shows a λ that is around 0.98 to 1.0 gives similar results, but a lower λ causes the modeling accuracy to decay. A higher λ value puts more equal weighting on all the measurements, where as a lower value puts much more weight on the newer measurements. Due to the complexities of the NLP solver and the PKPD model estimation, the linear versions of the C-ARX methods were selected to test the recursive controller algorithms. An estimation window length of 70 gives good accuracy of the hemoglobin predictions, but the linear C-ARX modeling method can be used on less data. In a clinical setting, there may not exist more than a years worth of data, but this shows the modeling method can be used with less data points, without too much deterioration in model accuracy.

Model Method	Non-Weighted	Weighted	Weighted	Weighted	Weighted
Training Window Size	70	30	50	70	70
Weighting Value (λ)	–	0.98	0.98	0.98	0.95
Mean	-0.05	-0.08	-0.04	-0.06	-0.08
Standard Deviation	1.04	1.26	1.20	1.05	1.09
Mean (absolute)	0.76	0.87	0.81	0.77	0.78
90% Confidence Interval	± 1.71	± 2.08	± 1.97	± 1.73	± 1.80

Table 2.9: Highlights of the Recursive Modeling 8-Step Residual Statistics for the Linear C-ARX modeling methods with various settings

2.5 Conclusions

In this chapter, three different modeling methods were explored. The classical ARX method was chosen as a base to compare the other models too. The classical ARX models that were estimated were of order [1 20 1]. A DDE modeling method was also used based on pharmacokinetics and pharmacodynamics. This method used a fixed model structure and eight parameters within the model structure were estimated by using an individual patients' data along with nonlinear least squares regression in

Matlab. The third method used was the method of attaining a [1 20 1] order ARX model through constrained optimization. In this modeling technique, the steady state values were also optimized. The magnitudes of the parameters were constrained to follow certain patterns learned from the first two methods. The three modeling methods were tested on the clinical patient data and compared for all 167 patients. It was found that on average the Constrained ARX models outperformed the other modeling methods. The classical ARX modeling method performed the worst as was expected due to the impact of large process and measurement noise in the clinical data, along with a relatively large amount of b parameters. These ARX models tended to over-fit the noise. The C-ARX modeling method performed quite similar to the DDE modeling method, but has the benefit of being linear, and efficiently estimated.

Model order reduction for the Constrained ARX models was also explored. It was found that reducing the model order to [1 8 1] resulted in a good balance between robustness and model accuracy. It resulted in comparable RMSE values to the [1 20 1] models, but with less parameters to estimate. The [1 8 1] model order was also shown to be more robust than the [1 5 1] model order. The [1 8 1] and [1 10 1] results were extremely close in values and were both considered for the final suggested model order. The final choice for the model order for the Constrained ARX modeling method is of order [1 8 1] because there are less parameters to estimate than the [1 10 1]. For the purpose of controller design, the [1 8 1] Constrained ARX models offer the best modeling solution.

A weighted and non-weighted linear version of the nonlinear C-ARX method was also introduced. The results show that the linear version of the C-ARX modeling methods yields similar results on the 50/50 training/validation tests as the nonlinear method. The linear C-ARX uses a simple QP formulation. QP solvers are more robust than NLP solvers are and are more desirable to use. Both the weighted and non-weighted versions performed similar on the 50/50 modeling results. The two linear methods were also selected to explore the effect of window size and weighting values on the 8-step prediction residuals. The results from the recursive modeling results suggested that a longer window and higher value of λ were better at predicting the hgb 8 weeks later. It should be noted that the accuracy of the 8-step predictions is highly dependent on the initial condition, which can be greatly affected by measurement noise. The data was filtered with an EWMA filter to try and remove some of the effect of the noise. Taken altogether, it is recommended that either the weighted or non-weighted linear C-ARX modeling method with an order of [1 8 1] should be used within the controller. Both the linear and nonlinear methods will be explored further in the controller performance tests.

Chapter 3

Hemoglobin Controller Designs

3.1 Introduction

Chapter 3 explores the development of several different types of model predictive controllers to be used to dose epoetin-alfa in the control of hemoglobin in CKD. The optimal hemoglobin target range is still up for debate (Singh, 2007) but generally lies somewhere between 9.5 and 12.0 g/dL for CKD patients. The tremendous cost of ESA therapy leaves a lot of room for debate on this issue, and there becomes a fine line where one could sacrifice patient health for monetary gain. For the purpose of this thesis, a control zone of 9.5 to 11.0 g/dL will be used. This range was chosen based on the available physician's protocol that the controllers will be compared to. There exist a few problems with a one-size-fits-all protocol for delivering ESA's to the patients. First, many of these protocols make doses based on a patient's weight, even though this is poorly correlated, as is shown in Figure 3.1. Secondly, the protocols lack the ability to counter acute disturbances in the hemoglobin in the patients, such as infection, blood loss or blood transfusions. The protocol that is used for comparison in this paper, is generally sluggish with its choice of ESA dosing and often fails to react quickly when presented with acute disturbances. Frequent disturbances, along with the reactive behaviour of the protocol, cause bouts of hemoglobin cycling. Thirdly, due to the large delay in the system caused by the pharmacokinetics and the delay in the production of red blood cells, it is extremely difficult to control by reactive measures as the protocol will always be a week or two behind the system dynamics.

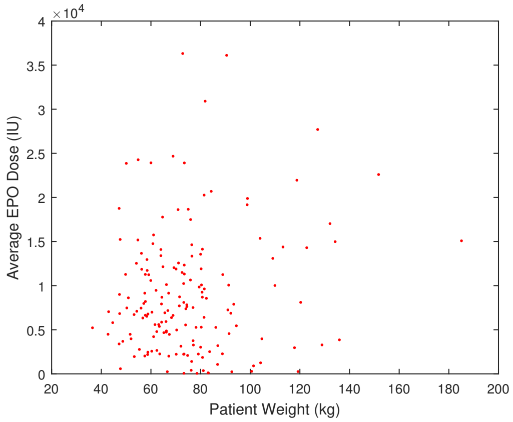

Figure 3.1: Relationship between Patient Weight and Average EPO dose for 167 clinical patients

With the aim of producing a more stable ESA protocol to overcome some of these issues, model based predictive controllers were explored. Gaweda et al. present one of the first published applications using a model predictive controller design and artificial neural networks for the control of hemoglobin (A. Gaweda *et al.*, 2008). Recent works on ESA dosing using model predictive control techniques have been used with improved clinical results as suggested in studies by Gaweda et al. (A. Gaweda *et al.*, 2014; M. Brier *et al.*, 2010). Hemoglobin variability was reduced significantly in these studies without compromising the safety of patient health. These studies suggest MPC may be a useful tool in the effective treatment of anemia in CKD. These studies were limited to traditional MPC and dose totals and controller aggressiveness were not tracked. This chapter seeks to develop and test new methods to aid in improved controller performance.

This chapter begins with an introduction to the model structure used in the MPC algorithms and outlines several predictive controllers, that are classified as either deterministic or stochastic. Deterministic controllers take the model structure to be a true model of the system, and the measurements to be a true measurement of the system and calculate an optimal dose based on this. The stochastic controllers take into account some of the uncertainties in the system, such as measurement noise in measuring the mass per volume of hemoglobin. Both classical MPC and Zone model predictive control will be explored within the framework of these two classifications.

The physician's protocol used for comparison in this thesis is shown on the next page, with sensitive information removed.

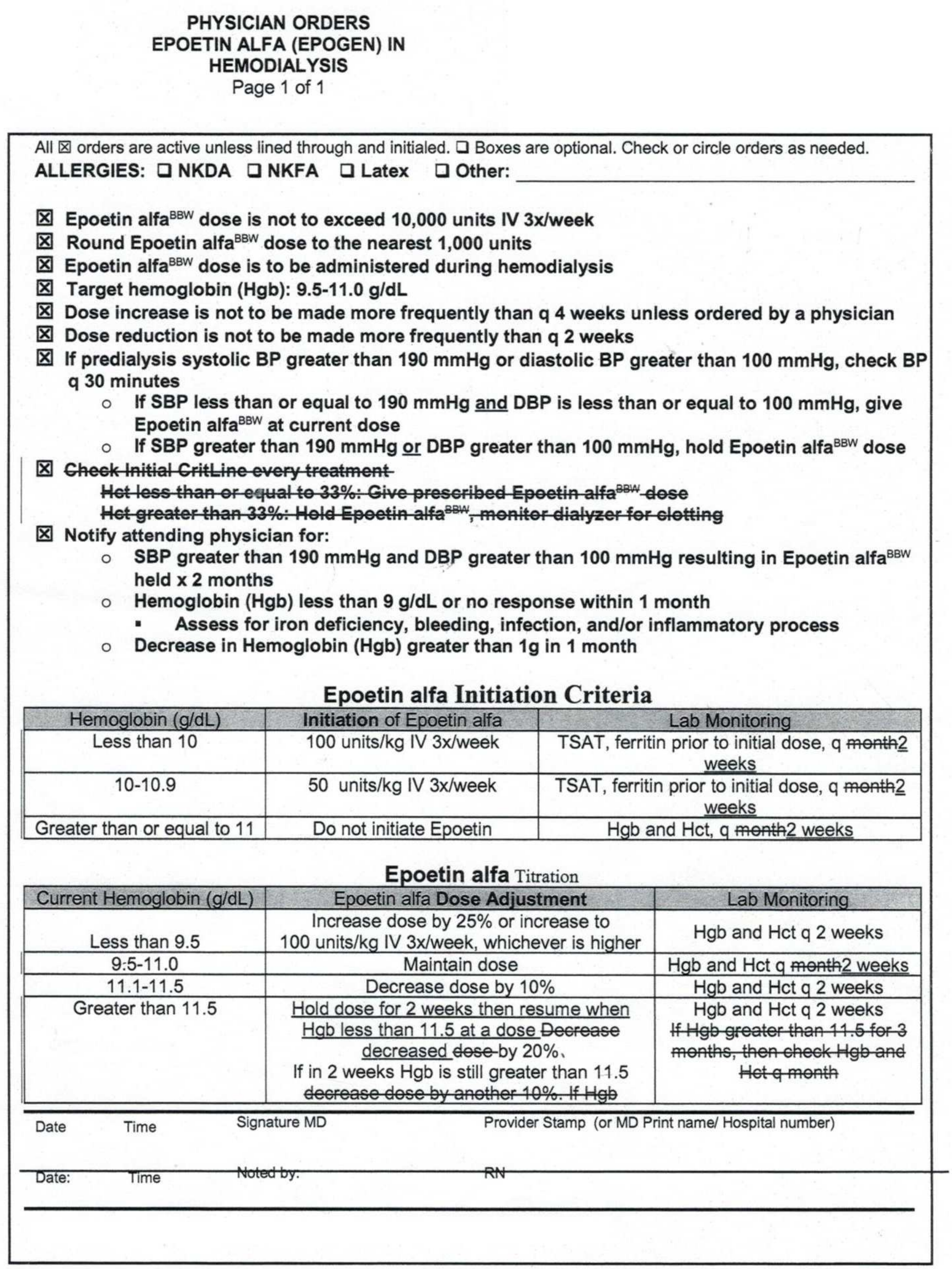

PHYSICIAN ORDERS
EPOETIN ALFA (EPOGEN) IN
HEMODIALYSIS
Page 1 of 1

All ☒ orders are active unless lined through and initialed. □ Boxes are optional. Check or circle orders as needed.

ALLERGIES: □ NKDA □ NKFA □ Latex □ Other: ____________________

☒ Epoetin alfa^{BBW} dose is not to exceed 10,000 units IV 3x/week
☒ Round Epoetin alfa^{BBW} dose to the nearest 1,000 units
☒ Epoetin alfa^{BBW} dose is to be administered during hemodialysis
☒ Target hemoglobin (Hgb): 9.5-11.0 g/dL
☒ Dose increase is not to be made more frequently than q 4 weeks unless ordered by a physician
☒ Dose reduction is not to be made more frequently than q 2 weeks
☒ If predialysis systolic BP greater than 190 mmHg or diastolic BP greater than 100 mmHg, check BP q 30 minutes

- **If SBP less than or equal to 190 mmHg and DBP is less than or equal to 100 mmHg, give Epoetin alfa^{BBW} at current dose**
- **If SBP greater than 190 mmHg or DBP greater than 100 mmHg, hold Epoetin alfa^{BBW} dose**

☒ ~~Check Initial CritLine every treatment~~
~~Hct less than or equal to 33%: Give prescribed Epoetin alfa^{BBW} dose~~
~~Hct greater than 33%: Hold Epoetin alfa^{BBW}, monitor dialyzer for clotting~~

☒ Notify attending physician for:

- **SBP greater than 190 mmHg and DBP greater than 100 mmHg resulting in Epoetin alfa^{BBW} held x 2 months**
- **Hemoglobin (Hgb) less than 9 g/dL or no response within 1 month**
  - **Assess for iron deficiency, bleeding, infection, and/or inflammatory process**
- **Decrease in Hemoglobin (Hgb) greater than 1g in 1 month**

Epoetin alfa Initiation Criteria

Hemoglobin (g/dL)	**Initiation** of Epoetin alfa	Lab Monitoring
Less than 10	100 units/kg IV 3x/week	TSAT, ferritin prior to initial dose, q ~~month~~2 weeks
10-10.9	50 units/kg IV 3x/week	TSAT, ferritin prior to initial dose, q ~~month~~2 weeks
Greater than or equal to 11	Do not initiate Epoetin	Hgb and Hct, q ~~month~~2 weeks

Epoetin alfa Titration

Current Hemoglobin (g/dL)	Epoetin alfa **Dose Adjustment**	Lab Monitoring
Less than 9.5	Increase dose by 25% or increase to 100 units/kg IV 3x/week, whichever is higher	Hgb and Hct q 2 weeks
9:5-11.0	Maintain dose	Hgb and Hct q ~~month~~2 weeks
11.1-11.5	Decrease dose by 10%	Hgb and Hct q 2 weeks
Greater than 11.5	Hold dose for 2 weeks then resume when Hgb less than 11.5 at a dose ~~Decrease~~ decreased ~~dose~~ by 20%、 If in 2 weeks Hgb is still greater than 11.5 ~~decrease dose by another 10%. If Hgb~~	Hgb and Hct q 2 weeks ~~If Hgb greater than 11.5 for 3 months, then check Hgb and Hct q month~~

Date Time Signature MD Provider Stamp (or MD Print name/ Hospital number)

~~Date: Time Noted by: RN~~

Figure 3.2: Physician's Protocol for dosing Epoetin-alfa

3.2 System Model

The system model that has been used in the following derivations is an autoregressive with exogenous inputs (ARX) model. This model can be obtained by either of the three methods mentioned in Chapter 2. The model structure for the [1 20 1] Constrained ARX model is as follows, where the inputs and outputs are represented as deviation variables. The derivations shown in this chapter will use a control horizon of N. In the next chapter on simulation results, the control horizon will be fixed to 8 weeks, which corresponds to $N = 8$ using a one week sampling time ($\Delta t \ = \ 1 \ week$). The theory for the following controller designs focus on the [1 20 1] ARX models. For models with less b parameters such as the [1 8 1] C-ARX models, the missing b parameters can simply be set to zero.

$$y_{k+1} = -a_1 \ y_k + b_1 u_k + \cdots + b_{20} u_{k-19} \tag{3.1}$$

3.3 Deterministic Model Predictive Controller Designs

3.3.1 Zone MPC Cost Function and Reformulation of Problem into Quadratic Program

The cost function that has been explored is a combination of state/output ($y_k \in \Re^n$) penalties from the target zone and penalties on the magnitude of the changes in the input ($\Delta u_k \in \Re^n$). This controller design using these cost function terms is commonly used in many emerging papers written on Type 1 Diabetes, and the control of blood glucose (B. Grosman *et al.*, 2010; V. Batora *et al.*, 2015; T. Knab and Parker, 2015). This penalty term allows the controller to eliminate erratic behaviour of the input; it aids in smoothing the optimized input. The cost function and constraints are outlined in Equation 3.2.

$$\min_{u,\delta} \frac{1}{2} \sum_{i=1}^{N} (y_{k+i} - \delta_{k+i})^T \ \hat{Q} \ (y_{k+i} - \delta_{k+i}) + \frac{1}{2} \sum_{i=0}^{N-2} \Delta u_{k+i}^T \ \hat{R} \ \Delta u_{k+i} \tag{3.2a}$$

$$s.t. \quad y_L \leq \ \delta_{k+i} \ \leq y_H \qquad i = 1, \ldots, N \tag{3.2b}$$

$$u_L \leq \ u_{k+i} \ \leq u_H \qquad i = 0, \ldots, N-2 \tag{3.2c}$$

$$\Delta u_L \leq \ \Delta u_{k+i} \ \leq \Delta u_H \qquad i = 0, \ldots, N-2 \tag{3.2d}$$

The controller achieves zone tracking through the use of the slack variable, $\hat{\delta}_k \in \{\Re^n : y_L \leq \delta_k \leq y_H\}$, in the cost function, along with its associated constraint in Equation 3.2b. The zone limits are set by choosing values for y_L and y_H in the constraint. The use of the slack variable in this way eliminates the cost of the state at that time instant as long as the state is in between the zone limits y_L and y_H. If the state is outside of the target zone, the cost associated with that point is the distance from the point to the nearest zone boundary, squared, and then multiplied by the state tuning parameter ($\hat{Q} \in \{\Re^n : \hat{Q} > 0\}$). In the following designs, no terminal state penalty is used and the prediction horizon is chosen large enough to ensure practical stability. $\hat{R} \in \{\Re^n : \hat{R} > 0\}$ is the tuning value on the rate change term and is always set to 1 and only $\hat{Q}$ is adjusted.

In order to solve the optimization algorithm efficiently, it is desired to generate a quadratic program reformulation (Rawlings, 2000). Using the chosen ARX model structure this can be achieved by making several substitutions and matrix manipulations. First start by separating the model in Equation 3.1 into the state response ($\tilde{y}_k = Ay_k$), future input response ($B\hat{u}_k$), and past input response ($P\tilde{U_k}$). From the perspective of the classical ARX modeling method, a_1 will always be a negative number, which eliminates the negative signs from the following equations. The following equations also do not show b_1 because it is assumed to be equal to zero due to the delay in the system.

$$\tilde{y}_k = \begin{bmatrix} (-a_1) \\ (-a_1)^2 \\ (-a_1)^3 \\ \vdots \\ (-a_1)^N \end{bmatrix} y_k \qquad B\ \hat{u}_k = \begin{bmatrix} 0 & 0 & 0 & \cdots & 0 \\ b_2 & 0 & 0 & \cdots & 0 \\ b_3 - a_1 b_2 & b_2 & 0 & \cdots & 0 \\ \vdots & \vdots & \ddots & \ddots & \vdots \\ poly_1 & poly_2 & \cdots & b_3 - a_1\ b_2 & b_2 \end{bmatrix} \begin{bmatrix} u_k \\ u_{k+1} \\ u_{k+2} \\ \vdots \\ u_{k+N-2} \end{bmatrix}$$

$$\begin{aligned} poly_1 &= b_N + (-a_1)\ b_{N-1} + (-a_1)^2\ b_{N-2} + \cdots + (-a_1)^{N-2}\ b_2 \\ poly_2 &= b_{N-1} + (-a_1)\ b_{N-2} + (-a_1)^2\ b_{N-3} + \cdots + (-a_1)^{N-3}\ b_2 \end{aligned} \tag{3.3}$$

$$P\ \tilde{U}_k = \begin{bmatrix} b_2 & b_3 & b_4 & \cdots & b_{20} \\ (-a_1)\ b_2 + b_3 & b_4 + (-a_1)\ b_3 & \cdots & \cdots & (-a_1)\ b_{20} \\ (-a_1)^2\ b_2 + (-a_1)\ b_3 + b_4 & \vdots & \cdots & \cdots & (-a_1)^2\ b_{20} \\ \vdots & \vdots & \ddots & \ddots & \vdots \\ poly_3 & poly_4 & \cdots & poly_5 & (-a_1)^{N-1}\ b_{20} \end{bmatrix} \begin{bmatrix} u_{k-1} \\ u_{k-2} \\ u_{k-3} \\ \vdots \\ u_{k-19} \end{bmatrix}$$

$$poly_3 = b_2\ (-a_1)^{N-1} + b_3\ (-a_1)^{N-2} + b_4\ (-a_1)^{N-3} + b_5\ (-a_1)^{N-4} + b_6\ (-a_1)^{N-5} + \ldots$$

$$poly_4 = b_3\ (-a_1)^{N-1} + b_4\ (-a_1)^{N-2} + b_5\ (-a_1)^{N-3} + b_6\ (-a_1)^{N-4} + b_7\ (-a_1)^{N-5} + \ldots$$

$$poly_5 = b_{19}\ (-a_1)^{N-1} + b_{20}\ (-a_1)^{N-2}$$

The following matrices are also needed in the reformulation.

$$\hat{y}_k = \begin{bmatrix} y_{k+1} \\ y_{k+2} \\ \vdots \\ y_{k+N} \end{bmatrix} \quad \hat{\delta}_k = \begin{bmatrix} \delta_{k+1} \\ \delta_{k+2} \\ \vdots \\ \delta_{k+N} \end{bmatrix} \quad \hat{y}_L = \begin{bmatrix} y_{L,k+1} \\ y_{L,k+2} \\ \vdots \\ y_{L,k+N} \end{bmatrix} \quad \hat{y}_H = \begin{bmatrix} y_{H,k+1} \\ y_{H,k+2} \\ \vdots \\ y_{H,k+N} \end{bmatrix}$$

$$\tilde{u}_k = \begin{bmatrix} u_{k-1} \\ 0 \\ \vdots \\ 0 \end{bmatrix} \quad \hat{u}_k = \begin{bmatrix} u_k \\ u_{k+1} \\ \vdots \\ u_{k+N-2} \end{bmatrix} \quad \Delta\hat{u}_k = \begin{bmatrix} \Delta u_k \\ \Delta u_{k+1} \\ \vdots \\ \Delta u_{k+N-2} \end{bmatrix} \tag{3.4}$$

$$\phi = \begin{bmatrix} 1 & 0 & \ldots & 0 \\ -1 & 1 & \ldots & 0 \\ \vdots & \ddots & \ddots & 0 \\ 0 & 0 & -1 & 1 \end{bmatrix} \quad Q = \begin{bmatrix} \hat{Q} & 0 & \ldots & 0 \\ 0 & \hat{Q} & \ldots & 0 \\ \vdots & \vdots & \ddots & \vdots \\ 0 & 0 & \ldots & \hat{Q} \end{bmatrix} \quad R = \begin{bmatrix} \hat{R} & 0 & \ldots & 0 \\ 0 & \hat{R} & \ldots & 0 \\ \vdots & \vdots & \ddots & \vdots \\ 0 & 0 & \ldots & \hat{R} \end{bmatrix}$$

It follows that

$$\Delta\hat{u}_k = \phi\ \hat{u}_k\ -\ \tilde{u}_k \tag{3.5}$$

Equation (3.2) can then be rewritten as a quadratic equation in matrix form as

$$\min_{\hat{u}_k,\hat{\delta}_k} \frac{1}{2}\ \left[\|\tilde{y_k}\ +\ B\ \hat{u}_k +\ P\ \tilde{U}_k\ -\ \hat{\delta}_k\|_Q^2\ +\ \|\Delta\hat{u}_k\|_R^2\right] \tag{3.6a}$$

$$s.t.\ \hat{y}_L\ \leq\ \hat{\delta}_k \leq \hat{y}_H \tag{3.6b}$$

$$\hat{u}_L\ \leq\ \hat{u}_k \leq \hat{u}_H \tag{3.6c}$$

$$\Delta\hat{u}_L\ \leq\ \Delta\hat{u}_k \leq \Delta\hat{u}_H \tag{3.6d}$$

where $\hat{u}_L,\ \hat{u}_H,\ \Delta\hat{u}_L,\ \Delta\hat{u}_H$ are vectors of the original constraint limits. Equation (3.6a) can be easily transformed into a standard Quadratic Program of the form

$$\min_{Z_k} \ \frac{1}{2} \ Z_k^T \ H \ Z_k \ + \ f^T \ Z_k \ + c \tag{3.7}$$

where

$$\begin{aligned}
H \ &= \ \begin{bmatrix} B & -I \\ \phi & 0 \end{bmatrix}^T \ \begin{bmatrix} Q & 0 \\ 0 & R \end{bmatrix} \ \begin{bmatrix} B & -I \\ \phi & 0 \end{bmatrix} \\
f \ &= \ \begin{bmatrix} B & -I \\ \phi & 0 \end{bmatrix}^T \ \begin{bmatrix} Q & 0 \\ 0 & R \end{bmatrix} \ \begin{bmatrix} \tilde{y}_k \ + P \ \tilde{U}_k \\ -\tilde{u}_k \end{bmatrix} \\
c \ &= \ \begin{bmatrix} \tilde{y}_k \ + P \ \tilde{U}_k \\ -\tilde{u}_k \end{bmatrix}^T \ \begin{bmatrix} Q & 0 \\ 0 & R \end{bmatrix} \ \begin{bmatrix} \tilde{y}_k \ + P \ \tilde{U}_k \\ -\tilde{u}_k \end{bmatrix} \\
Z_k \ &= \ \begin{bmatrix} \hat{u}_k \\ \hat{\delta}_k \end{bmatrix}
\end{aligned}$$

Problems in the QP form can be solved easily and efficiently by many conventional solvers. Matlab's quadprog function utilizing the interior-point optimization algorithm will be used to solve these problems within the MPC controller.

3.3.2 Classical Model Predictive Control (MPC)

Classical Model Predictive control has a much simpler derivation of the Quadratic Program (J. Rawlings, 1993), but the derivation in the previous section can be reverted back to classical MPC by setting all the zone boundaries (y_H and y_L), in terms of deviation variables, to be equal to the desired setpoint.

One of the potential downfalls of using classical MPC, is the controllers' aggressiveness when using a one-size-fits-all set of tuning parameters. When controlling around the setpoint, the controller will often make excessive dose changes, while it tries to regulate back to exactly the setpoint. For a single process system, it is often ok to tune the controller to try and eliminate much of this aggression, but this may not be a viable solution when the controllers can't be individually tuned to the patient due to the sheer volume of patients. Each patient will have different hemoglobin response dynamics, as well as a different steady state EPO dose.

3.3.3 Zone Model Predictive Control (ZMPC)

Zone Model Predictive Control is a control algorithm that has been gaining a lot of attention in the medical field, where clinically acceptable setpoints often do not exist.

It has been successfully used in clinical trials for the treatment of Type 1 Diabetes (R. Gondhalekar *et al.*, 2013). Zone MPC has been shown to provide robustness against plant model mismatch as well as against measurement noise (R. Gondhalekar *et al.*, 2013). Paralleling this experience to the case presented here, hemoglobin measurement techniques suffer from a large amount of measurement uncertainty. The system is also time-varying, which results in plant model mismatch.

Zone MPC is achieved by setting y_H and y_L to the desired limits. A problem exists with leaving the zone boundaries as static values along the prediction horizon. Due to the controller's cost function offering no state penalties within the zone, the nominal solution is often allowed to settle near the boundaries of the zone. This is an undesirable feature of ZMPC because plant model mismatch, as well as measurement and process noise, will often push the state outside of the desired region. One way to remedy this situation is to set a tighter control zone than actually desired. Another way to remedy this situation is to modify the constraints on the slack variable, $\hat{\delta}_k$, in Equation 3.6b. They can be modified to allow the zone boundaries to decay back toward the middle of the zone over the prediction horizon. An example of this is portrayed in Equation 3.8. Here the variable p can be chosen ($p < 1$) to tune the decay rate of the constraints over the prediction horizon, N. A pictorial view of the constraints is shown for an example in Figure 3.3. Here the target zone is chosen to be between 9.5 and 11.0 g/dl, and the shape tuning parameter, p, is chosen to be equal to 0.6.

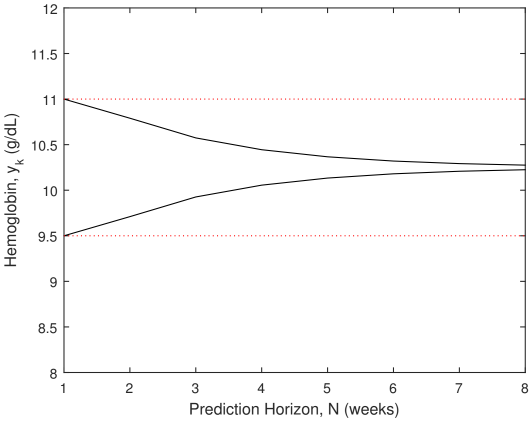

Figure 3.3: Constraint boundaries for the slack variable δ_k when the shape tuning parameter (p) is set to 0.6

The zone boundaries can be calculated with the following equations to facilitate a funnel-like control region.

$$\hat{y}_L = \begin{bmatrix} y_L \\ \frac{y_H+y_L}{2} - p\frac{y_H-y_L}{2} \\ \frac{y_H+y_L}{2} - p^2\frac{y_H-y_L}{2} \\ \vdots \\ \frac{y_H+y_L}{2} - p^{N-1}\frac{y_H-y_L}{2} \end{bmatrix} \quad \hat{y}_H = \begin{bmatrix} y_H \\ \frac{y_H+y_L}{2} + p\frac{y_H-y_L}{2} \\ \frac{y_H+y_L}{2} + p^2\frac{y_H-y_L}{2} \\ \vdots \\ \frac{y_H+y_L}{2} + p^{N-1}\frac{y_H-y_L}{2} \end{bmatrix} \qquad (3.8)$$

An example of the Zone MPC controllers using static boundaries and funnel constraints is shown in Figure 3.4. Here the controller with static boundaries settles exactly on the upper bound while the controller using the funnel constraints still regulates to the center of the zone.

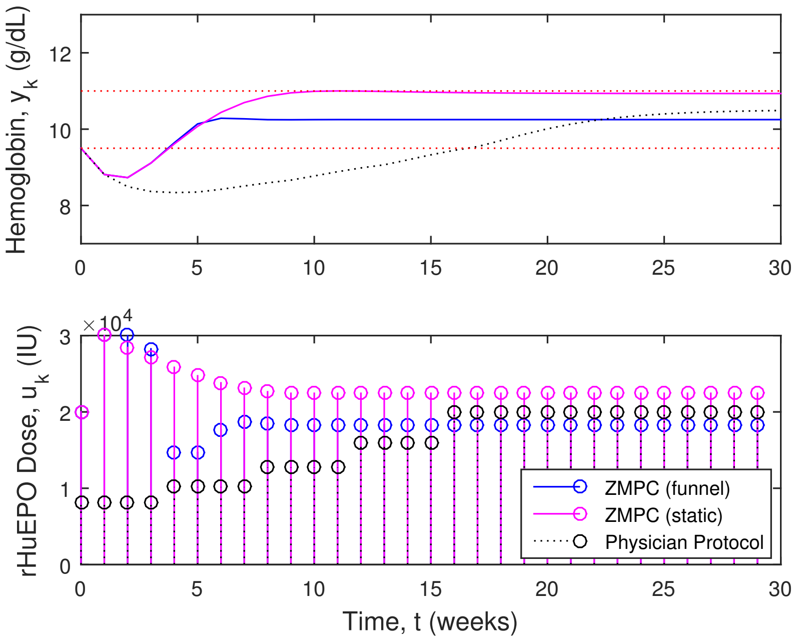

Figure 3.4: Comparison of Zone MPC with static vs decaying constraints on the slack variable under nominal conditions

Depending on the funnel shape, funnel controller performance will typically lie somewhere between that of the zone MPC controller and the classical MPC controller. That is, it will be more aggressive than the zone MPC controller, but have better state management. It will be less aggressive than the classical MPC controller, but often not yield as good of state management as the classical MPC. The funnel shape allows the controller to weakly track a setpoint. It is still desired to have a relatively low average Δu_k value, and the funnel shaped control zone allows the controller to be tuned to a more optimal level somewhere in between classical MPC and traditional zone MPC.

3.3.4 Economic Model Predictive Control (EMPC)

A simple Economic Zone MPC controller can be created by modifying the cost function equation to that of Equation 3.9, where the input, $u_{k+i} \in \{\Re^n : 0 \leq u_k \leq u_{max}\}$, is the absolute value of the input. The cost function then includes a penalty on the state deviation from the zone (primary objective), a penalty on change in the input (secondary objective), along with a penalty on the total drug use (secondary objective). In this fashion, the controller will regulate the state to the zone, while balancing the minimization of both the cost of the ESA treatment and the aggressiveness of the controller.

$$\min_{U,\delta} \frac{1}{2} \sum_{i=1}^{N} (y_{k+i} - \delta_{k+i})^T \; Q \; (y_{k+i} - \delta_{k+i}) + \frac{1}{2} \sum_{i=0}^{N-2} (\Delta u_{k+i}^T \; R \; \Delta u_{k+i} + u_{k+i}^T \; S) \tag{3.9a}$$

$$s.t. \quad y_L \leq \; \delta_{k+i} \; \leq y_H \qquad i = 1, \ldots, N \tag{3.9b}$$

$$u_L \leq \; u_{k+i} \; \leq u_H \qquad i = 0, \ldots, N-2 \tag{3.9c}$$

$$\Delta u_L \leq \; \Delta u_{k+i} \; \leq \Delta u_H \qquad i = 0, \ldots, N-2 \tag{3.9d}$$

In theory, significant drug costs can be saved by implementing EMPC on the patients. For demonstration purposes, both the controllers used in this section have a point target and their tuning parameter R is set to 0. Figure 3.5 depicts a 100 week simulation that compares economic MPC to classical MPC under additive process noise drawn from the distribution $N(0, 0.25^2)$. The setpoint is set in the middle of the zone at 10.25 g/dL. The state management is quite similar between both controllers, but the EMPC nets a drug dose reduction of 17.1% over the classical MPC controller. The tuning parameters Q and S are set at 400 and 1 for EMPC and 110 and 1 for MPC, respectively. The economic MPC controller results in a small negative offset compared to the classical MPC controller, which is the result of the economic term. The EMPC controller has a lower average hemoglobin value.

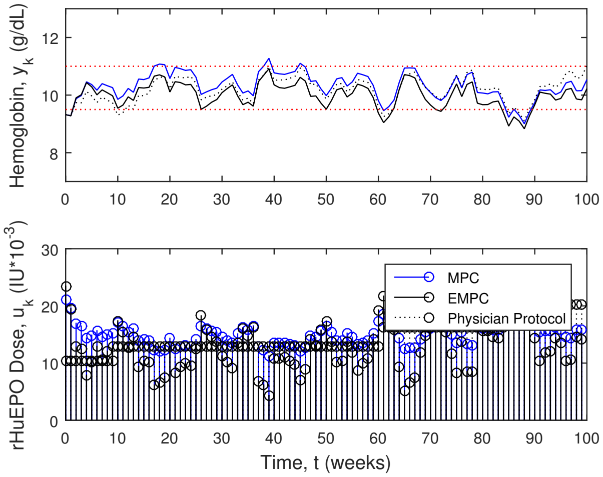

Figure 3.5: Comparison of EMPC with classical MPC for a 100 week patient simulation using additive process noise drawn from $N(0, 0.25^2)$

Figure 3.6a,b depicts two more simulations, when changing the tuning parameter Q from 400 to 110 and 10000, respectively. The improper tuning parameters cause significant offset to the downside of the system in Figure 3.6a. Figure 3.6b actually shows the EMPC controller using more drug dose than the classical MPC controller, a 4.4% increase.

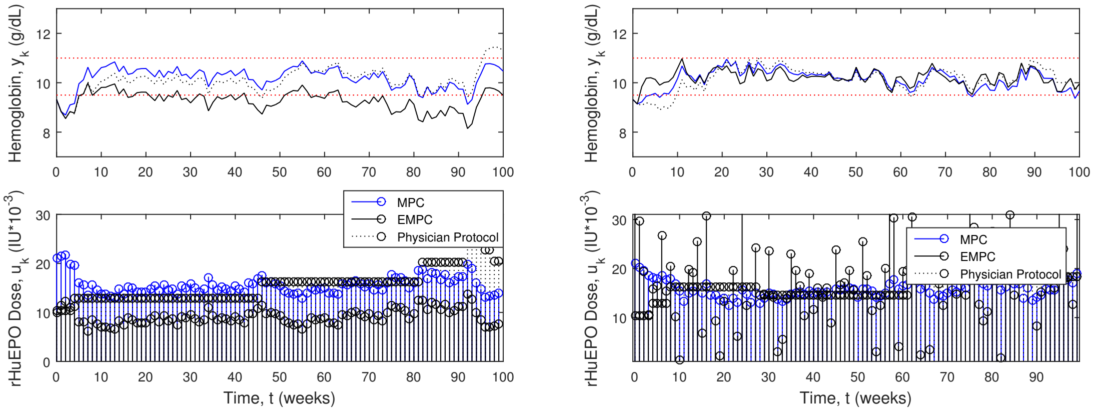

(a) EMPC Tuning Parameter Q=110 **(b)** EMPC Tuning Parameter Q=10000

Figure 3.6: Simulations comparing different tuning parameters for the EMPC controller

Minimizing the drug costs in the cost function can be performed, but the tuning parameters are highly sensitive. To aid in the tuning of this controller, the economic term was changed to a linear term versus a quadratic term, and the doses are scaled by 5000 IU. One of the complexities in tuning the controller is that drug doses come in multiples of 1000 and range from 0 to as high as 40000 IU. With each patient having different drug sensitivities, this controller becomes extremely difficult to tune properly for each patient. If tuned incorrectly, the controller will jeopardize the patients' health. This controller will be explored further in Chapter 4.

3.3.5 Nonlinear Zone MPC

Another possible solution for control is through the use of a nonlinear Zone MPC controller. This controller uses the PK/PD model from Equation 2.2 directly, and coupled together with Matlab's fmincon function, can solve for optimal control inputs. Nonlinear MPC has become more viable in recent years due to the advancement in modern computational speed and efficiencies, but it is still quite computationally expensive to solve a nonlinear programming problem (F. Allgower and Nagy, 2004). Matlab's fmincon function uses an interior-point algorithm to solve this problem. The algorithm simulates the system numerically, using a DDE solver similar to the one developed in Chapter 2, and then calculates a new step size by estimating the gradient at that point. The numerical method for simulating the DDE model is again an explicit method, so it does run the risk of being unstable for some time points which would greatly impact the solution from fmincon.

Figure 3.7 depicts a short 100 week simulation using measurement and additive process noise for the Nonlinear MPC controller versus a Linear MPC controller using an ARX model. The PK/PD model is used to simulate the patient, which makes almost identical models within the nonlinear MPC controller and the patient simulator. The ARX model chosen for this simulation offers only a minor amount of plant model mismatch, and does not produce a great deal of offset. In this simulation, the measurement noise was drawn from a distribution of $N(0, 0.166^2)$ which corresponds to a measurement error of approximately ±0.5 g/dL. The PK/PD model parameters in the patient were also allowed to vary with each parameter following a distribution of zero mean with the standard deviation being set to 10% of the original parameter value. It is clear from the the simulation that the NMPC controller does not offer improved accuracy over the linear counterpart. The time taken for the entire NMPC controller for the 100 week simulation was 8.26 hours, while the linear MPC controller completed the simulation in 2 minutes. If the purpose of this project was to control a single system, nonlinear MPC would certainly be a viable solution for many of the patients, but due to the sheer volume of patients that will be controlled using the proposed algorithm, it would require an incredible amount of computer processing power to calculate all the patients' control inputs. For this reason Nonlinear Zone MPC has not been explored further.

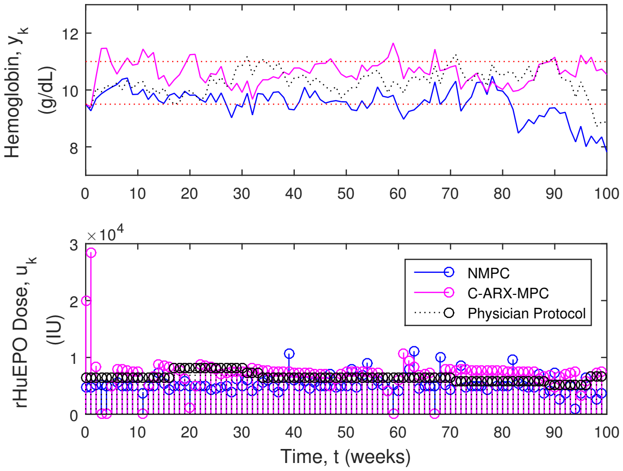

Figure 3.7: Example 100 week Simulation for a Nonlinear MPC controller versus a linear MPC controller for a single patient when trying to control the PK/PD model with measurement noise and parameter variation

3.4 Stochastic Model Predictive Controller Designs

Stochastic controllers have the ability to take into account some of the known uncertainties within a system. The constraints of the system are determined probabilistically which allows a small portion of violation. Uncertainties can manifest themselves within process and measurement noise, or within the model parameters themselves. This chapter focuses on the development of stochastic controllers that take into account the uncertainties in the measurement and process noise. These stochastic controllers take into account the randomly distributed vector $\hat{S}_k$, that will be taken from a distribution that approximates some additive process uncertainty. By utilizing the random variables and it's probability distribution, several methods for regulating to a zone can be explored and will be discussed in this section.

3.4.1 Stochastic System Model

Due to the propagation of error from each time instant along the prediction horizon, the random vector $\hat{S}_k$ is multiplied to a variation of the state response matrix which will be denoted as matrix D. Adding the additional random vector contribution to the system, the model takes on the following form

$$\hat{y}_k \;=\; A\,y_k \;+\; B\,\hat{u}_k \;+\; P\,\tilde{U}_k \;+\; D\,\hat{S}_k \tag{3.10}$$

where

$$D\;\hat{S}_k = \begin{bmatrix} I & 0 & \cdots & 0 \\ (-a_1) & I & \cdots & 0 \\ (-a_1)^2 & (-a_1) & \cdots & 0 \\ \vdots & \vdots & \ddots & \vdots \\ (-a_1)^{N-1} & (-a_1)^{N-2} & \cdots & I \end{bmatrix} \begin{bmatrix} s_k \\ s_{k+1} \\ s_{k+2} \\ \vdots \\ s_{k+N-1} \end{bmatrix}$$

3.4.2 Chance Constraints with Gaussian Uncertainty

The use of individual chance constraints was explored. In this method, these constraints use the properties of the distribution of the random vector $\hat{S}_k$ and then these chance constraints are formulated into hard constraints. If the random variables inside the vector follow a Gaussian distribution they can be converted directly to hard constraints (J. Grosso *et al.*, 2014). If we consider the variable s_{k+i} to be part of the distribution $N(\bar{s}, \Sigma)$ where vector D_j refers to the j^{th} row of the matrix D, the hard constraints can be formulated from the following method (J. Grosso *et al.*, 2014). In zone control, chance constraints would be applied to both the upper and lower bounds of the control region. For example purposes, the following upper bound chance constraint will be used to illustrate the method.

$$Pr(y_{k+i} < y_H) \geq 1 - \varepsilon \qquad where \;\; y_{k+i} = f(y_k, \hat{u}_k, \tilde{U}_k) \;+\; D_j\hat{S}_k \tag{3.11}$$

In Equation (3.11), ε refers to the probability level in which the chance constraint is allowed to be violated. The distribution of s_{k+i} is not normal. To normalize this distribution in the chance constraint, it follows that the mean of the distribution should be subtracted from both sides and then both sides can be divided by the standard deviation of the distribution of the random variable $D_j\hat{S}_{k+i}$ (ie. $N(\bar{s}^T D_j^T, D_j \Sigma D_j^T)$).

The resulting equation is

$$Pr\left(\frac{D_j\hat{S}_k - \bar{s}^T D_j^T}{\sqrt{D_j \Sigma D_j^T}} \;<\; \frac{y_H - f(y_k, \hat{u}_k, \tilde{U}_k) - \bar{s}^T D_j^T}{\sqrt{D_j \Sigma D_j^T}}\right) \;\geq\; 1 - \varepsilon \tag{3.12}$$

Equation (3.12) follows a standard normal distribution, $N(0,1)$, and can be represented by

$$\Phi\left(\frac{y_H - f(y_k, \hat{u}_k, \tilde{U}_k) - \bar{s}^T D_j^T}{\sqrt{D_j \Sigma D_j^T}}\right) \;\geq\; 1 - \varepsilon \tag{3.13}$$

where $\Phi\ (\cdot)$ is the cumulative distribution function (CDF) of the standard normal distribution. Taking the inverse CDF of both sides, and rearranging the equation results in the deterministic hard constraint representing Equation (3.11)

$$y_H \;\geq\; \phi^{-1}(1-\varepsilon)\,\sqrt{D_j \Sigma D_j^T} + \;\bar{s}^T D_j^T \;+\; f(y_k, \hat{u}_k, \tilde{U}_k) \tag{3.14}$$

Similarly, hard constraints can be determined for the lower zone boundary.

$$y_L \;\leq\; -\phi^{-1}(1-\varepsilon)\,\sqrt{D_j \Sigma D_j^T} + \;\bar{s}^T D_j^T \;+\; f(y_k, \hat{u}_k, \tilde{U}_k) \tag{3.15}$$

Due to the constraints being hard constraints, the controller will naturally have feasibility issues. This problem can be overcome by using a hybrid controller or using soft constraints which will be discussed in the following sections.

3.4.3 Conditional Value at Risk (CVaR) Constraints

CVaR is a popular tool used in risk management. CVaR was introduced by Rockafellar and Uryasev (R. Rockafellar, 2000). It is widely used in the finance industry for portfolio management. Before the advent of CVaR, the Value at Risk (VaR) was the standard for optimization problems involving finances (R. Rockafellar, 2000). In the finance industry, $p - VaR$ is defined as the maximum loss value that is assigned to some desired probability , p, over a given prediction horizon. That is to mean that a loss $\leq p - VaR$ will occur $p\%$ of the time.

One of the main benefits over the previous chance constraint formulation, is that CVaR is usable for any type of distribution and doesn't rely on the noise distribution being Gaussian. The following upper bound chance constraint will be used as an example for the derivation of a CVaR constraint. Here, it is desired to have the output remain underneath some upper bound within a certain probability. Opposite to intuition, the following derivation is completed using a probability of violation (ϵ) of the constraint. The uncertainty is again located within the output, y_k, in the form of a random variable s_{k+i}. s_{k+i} is part of the distribution $N(\bar{s}, \Sigma)$. For brevities sake in notation, the output in the derivation will remain as y_k and it will be assumed it contains the random variable.

$$Pr\{y_k > y_H\} \leq \epsilon \tag{3.16}$$

Equation 3.17 is the definition for the indicator function. This function holds a value of 1 if $u > 0$ and a value of 0 if $u \leq 0$.

$$1_{(0,\infty)}(u) = 1 \; if \;\; u > 0 \tag{3.17a}$$

$$1_{(0,\infty)}(u) = 0 \; if \;\; u \leq 0 \tag{3.17b}$$

Inserting the positive variable α into the indicator function changes the input to the indicator function but makes no difference in its output.

$$1_{(0,\infty)}(u) = 1_{(0,\infty)}(\frac{1}{\alpha}u) \tag{3.18a}$$

$$\alpha > 0 \tag{3.18b}$$

Defining an upper bounding function $\phi(u)$ for the indicator function, the following inequality can be written.

$$1_{(0,\infty)}(\frac{1}{\alpha}u) \leq \phi(\frac{1}{\alpha}u) \tag{3.19}$$

Replacing u with $y_k - y_H$, the following inequality can be written. If $y_k - y_H > 0$ the constraint is violated and the indicator function holds a value of 1, and vice versa. $\phi(u)$ is the upperbounding function for the indicator function and it is a conservative estimate of the probability of violation, ϵ.

$$Pr\{y_k - y_H > 0\} = \mathrm{E}[1_{(0,\infty)}(y_k - y_H)] \leq \mathrm{E}[\phi(\frac{1}{\alpha}(y_k - y_H))] \;\; \leq \epsilon \tag{3.20}$$

From this, any solution that satisfies the inequality will also satisfy the constraint. The focus will remain on the right side of this inequality. (u)$^+$ is defined as the maximum operator, which will hold the maximum value between 0 and the input u. Applying the upper bounding function $\phi(u) = (u+1)^+$, a conservative approximation of the chance constraint is defined as

$$\mathrm{E}\left[(\tfrac{1}{\alpha}(y_k - y_H) + 1)^+\right] \leq \epsilon \tag{3.21}$$

multiply by $\frac{\alpha}{\epsilon}$

$$\frac{1}{\epsilon}\ \mathrm{E}\left[((y_k - y_H) + \alpha)^+\right] \leq \alpha \tag{3.22}$$

moving α to the left hand side

$$-\alpha\ + \frac{1}{\epsilon}\ \mathrm{E}\left[((y_k - y_H) + \alpha)^+\right] \leq 0 \tag{3.23}$$

To reduce conservatism, find the minimum α that satisfies the inequality. That is, it is desired to find the smallest upperbound. This results in the CVaR constraint, but it is difficult to calculate its value in its present form.

$$\min_{\alpha}\quad -\alpha\ + \frac{1}{\epsilon}\ \mathrm{E}\left[((y_k - y_H) + \alpha)^+\right] \leq 0 \tag{3.24}$$

The expectation operator is removed with the introduction of sampling to approximate the CVaR constraint. M is the total number of scenarios. For instance, if there were a single random variable per scenario, and the prediction horizon was 1, it would be necessary to sample the random variables' distribution M times. π_j is the probability that a single scenario will occur, and will be equal to $\frac{1}{M}$.

$$-\alpha\ + \frac{1}{\epsilon}\ \sum_{j=1}^{M} \pi_j \left[((y_{k,j} - y_H) + \alpha)^+\right] \leq 0 \tag{3.25}$$

The above equation is still not usable within an optimization constraint function. The expression inside of the max operator can be replaced by two separate constraints. The following equation replaces the max operator term with the variable v_j, and constraints are set on v_j to satisfy the original max operator's function. The combination of all three constraints in Equation 3.26 can be used to provide a conservative estimate of the original chance constraint in Equation 3.16 through the use of sampling (A. Parisio *et al.*, 2013). These constraints are solved using many different scenarios of the random variable distribution, leading to it being part of a class of controllers called Scenario-Based MPC.

$$-\alpha + \frac{1}{\epsilon}\sum_{j=1}^{M}\pi_j v_j \leq 0 \tag{3.26a}$$

$$v_j \geq (y_{k,j} - y_H) + \alpha \qquad j = 1, ..., M \tag{3.26b}$$

$$v_j \geq 0 \qquad j = 1, ..., M \tag{3.26c}$$

3.4.4 Zone MPC Hybrid Controller using Hard Chance Constraints

The controller outlined in this section uses the Quadratic Program formulation in Equation 3.7, along with a number of chance constraints. The controller adds chance constraints only when the system output enters the zone and the regular Zone MPC controller is used while the output is outside of the desired zone. This controller type leads to stable solutions but it reduces the ability to analytically explain the probability of having the output within the bounds because the chance constraints are not always used. It is typically not feasible for a large prediction horizon to have a chance constraint at each time instant, k, along the predicted trajectory because the constraints will end up converging at some point before the prediction horizon ends making every solution infeasible. One way around this is to use less chance constraints and then extend the final chance constraint to create a zone constraint for the remaining portion of the prediction horizon. The constraint extension will not be necessary in the control of hemoglobin because the prediction horizon is short and does not allow the constraint convergence.

3.4.5 Zone MPC using Soft Chance Constraints

Another way to deal with the infeasibility of the chance constraints is to introduce the addition of slack variables that relax the chance constraints if necessary. These same slack variables are then penalized heavily in the cost function. In this way, the relaxation of the constraints only occurs if the chance constraints are infeasible. In these cases, the solution should then always touch the boundary of the relaxed constraint. The hard constraints in Equations 3.14 and 3.15 with the introduction of these slack variables become

$$y_H \ + \xi_1 \ > \ \phi^{-1}(1-\varepsilon)\ \sqrt{D_j \Sigma D_j^T} + \ \bar{s}^T D_j^T \ + \ f(y_k, \hat{u}_k, \tilde{U}_k) \tag{3.27a}$$

$$y_L - \ \xi_2 \ < \ -\phi^{-1}(1-\varepsilon)\ \sqrt{D_j \Sigma D_j^T} + \ \bar{s}^T D_j^T \ + \ f(y_k, \hat{u}_k, \tilde{U}_k) \tag{3.27b}$$

The Quadratic Program in Equation 3.7 can be augmented to include the two slack variables $\xi_1 \in \{\Re^n : \xi_1 > 0\}$ and $\xi_2 \in \{\Re^n : \xi_2 > 0\}$. The new H, f, and c will be subscripted with 1 while the previous H, f, and c from Equation 3.7 will be used without subscripts. The new penalty on the slack variables ξ_1 and ξ_2 will be $\xi_P \in \{\Re^n : \xi_P > 0\}$ and hold a very high value.

$$\min_{Z_k} \ \frac{1}{2}\ Z_k^T \ H_1 \ Z_k \ + \ f_1^T \ Z_k \ + c_1 \tag{3.28}$$

where

$$H_1 \ = \ \begin{bmatrix} H & 0 & 0 \\ 0 & \xi_P & 0 \\ 0 & 0 & \xi_P \end{bmatrix} \qquad and\ Z_k = \begin{bmatrix} \hat{u}_k \\ \hat{\delta}_k \\ \xi_1 \\ \xi_2 \end{bmatrix}$$

$$f_1 \ = \ \begin{bmatrix} f & 0 & 0 \end{bmatrix}^T$$

$$c_1 \ = \ c$$

Subject to the previous constraints as well as two new constraints on the new slack variables

$$\hat{y}_L \ \le \ \hat{\delta}_k \le \hat{y}_H$$

$$\hat{u}_L \ \le \ \hat{u}_k \le \hat{u}_H$$

$$\Delta\hat{u}_L \ + \ \tilde{u}_k \ \le \ \phi\ \hat{u}_k \le \Delta\hat{u}_H \ + \ \tilde{u}_k$$

$$0 \ \le \ \xi_1$$

$$0 \ \le \ \xi_2$$

$$y_{H,i} \ + \xi_1 \ > \ \phi^{-1}(1-\varepsilon)\ \sqrt{D_j \Sigma D_j^T} + \ \bar{s}^T D_j^T \ + \ f(y_k, \hat{u}_k, \tilde{U}_k) \qquad i, j = 2, \ldots, 8 \tag{3.29a}$$

$$y_{L,i} - \ \xi_2 \ < \ -\phi^{-1}(1-\varepsilon)\ \sqrt{D_j \Sigma D_j^T} + \ \bar{s}^T D_j^T \ + \ f(y_k, \hat{u}_k, \tilde{U}_k) \qquad i, j = 2, \ldots, 8 \tag{3.29b}$$

3.4.6 Scenario Based Zone MPC using Hard CVaR Constraints

The controller described in this section belongs to the family of Scenario-Based Controllers. The controller is designed to take into account an additive process noise from a known distribution. Using this known distribution, the chance constraints are created as outlined in Section 3.4.3. This controller design will have 2 CVaR constraints on the output of the system, 1 on the lower bound and 1 on the upper bound. The constraints will be used for $k = 3$ as shown in Equation 3.30.

$$
\begin{aligned}
& -\alpha_k + \frac{1}{\epsilon}\sum_{j=1}^{M} \pi_j v_{j,k} \leq 0 \qquad k = 3 && (3.30a)\\
& v_{j,k} \geq (y_{k,j} - y_H) + \alpha_k \quad j = 1, ..., M, \quad k = 3 && (3.30b)\\
& v_{j,k} \geq 0 \qquad j = 1, ..., M, \quad k = 3 && (3.30c)\\
& -\beta_k + \frac{1}{\epsilon}\sum_{j=1}^{M} \pi_j \omega_{j,k} \leq 0 \qquad k = 3 && (3.30d)\\
& \omega_{j,k} \geq (y_L - y_{k,j}) + \beta_k \quad j = 1, ..., M, \quad k = 3 && (3.30e)\\
& \omega_{j,k} \geq 0 \qquad j = 1, ..., M, \quad k = 3 && (3.30f)
\end{aligned}
$$

The controller that will be tested for this section will, for example, use 100 scenarios ($M = 100$). It should quickly become apparent that scenario-based constraints such as these lead to a very large number of constraints. In this case, there will be $4M + 2$ constraints related to the CVaR constraints, leading to a total of 402 constraints. With this in mind, the cost function used was changed to a linear program for the ability of that solver type to handle a large number of constraints. In this case Matlab's linprog function was used along with its dual-simplex optimization solver. The cost function is outlined in Equation 3.4.6.

$$\min Q \sum_{k=1}^{8} |y_k - \delta_k| + R \sum_{k=0}^{6} |\Delta u_k| \tag{3.31}$$

This equation can be manipulated to remove the absolute sign and the resulting linear program with all the constraints is outlined in Equation 3.32.

$$\min Q \sum_{k=1}^{8} h_k + R \sum_{k=0}^{6} g_k \tag{3.32a}$$

$$-\alpha_k + \frac{1}{\epsilon}\sum_{j=1}^{M}\pi_j v_{j,k} \leq 0 \qquad k = 3 \tag{3.32b}$$

$$v_{j,k} \geq (y_{k,j} - y_H) + \alpha_k \qquad j = 1, ..., M, \quad k = 3 \tag{3.32c}$$

$$v_{j,k} \geq 0 \qquad j = 1, ..., M, \quad k = 3 \tag{3.32d}$$

$$-\beta_k + \frac{1}{\epsilon}\sum_{j=1}^{M}\pi_j \omega_{j,k} \leq 0 \qquad k = 3 \tag{3.32e}$$

$$\omega_{j,k} \geq (y_L - y_{k,j}) + \beta_k \qquad j = 1, ..., M, \quad k = 3 \tag{3.32f}$$

$$\omega_{j,k} \geq 0 \qquad j = 1, ..., M, \quad k = 3 \tag{3.32g}$$

$$h_k \geq y_k - \delta_k \qquad k = 1, \ldots, 8 \tag{3.32h}$$

$$h_k \geq -(y_k - \delta_k) \qquad k = 1, \ldots, 8 \tag{3.32i}$$

$$g_k \geq \Delta u_k \qquad k = 0, \ldots, 6 \tag{3.32j}$$

$$g_k \geq -\Delta u_k \qquad k = 0, \ldots, 6 \tag{3.32k}$$

$$\delta_k \leq y_H \qquad k = 1, \ldots, 8 \tag{3.32l}$$

$$-\delta_k \leq -y_L \qquad k = 1, \ldots, 8 \tag{3.32m}$$

$$u_k \leq U_{max} \qquad k = 0, \ldots, 6 \tag{3.32n}$$

$$-u_k \leq U_{min} \qquad k = 0, \ldots, 6 \tag{3.32o}$$

$$\Delta u_k \leq \Delta U_{max} \qquad k = 0, \ldots, 6 \tag{3.32p}$$

$$-\Delta u_k \leq \Delta U_{min} \qquad k = 0, \ldots, 6 \tag{3.32q}$$

Equation 3.32 leads to a total of 470 constraints and an optimization vector Z_k as outlined below. There are $2M + 30$ variables to be optimized (232).

$$Z_k = \begin{bmatrix} u_0 \\ \vdots \\ u_6 \\ \delta_1 \\ \vdots \\ \delta_8 \\ \alpha_3 \\ \vdots \\ v_{1,3} \\ \vdots \\ v_{100,3} \\ \beta_3 \\ \omega_{1,3} \\ \vdots \\ \omega_{100,3} \\ h_1 \\ \vdots \\ h_8 \\ g_0 \\ \vdots \\ g_6 \end{bmatrix} \tag{3.33}$$

Due to in-feasibility issues, if the controller fails to find a feasible solution, a backup classical MPC controller will be used for that time instant. This is a hybrid controller solution similar to that used in the controller with Hard Chance Constraints.

3.4.7 Scenario Based Zone MPC using Soft CVaR Constraints

Similar to the formulation for soft constraints previously mentioned in the Gaussian case, the CVaR constraints can be relaxed to facilitate feasibility. Again, a slack variable is introduced to relax the constraints in Equation 3.34b,e. The constraints in Equation 3.34r,s are also added to ensure the new slack variables are always positive.

$$\min Q \sum_{k=1}^{8} h_k + R \sum_{k=0}^{6} g_k + \xi_P(\xi_1 + \xi_2) \tag{3.34a}$$

$$-\xi_1 - \alpha_k \ + \frac{1}{\epsilon} \sum_{j=1}^{M} \pi_j v_{j,k} \leq 0 \qquad k = 3 \tag{3.34b}$$

$$v_{j,k} \geq (y_{k,j} - y_H) + \alpha_k \quad j = 1, ..., M, \quad k = 3 \tag{3.34c}$$

$$v_{j,k} \geq 0 \qquad j = 1, ..., M, \quad k = 3 \tag{3.34d}$$

$$-\xi_2 - \beta_k + \frac{1}{\epsilon} \sum_{j=1}^{M} \pi_j \omega_{j,k} \leq 0 \qquad k = 3 \tag{3.34e}$$

$$\omega_{j,k} \geq (y_L - y_{k,j}) + \beta_k \quad j = 1, ..., M, \quad k = 3 \tag{3.34f}$$

$$\omega_{j,k} \geq 0 \qquad j = 1, ..., M, \quad k = 3 \tag{3.34g}$$

$$h_k \geq y_k - \delta_k \qquad k = 1, \ldots, 8 \tag{3.34h}$$

$$h_k \geq -(y_k - \delta_k) \qquad k = 1, \ldots, 8 \tag{3.34i}$$

$$g_k \geq \Delta u_k \qquad k = 0, \ldots, 6 \tag{3.34j}$$

$$g_k \geq -\Delta u_K \qquad k = 0, \ldots, 6 \tag{3.34k}$$

$$\delta_k \leq y_H \qquad k = 1, \ldots, 8 \tag{3.34l}$$

$$-\delta_k \leq -y_L \qquad k = 1, \ldots, 8 \tag{3.34m}$$

$$u_k \leq U_{max} \qquad k = 0, \ldots, 6 \tag{3.34n}$$

$$-u_k \leq U_{min} \qquad k = 0, \ldots, 6 \tag{3.34o}$$

$$\Delta u_k \leq \Delta U_{max} \qquad k = 0, \ldots, 6 \tag{3.34p}$$

$$-\Delta u_k \leq \Delta U_{min} \qquad k = 0, \ldots, 6 \tag{3.34q}$$

$$\xi_1 \geq 0 \tag{3.34r}$$

$$\xi_2 \geq 0 \tag{3.34s}$$

3.4.8 Scenario Based Zone MPC using Conditional Value at Risk in Cost Function

Another controller method for dealing with uncertainty is the scenario based MPC controller using CVaR in the cost function, rather than in the constraints. The controller discussed here, will look at optimizing the control inputs using conditional value at risk, directly within the cost function which leads to a solution that is always feasible. The scenario based Zone MPC controller uses the distribution of the random variable s_k to generate several different plausible scenarios of noise. Instead of optimizing a linear or quadratic objective as before, the controller optimizes the Conditional Value at Risk (β-CVaR) as introduced by Bemporady et al. (A. Bemporady and Gabbriellin, 2011). The formulation of this problem requires several steps and starts with the definition of a linear program similar to the previous quadratic objective function used. The linear program used as the loss function is $\in \Re^{n+i}$ which is associated with decision vectors $\hat{u}_k \in \{\Re^n : u_{min} \leq u_k \leq u_{max}\}$ and $\hat{\delta}_k \in \{\Re^n : y_L \leq \delta_k \leq y_H\}$ and random vector $\hat{S}_k \in \Re^n$. $\tilde{U}_k \in \Re^n$ is associated with the past inputs. Note that Q and R are again used as the tuning parameters in this equation.

$$f(\hat{u}_k, \tilde{U}_k, \hat{\delta}_k, \hat{S}_k) \;=\; Q\sum_{i=1}^{N}|y_{k+i} - \delta_{k+i}| \;+\; R\sum_{i=0}^{N-2}|\Delta u_{k+i}| \tag{3.35}$$

Let $p(s)$ be the probability density function of the random variable s_k. Used in the calculation of β-CVaR is another parameter β-VaR (Value at Risk) which is defined as the smallest value for which the probability that the loss function will not exceed its value is β. β is the fixed value confidence level and typically holds a value greater than 0.9. The downside of using only β-VaR (ℓ) is that the loss greater than ℓ is not accounted for. β-CVaR allows for the quantification of losses greater than ℓ. The variable β-VaR is defined as

$$\ell_\beta(\hat{u}_k, \tilde{U}_k, \hat{\delta}_k) \;= min\{\ell \in \Re : \psi(\hat{u}_k, \tilde{U}_k, \hat{\delta}_k, \ell) \geq \beta\} \tag{3.36}$$

where the probability of $f(\hat{u}_k, \tilde{U}_k, \hat{\delta}_k, \hat{S}_k)$ not exceeding ℓ is

$$\psi(\hat{u}_k, \tilde{U}_k, \hat{\delta}_k, \ell) = \int_{f(\hat{u}_k, \tilde{U}_k, \hat{\delta}_k, \hat{S}_k) \leq \ell} p(s)ds \tag{3.37}$$

β-CVaR is defined as

$$\phi_\beta(\hat{u}_k, \tilde{U}_k, \hat{\delta}_k) = (1-\beta)^{-1} \int_{f(\hat{u}_k, \tilde{U}_k, \hat{\delta}_k, \hat{S}_k) \geq \ell_\beta(u)} f(\hat{u}_k, \tilde{U}_k, \hat{\delta}_k, \hat{S}_k)\; p(s)ds \tag{3.38}$$

The loss associated with any $\hat{u}_k$,$\tilde{U}_k$ and $\hat{\delta}_k$ can be determined from the addition of both β-VaR and β-CVaR.

$$F_\beta(\hat{u}_k, \tilde{U}_k, \hat{\delta}_k, \ell) = \ell + (1-\beta)^{-1} \int_{\hat{S}_k \in \Re^m} [f(\hat{u}_k, \tilde{U}_k, \hat{\delta}_k, \hat{S}_k) - \ell]^+ p(s)ds \tag{3.39}$$

$[f]^+$ denotes the max of $[f, 0]$. The integral in the above equation is difficult to solve explicitly which brings about the need to perform sampling to approximate it. M number of scenarios (or M vectors of $\hat{S}_k$) are randomly generated from the distribution of s_k, with each scenario having a probability of π_j of occurring. Then Equation (3.39) can be approximated by

$$\hat{F}_\beta(\hat{u}_k, \tilde{U}_k, \hat{\delta}_k, \ell) = \ \ell + (1-\beta)^{-1} \sum_{j=1}^{M} \ \pi_j \ [f(\hat{u}_k, \tilde{U}_k, \hat{\delta}_k, \hat{S}_k) - \ell]^+ \tag{3.40}$$

Combining Equations (3.35) and (3.40) and adding the previous system constraints, the final form of the SMPC problem results in a linear program minimizing the β-CVaR as follows where k, j, i represent the sampling instant, scenario number and sampling instant along the prediction horizon, respectively.

$$\begin{aligned}
\min_{\hat{u}_k, \hat{\delta}_k, \ell, v_j} \quad & \ell + (1-\beta)^{-1} \sum_{j=1}^{M} \ \pi_j \ v_j & & \text{(3.41a)}\\
s.t. \ \ & v_j \geq \ Q \sum_{i=0}^{N-1} h_{k+i,j} + R \sum_{i=0}^{N-2} g_{k+i} \quad - \ell & & \text{(3.41b)}\\
& v_j \geq 0 & \forall \ j & \quad \text{(3.41c)}\\
& h_{k+i,j} \geq y_{k+1+i,j} - \delta_{k+i,j} & \forall \ i,j & \quad \text{(3.41d)}\\
& h_{k+i,j} \geq -(y_{k+1+i,j} - \delta_{k+i,j}) & \forall \ i,j & \quad \text{(3.41e)}\\
& g_{k+i} \geq \Delta u_{k+i} & \forall \ i & \quad \text{(3.41f)}\\
& g_{k+i} \geq -\Delta u_{k+i} & \forall \ i & \quad \text{(3.41g)}\\
& u_{min} \leq u_{k+i} \leq u_{max} & \forall \ i & \quad \text{(3.41h)}\\
& \Delta u_{min} \leq \Delta u_{k+i} \leq \Delta u_{max} & \forall \ i & \quad \text{(3.41i)}\\
& y_L \leq \delta_{k+i,j} \leq y_H & \forall \ i,j & \quad \text{(3.41j)}
\end{aligned}$$

The above Equation results in $4MN + 2M + 6N$ constraints and an optimization vector length of $2MN + 2N + M + 1$.

3.5 Time-varying System Controllers for Disturbance Rejection and Offset-Free Control

Traditional MPC controllers tend to break down in the presence of large plant model mismatch as well as when significant unmeasured disturbances are introduced into the plant process. These can produce large offsets between the actual process variables and the setpoint. This section explores a few potential methods for dealing with these scenarios.

3.5.1 ZMPC with Internal Model Control and Integrator

The first such method is a simple version of offset-free MPC (D. Seborg *et al.*, 2011). The aim of this controller was to explore a way to deal with plant-model mismatch as well as any unmodeled disturbances. It is already known that most patients' health will deteriorate slowly overtime, similar to the introduction of a slow continuous ramp disturbance. The idea behind this MPC algorithm is to calculate the 1-step error between the ARX model and the actual measurement and adjust the reference targets for the zone boundaries to reflect the estimate for the estimated steady state offset (alternatively one could include the disturbance estimate $\hat{D}_k$ in the model instead of adjusting the targets). Offset-Free MPC algorithms similar to this have been shown to work well for constant steady state disturbances (G. Pannocchia, 2003). This method can be expressed in the following equations in terms of deviation variables. The ARX model is in the form

$$\hat{y}_k = a_1 y_{k-1} + \sum_{i=1}^{20} b_i u_{k-i} + \hat{D}_{k-1} \tag{3.42}$$

and gives a 1-step ahead estimate of the system when using the past data on and before time $k-1$.

$$\hat{d}_k = y_k - \hat{y}_k \tag{3.43}$$

gives an estimate for the 1-step residual at time k. This residual is multiplied by a filter value, K, and added to the summation of the previous time step estimate for d_k. Equation 3.5.1 represents the total integrated output 1-step error.

$$\hat{D}_k = \sum_{1}^{k} K \hat{d}_k \tag{3.44}$$

The model inside the controller remains static, but the targets of the MPC routine are adjusted to reflect the steady state offset estimate. This is represented by

$$y_{L,new} = y_L - \hat{D}_k \tag{3.45a}$$

$$y_{H,new} = y_H - \hat{D}_k \tag{3.45b}$$

A block diagram of the simulation setup is shown in Figure 3.8. The DDE solver along with a random additive disturbance is used as the patient simulator. The DDE solver is in continuous time and sampled weekly, while the designed control system is in discrete time with a sampling interval equal to the hemoglobin sampling rate. In cases of constant steady state offset, this algorithm will capture the full offset over time.

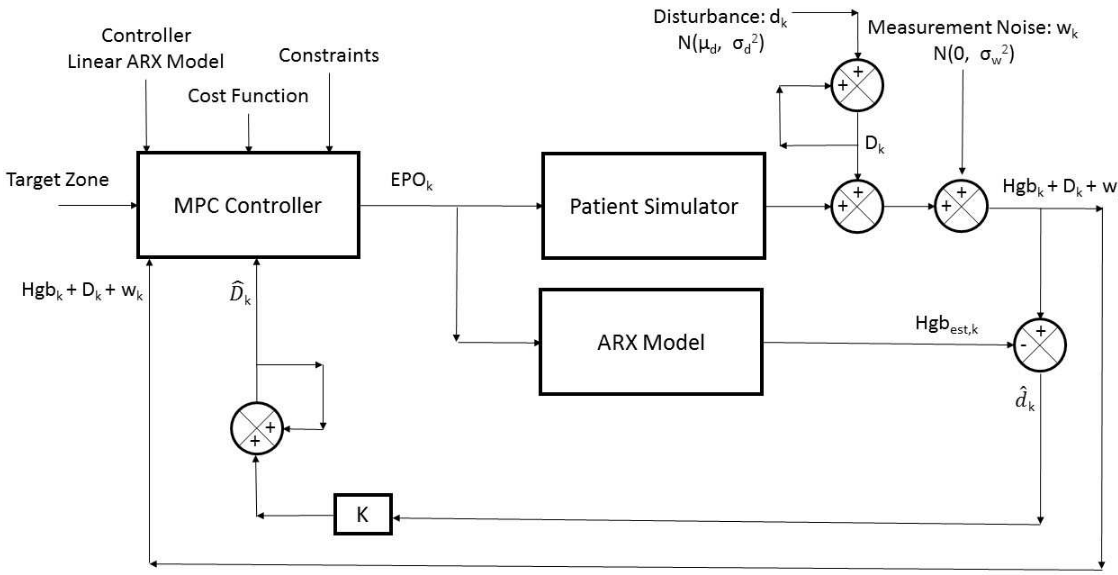

Figure 3.8: Block Diagram of the MPC and IMC algorithm with a filtered integrator when simulated using a disturbance variable and measurement noise

Figure 3.9 shows a 500 week simulation where an additive noise disturbance accumulates a negative sum in the first 250 weeks and then switches to accumulating a positive sum in the last 250 weeks. The filter value K is equal to 0.2, 0.5 and 0.8 in these simulations. The low filter value helps to reject any acute disturbances and zero mean measurement noise but still captures the long-term disturbance dynamics. As the filter value increases, the input response becomes much noiser, and the gains in state management are minimal. The shortcomings of this configuration can be seen in this figure. In cases of steady ramp disturbances such as the simulation in Figure 3.9, this algorithm will often lag behind the actual disturbance, as can be seen in the middle of the simulation where the system settles on or below the control zone limit. This lag presents a large problem for the time-varying nature of the steady state EPO dose. It is likely that the steady state dose may oscillate up and down over the course of the patient's life. The IMC configuration works well for steady state offset, but fails to provide adequate control when the steady-state dose changes quickly. For this reason, the IMC configuration was not explored further in the following chapters.

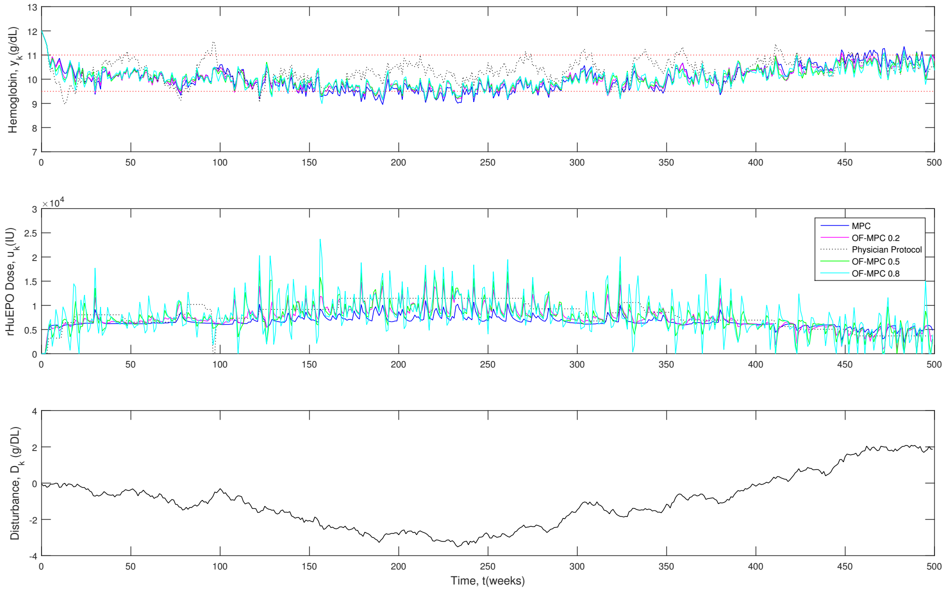

Figure 3.9: Comparison of different filter values with an Offset-Free MPC controller versus a classical MPC controller for a single patient when trying to control the PK/PD model with uncertainties

3.5.2 ZMPC with Recursive Modeling

To overcome the dynamic nature of a patients' health over time, this algorithm recursively estimates a new constrained ARX model at each specified time instant. This method relies on the fixed structure of the C-ARX models to ensure that the model attained at each time step is open-loop stable and representative of a physiologically acceptable model (K. Turksoy *et al.*, 2014). The estimation phase uses a moving window of historical data that is 50 data points in length. A longer window is typically better for model estimation, but patient health may change over time, making the initial data counter-productive in estimating a present time model. If too little data is used, it is difficult mathematically to find a proper solution, given the large number of degrees of freedom in the model. A block diagram of the simulation is shown in Figure 3.10 . The controller model, steady states, and constraints must be updated after each new model is obtained.

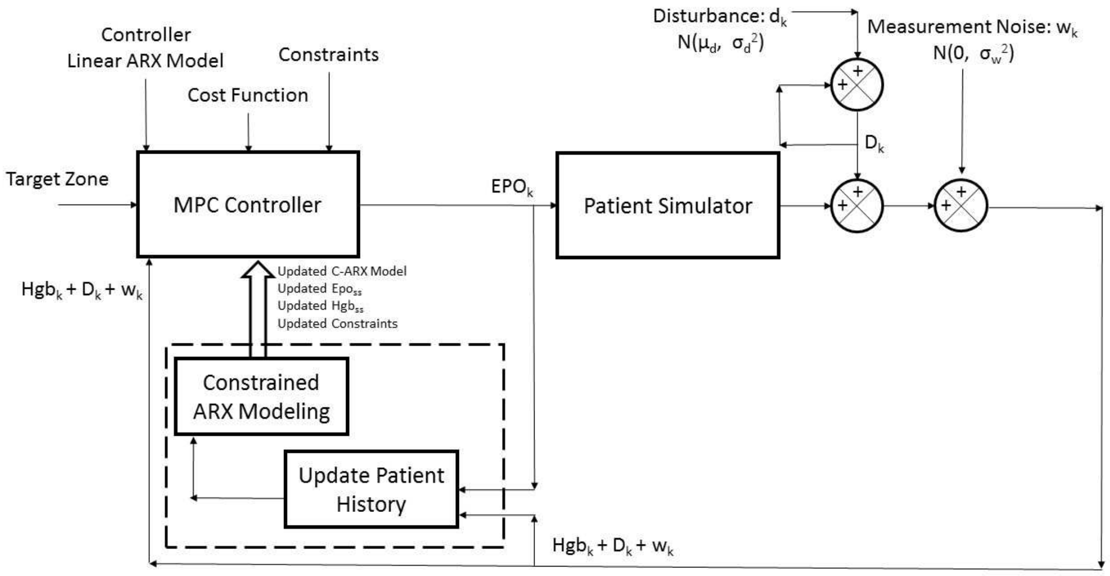

Figure 3.10: Block Diagram of the MPC algorithm with recursive modeling when simulated using disturbance and measurement noise

Figure 3.11 shows a comparison of the response of the recursive ZMPC controller to that of the IMC-MPC configuration discussed previously. Recursively estimating the patient model can help to overcome the time-varying nature of the patient model.

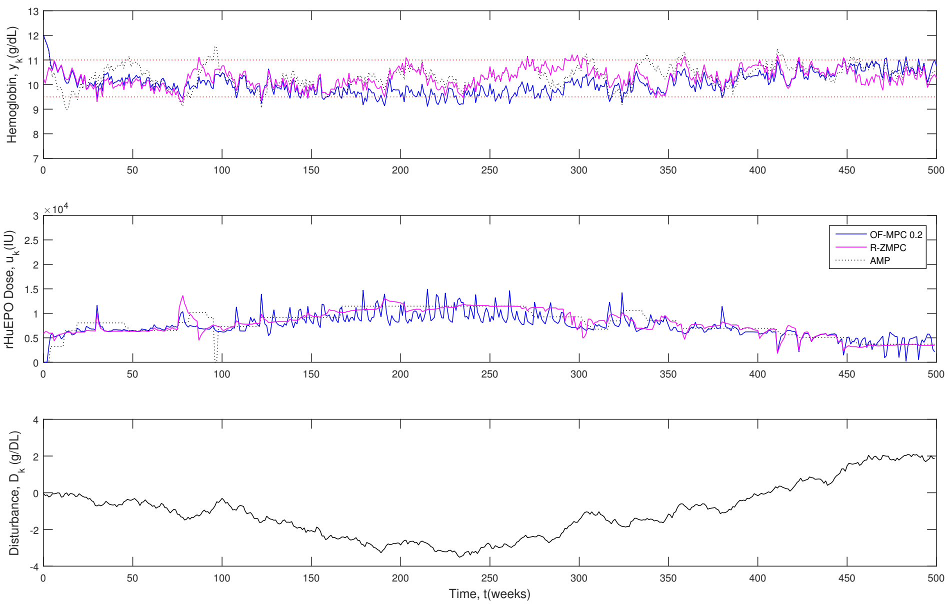

Figure 3.11: Comparison of Recursive ZMPC and the IMC-MPC configuration for a single patient when trying to control the PK/PD model with uncertainties

3.5.3 Digital PID Control

Another appropriate method for control is to use a Digital PID controller. PID control is a very mature technology and used widely across many industries. PID controllers have the advantage of being able to be tuned for disturbance rejection which may offer improved state management in scenarios where the patient model is time-varying. PID controllers have been used successfully in the control of Type 1 Diabetes and the first FDA approved automatic insulin pump (Medtronic's Minimed 670G, approved by FDA Sept 28, 2016) is equipped with PID control (S. Trevitt and Wood, 2016). PID controllers typically perform quite well for SISO systems, if designed and tuned properly (O'Dwyer, 2006).

To design the PID controllers, a First Order Plus Deadtime (FOPDT) transfer function estimate for the patient model is first needed. Due to health consequences and liabilities, it is not feasible to perform step tests on the patients in practice. One method to derive a FOPDT model is to first estimate a Constrained ARX model, and subsequently perform a step test on the attained model. The steady state values from the C-ARX model identification will be used for the FOPDT model. The dosing levels are chosen appropriately to center the step response over the control zone, having the initial hemoglobin approximately equal to 9.5 and the final hemoglobin appropriately equal to 11 g/dL. In order to identify the FOPDT model automatically, the dosing levels are chosen automatically through the use of a simple Interval Halving Optimization Method. The deadtime (θ) for each system will be assumed to be 2 weeks to avoid having to get the tangent line to the curve in the transfer function estimate. Using linear interpolation between the simulated data points, and the beginning and final simulated measurements, a FOPDT model can be easily attained automatically using the a graphical method outlined in Figure 3.12.

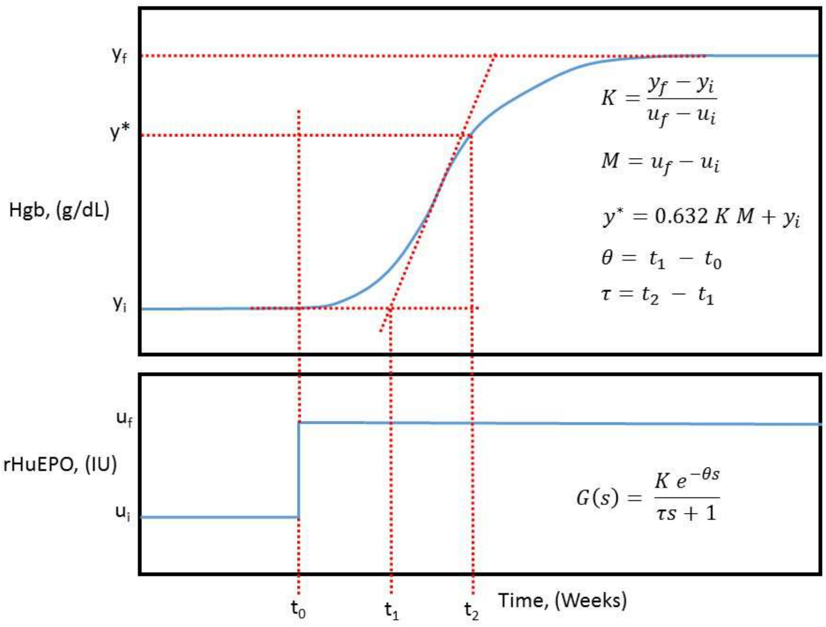

Figure 3.12: Graphical Approach to estimating a First Order plus Deadtime transfer function that is used to attain continuous time transfer functions for PID controller design

As a starting point for the PID controller (parallel form), IMC-based PID controller settings were selected from the works of Chien and Fruehauf (D. Seborg *et al.*, 2011). Due to the large amount of uncertainty in the process model and disturbances, it is desired to make the controller more robust. This can be accomplished by reducing the controller gain (K_c) and increasing the integral time constant (τ_I) (D. Seborg *et al.*, 2011). The reduction factor for K_c was determined empirically through simulation tests and found to be approximately 0.3. τ_I was increased by a factor of 35, which was also determined empirically. τ_D remains the same.

The continuous time PID controller is then converted to a discretized version using a sampling time of 1 week (T_s). Continuous time transfer functions can be discretized using finite difference methods (FDM). One such form for discretizing the PID controller is represented in Equation 3.46 (V. Bobal *et al.*, 2005).

$$\frac{U(z)}{E(z)} = \frac{(K_c + \tau_I \frac{T_s}{2} + \frac{\tau_D}{T_s})z^2 + (-K_c + \tau_I \frac{T_s}{2} - \frac{2\tau_D}{T_s})z + \frac{\tau_D}{T_s}}{z^2 - z} \tag{3.46}$$

which can be rearranged into the discrete time domain to attain the following equation for the next time instants' input. The continuous time PID parameters and sampling time (in weeks) are substituted into the equation.

$$u(k) = u(k-1)+(K_c+\tau_I\frac{T_s}{2}+\frac{\tau_D}{T_s})e(k)+(-K_c+\tau_I\frac{T_s}{2}-\frac{2\tau_D}{T_s})e(k-1)+\frac{\tau_D}{T_s}e(k-2) \quad (3.47)$$

3.6 Conclusion

Several model based predictive controllers were designed and discussed in this chapter. Two main classifications of controllers were explored, deterministic and stochastic. Deterministic controllers do not take into account the possible uncertainty in the measurements and process noise. The stochastic controllers are able to take into account these uncertainties and should be more effective than their deterministic counterparts when the uncertainty distributions are known. The stochastic controllers introduced here however, do not take into account parameter uncertainty. It is possible that plant model mismatch may adversely affect these controller types.

Three methods for dealing with the Time-varying nature of the models were presented. These included the internal model control based MPC, Recursive MPC and Digital PID controller methods. The IMC based MPC will not be explored further due to its inability to provide good control for ramp disturbances. The PID controller and the recursive ZMPC algorithm will be tested rigorously, under different simulation scenarios in Chapter 4.

Chapter 4

Simulation Results and Discussion

4.1 Introduction

This Chapter focuses on many aspects of the controller simulation results. The first section uses the C-ARX models within the MPC controllers, and performs several test scenarios to determine the effectiveness of the MPC controllers against one another as well as against the current anemia management protocol obtained from an actual hemodialysis unit from a hospital.

The first set of simulations will focus on the controller algorithms. The ARX models will be used in the both the controller and as the patient simulator. The tuning parameters for each controller will first be discussed. The controllers will be tested using different types of disturbances and process noise. These tests represent the nominal case and will provide good results to eliminate some of the less effective controllers designed in Chapter 3.

The last section includes simulation results which represent a more realistic test scenario, where the controllers are used to control the PK/PD model as it is subjected to process noise and disturbances. These simulations use a designed patient simulator which includes measurement noise, integrating process disturbance noise as well as random acute disturbances. The random integrating disturbance causes the average patient dose to drift away from its original value. The random acute disturbances simulate infections and blood loss which are common to CKD patients. To overcome the time-varying nature of the patient simulator, recursive modeling will be used. The chapter will conclude with the final recommendation for the control system.

4.2 Simulation Results using Identified ARX Models to Simulate Patients

4.2.1 MPC Tuning

The tuning parameters for an MPC controller are often difficult to choose. It is typically necessary to strike a balance between them, which is often found empirically through testing in simulations. Some guidelines do exist for tuning parameters in general (J. Garriga, 2010). The difficulty with this particular case, is that each patient is different, and hence follows a different system model. It would be very difficult to tune a controller that has performance tied closely to the correct tuning parameters for each patient. This is one of the advantages of the Zone MPC formulation presented, it is not overly sensitive to tuning parameters. The tuning parameter for the states (Q) are typically set much higher than the tuning parameter for the change in input term (R). This allows the controller to have a primary objective, which is to regulate the hemoglobin into the zone, as well as a secondary objective, which is to keep the same dose as long as the hemoglobin will stay within the control zone. In nearly all of the proposed cases, the tuning parameter Q will be set much higher than that of R. The classical MPC controller will have $Q = 500$ and $R = 1$ chosen for its tuning parameters.

Due to the complexities apparent in the design of the stochastic controllers, it is worth mentioning some of the other tuning parameters in more detail.

ZMPC

Zone MPC will be used in multiple configurations. For comparison purposes, a ZMPC controller with static boundaries equal to the target will be used. Another configuration of the ZMPC controller will use decaying constraints on the δ_k slack variable. The final tuning parameters for these two controllers are outlined in Table 4.1. An example simulation is shown in Figure 4.1.

Tuning Parameter	static	funnel
Q	500	500
R	1	1
y_L (δ_k constraint)	9.5 g/dL	9.75 g/dL
y_H (δ_k constraint)	11 g/dL	10.75 g/dL
y_L (target)	9.5 g/dL	9.5 g/dL
y_H (target)	11 g/dL	11 g/dL
p, (y_L decay ratio on δ_k constraint)	0	0.6
p, (y_H decay ratio on δ_k constraint)	0	0.6

Table 4.1: Final tuning settings for the ZMPC controllers that will be tested

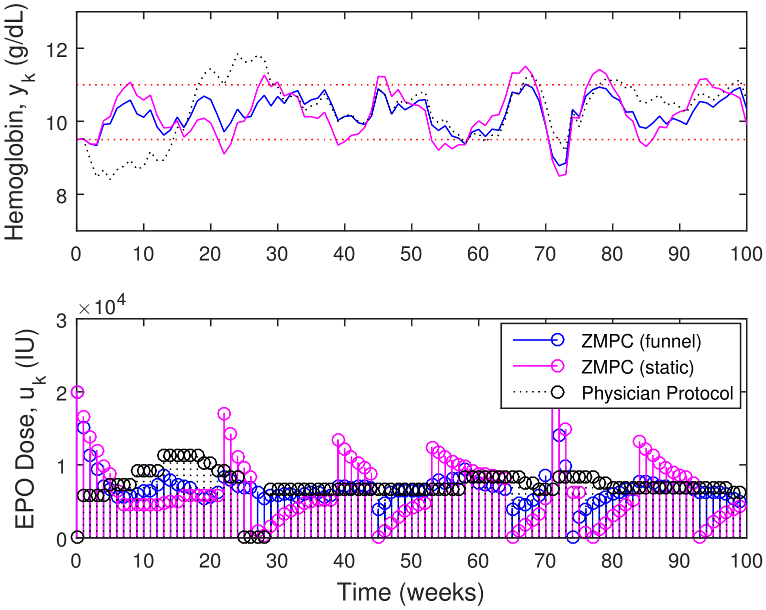

Figure 4.1: Example simulation comparing ZMPC with static boundaries and decaying boundaries on the δ_k constraints

ZMPC Hybrid with 1 CVaR Constraint

The first controller discussed here is the ZMPC controller with CVaR constraints. This controller requires an estimate for the process noise distribution to draw random samples from, for the scenarios. It also requires tuning parameters Q and R, along with control zone boundaries for the constraints, as well as control zone boundaries for δ_k. The number of scenarios M and the CVaR constraint violation probability ϵ is also needed. It should be noted that the CVaR constraints cannot be combined with a ZMPC controller that has a control boundary larger than what the CVaR constraints will typically be solved as, because this eliminates the state term in the cost function. The CVaR constraint will be added for y_{k+3} and use the target bounds for the upper and lower limit. A constraint on y_{k+2} is also avoided because the solution to the optimization problem is typically very aggressive in trying to reach the target zone in a single move if the current state starts outside of the desired control region.

Without delving into specifics, Figure 4.2 shows a simulation figure that compares classical MPC directly to classical MPC using the CVaR constraint. In this simulation, the tuning parameter Q is set too low, but it allows the effect of the CVaR constraints to be demonstrated. The figure clearly shows that the addition of the CVaR constraint greatly improves the performance as compared to the controller without the CVaR constraints.

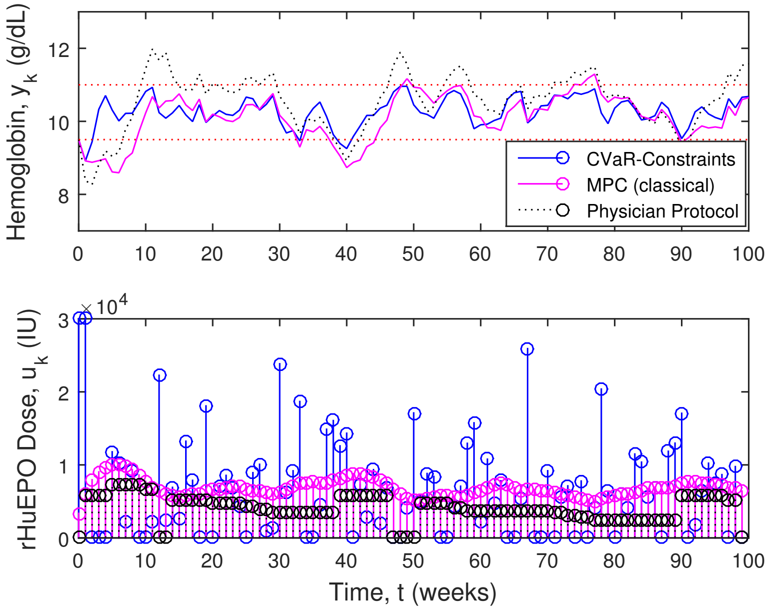

Figure 4.2: Example simulation showcasing the ability of CVaR constraints to regulate the zone boundary

Figure 4.3 shows an example simulation where the tuning parameter Q is set much higher to align with the previously stated guidelines of having a primary and secondary objective, to avoid patient specific tuning. It can be seen that the effect of the CVaR constraint is small, but it does offer an improvement in performance for this case. For this short simulation, the percent of points within the zone was 90.6% compared to 88.8% for MPC with CVaR constraints, and classical MPC, respectively.

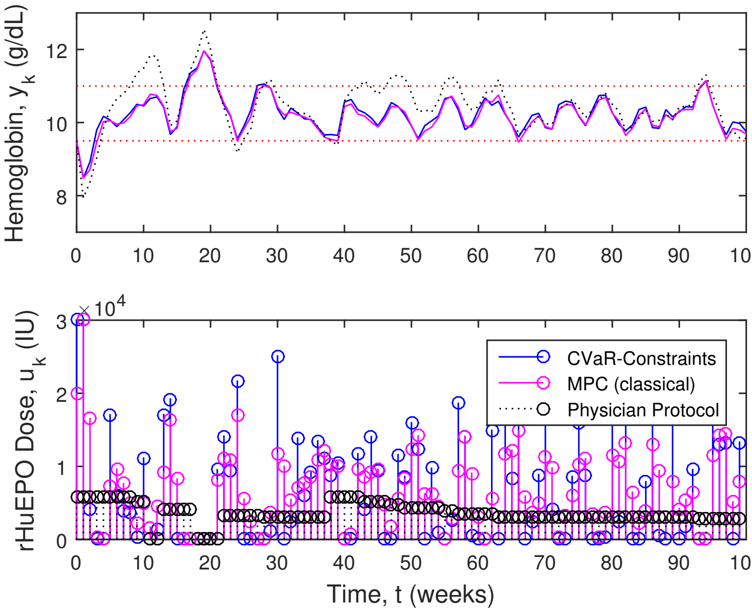

Figure 4.3: Example simulation showcasing that if Q is set too high, the CVaR constraints have little impact on the solution

The final controller to be tested will be a ZMPC controller with 1 CVaR constraint. The constraints on δ_k will also be reduced to 10.15 to 10.45 g/dL. This will allow a small penalty-free zone in the center of the actual control zone to try and reduce control input chatter, while still allowing the CVaR constraints to do their proposed purpose. Figure 4.4 shows an example simulation as compared to a classical MPC controller. The final parameter settings for the controller are shown in Table 4.2. ϵ is set relatively high in order to facilitate the feasibility of the optimization problem. Due to the conservativeness of the CVaR constraints, if ϵ is set too low, the upper and lower bound constraints will overlap and the problem will become infeasible. With such a tight boundary of control, this becomes a severe problem for this controller. The control region tested in this section is from 9.5 to 11.0 g/dL. This is a very tight range for CVaR approximations. Not shown here, but simulations were performed with zone boundaries of 9.5 - 12.0 g/dL and ϵ equal to 0.05 and this eliminates most of the in-feasibility issues encountered with the smaller control zone. ϵ can be also be tuned to the choice of $\sigma^2_{S_k}$. The larger the value used, the larger ϵ will have to be to facilitate feasibility. The number of infeasible optimization solutions will be tracked during the simulations.

Tuning Parameter	Value
Q	100
R	1
y_L (δ_k constraint)	10.05 g/dL
y_H (δ_k constraint)	10.45 g/dL
y_L (target)	9.5 g/dL
y_H (target)	11 g/dL
M	100
ϵ	0.25
$\bar{S}_k$	*
$\sigma^2_{S_k}$	*

Table 4.2: Final tuning settings for the ZMPC-CVaR (constraint) controller that will be tested.

*note the mean and variance of the random distribution will be set during specific simulation tests

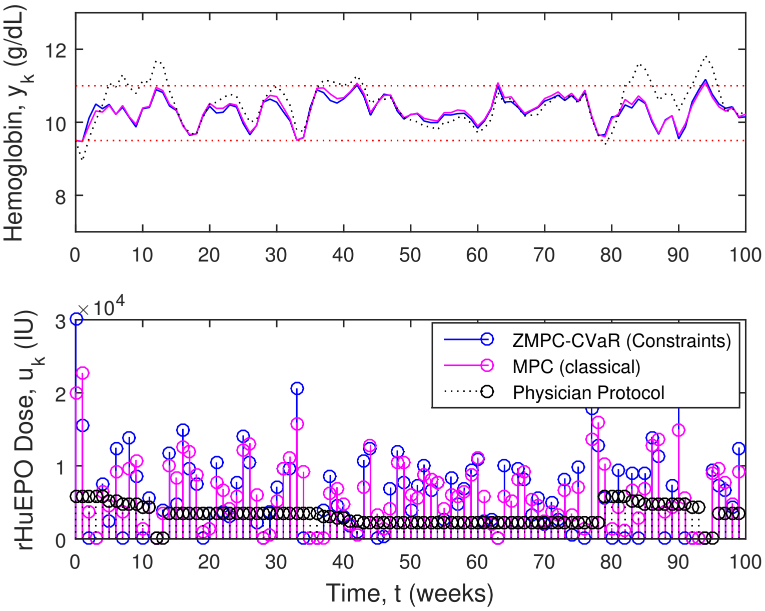

Figure 4.4: Example simulation using the final controller tuning settings for the ZMPC-CVaR (constraints) controller to be tested as compared to classical MPC

ZMPC with 1 Soft CVaR Constraint

This controller is exactly the same as the previous controller using a CVaR constraint on time instant y_{k+3}, but instead of using a backup controller in the event of in-feasibility, an additional slack variable will be used to loosen the constraints to make the problem feasible when necessary. The slack variable will then be penalized heavily in the cost function. Figure 4.5 shows an example simulation of this controller compared to a ZMPC controller with static bounds on δ_k. The table of final tuning parameters for this controller is shown in Table 4.3. The control zone for the controller will be a small region in the center of the actual target hemoglobin.

Tuning Parameter	Value
Q	100
R	1
ξ_P	10^7
y_L (δ_k constraint)	10.05 g/dL
y_H (δ_k constraint)	10.45 g/dL
y_L (target)	9.5 g/dL
y_H (target)	11 g/dL
M	100
ϵ	0.05
ΔU_{max}	20 000 IU
$\bar{S}_k$	*
$\sigma^2_{S_k}$	*

Table 4.3: Final tuning settings for the ZMPC-CVaR (Soft Constraint) controller that will be tested.

*note the mean and variance of the random distribution will be set during specific simulation tests

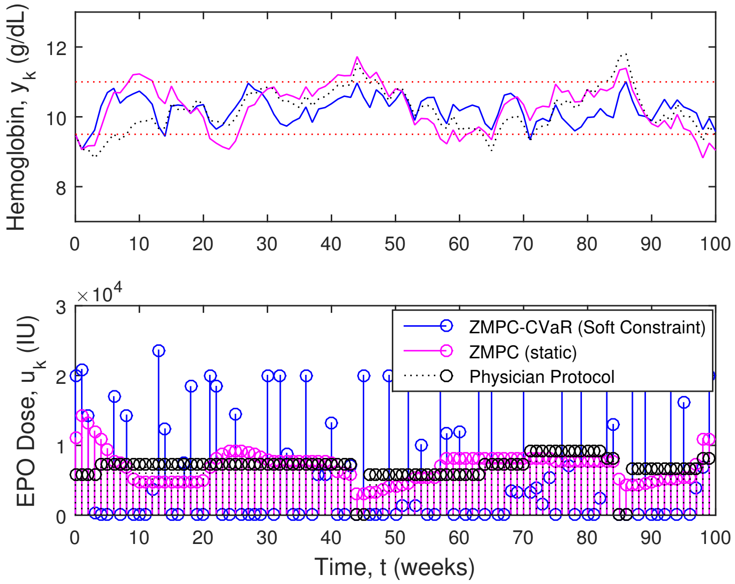

Figure 4.5: Example simulation using the final controller tuning settings for the ZMPC-CVaR (Soft Constraint) controller to be tested as compared to ZMPC with static boundaries

ZMPC with CVaR in the Cost Function

This controller, unlike it's CVaR constraint counterpart, is always feasible. It is not necessary to use a backup controller. This controller is still a scenario-based controller and uses the linear program over the quadratic program due to its large number of constraints. An example simulation of the ZMPC-CVaR (Cost) controller as compared to a ZMPC controller is shown in Figure 4.6. Here both zone boundary conditions on δ_k are equal to the target zone of 9.5-11 g/dL. The ZMPC-CVaR (Cost) controller regulates the points in the zone at an accuracy of 93.0%, compared to that of the ZMPC controller with 72.2%. One thing to note is the aggressiveness of the controller. This controller exhibits the largest average changes in the input out of all the controllers discussed. For this reason, a constraint on ΔU_k is also used to cap the changes to a max of 20000 IU.

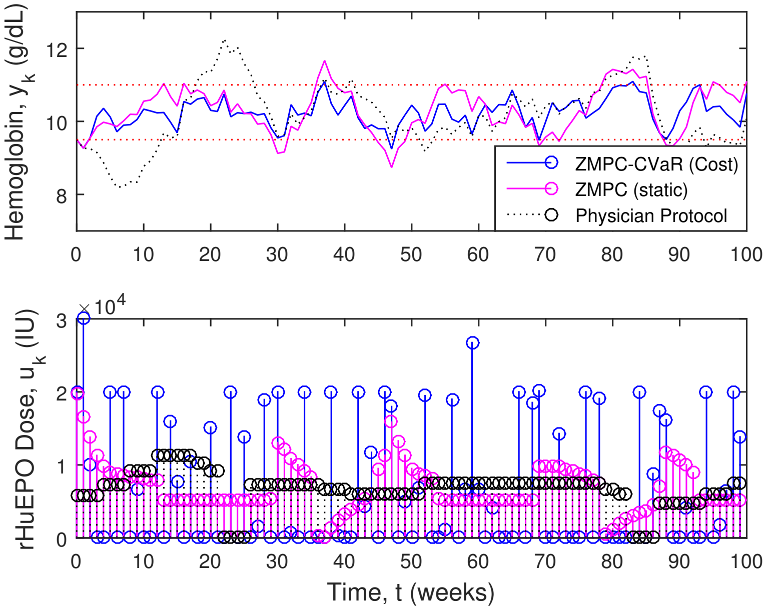

Figure 4.6: Example simulation using the final controller tuning settings for the ZMPC-CVaR (Cost) controller to be tested as compared to ZMPC with static boundaries

The final tuning parameters for this controller are outlined in Table 4.4.

Tuning Parameter	Value
Q	100
R	1
y_L (δ_k constraint)	10.05 g/dL
y_H (δ_k constraint)	10.45 g/dL
y_L (target)	9.5 g/dL
y_H (target)	11 g/dL
M	200
β	0.99
ΔU_{max}	20 000 IU
$\bar{S}_k$	*
$\sigma^2_{S_k}$	*

Table 4.4: Final tuning settings for the ZMPC-CVaR (cost) controller that will be tested. *note the mean and variance of the random distribution will be set during specific simulation tests

ZMPC Hybrid with 7 Hard Chance Constraints

This controller will use the standard ZMPC controller formulation with the addition of 7 chance constraints on y_{k+2} to y_{k+8} using the target limits for the boundaries. There was no chance constraint placed on y_{k+1} as it cannot be affected by u_k. Due to the nature of the hard constraints, a backup classical MPC controller will be used in case the optimization problem becomes infeasible. Figure 4.7 shows the controller as compared to a ZMPC controller with again the same boundaries used on δ_k that are equal to the target zone of 9.5 to 11.0 g/dL.

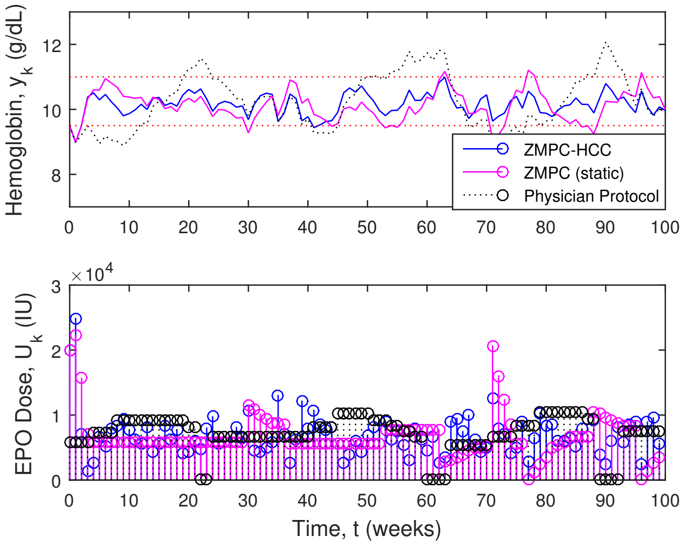

Figure 4.7: Example simulation using the final controller tuning settings for the ZMPC-HCC (7) to be tested as compared to ZMPC with static boundaries

For the final tuning parameters, the constraints on y_L and y_H will decrease exponentially to create a funnel. Figure 4.8 shows an example of the δ_k constraints and chance constraints visually.

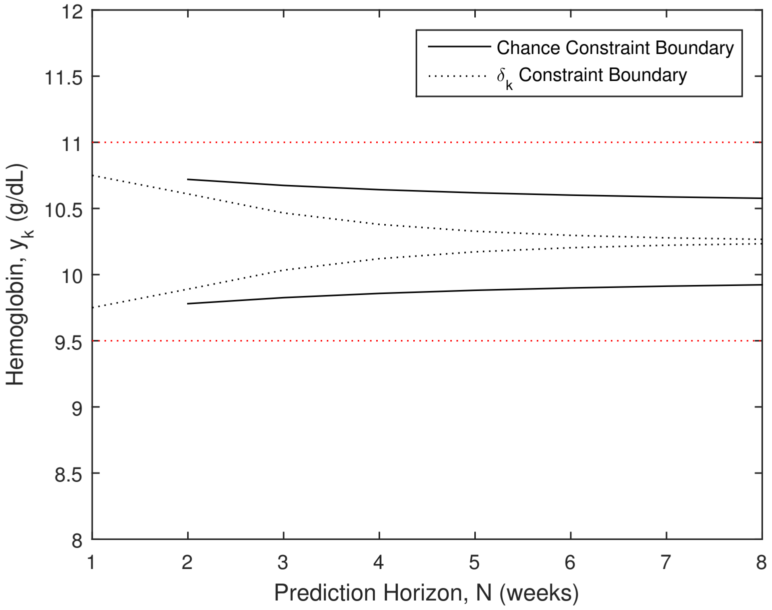

Figure 4.8: Example simulation using the final controller tuning settings for the ZMPC-HCC (7) to be tested as compared to ZMPC with static boundaries

The final tuning parameters that will be used for this controller are outlined in Table 4.5. The constraints on δ_k will decay back towards the center of the zone at the ratio specified.

Tuning Parameter	Value
Q	500
R	1
y_L (δ_k constraint)	9.75 g/dL
y_H (δ_k constraint)	10.75 g/dL
y_L decay ratio (δ_k constraint)	0.6^k g/dL
y_H decay ratio (δ_k constraint)	0.6^k g/dL
y_L (target)	9.5 g/dL
y_H (target)	11 g/dL
ϵ	0.01
$\bar{S}_k$	*
$\sigma^2_{S_k}$	*

Table 4.5: Final tuning settings for the ZMPC-HCC (7) controller that will be tested. *note the mean and variance of the random distribution will be set during specific simulation tests

ZMPC with 7 Soft Chance Constraints

This controller will use the standard ZMPC controller formulation with the addition of 7 soft chance constraints on y_{k+2} to y_{k+8}. There was no chance constraint placed on y_{k+1} as it cannot be affected by u_k. Figure 4.9 shows the controller as compared to a ZMPC controller with again the same boundaries used on δ_k that are equal to the target zone of 9.5 to 11.0 g/dL.

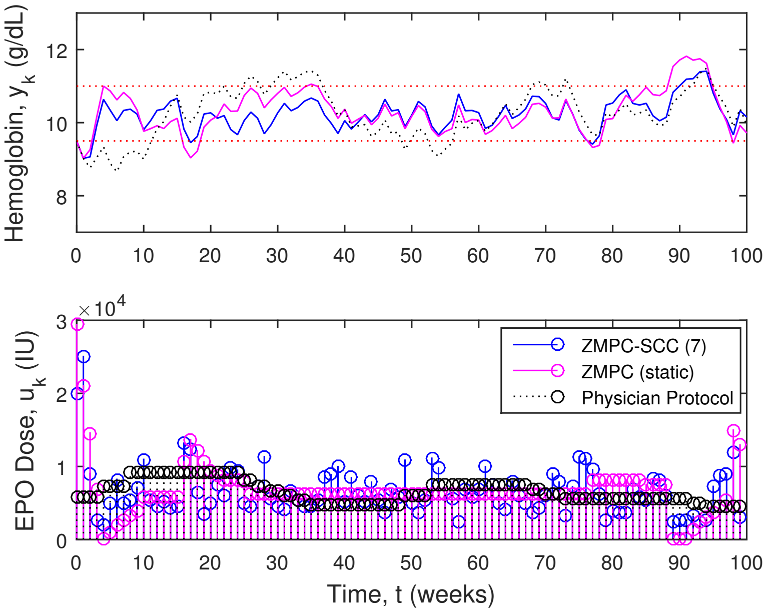

Figure 4.9: Example simulation using the final controller tuning settings for the ZMPC-SCC (7) to be tested as compared to ZMPC with static boundaries

For the final tuning parameters, the constraints using y_L and y_H will decrease exponentially to create a funnel similar to the hard chance constraint version. The final tuning parameters that will be used for this controller are outlined in Table 4.6. The constraints on δ_k will decay back towards the center of the zone at the ratio specified.

Tuning Parameter	Value
Q	500
R	1
ξ_P	10^9
y_L (δ_k constraint)	9.75 g/dL
y_H (δ_k constraint)	10.75 g/dL
y_L decay ratio (δ_k constraint)	0.6^k g/dL
y_H decay ratio (δ_k constraint)	0.6^k g/dL
y_L (target)	9.5 g/dL
y_H (target)	11 g/dL
ϵ	0.01
$\bar{S}_k$	*
$\sigma^2_{S_k}$	*

Table 4.6: Final tuning settings for the ZMPC-SCC (7) controller that will be tested. *note the mean and variance of the random distribution will be set during specific simulation tests

4.2.2 Additive Process Noise Simulation Results

The first test used to assess the different controllers' performance was a simulation using the Constrained ARX models within the controller, as well as for the patient. The Constrained ARX models were the nonlinear version estimated using an NLP solver. This represents the nominal case, with perfect modeling. A block diagram of the simulations in shown in Figure 4.10.

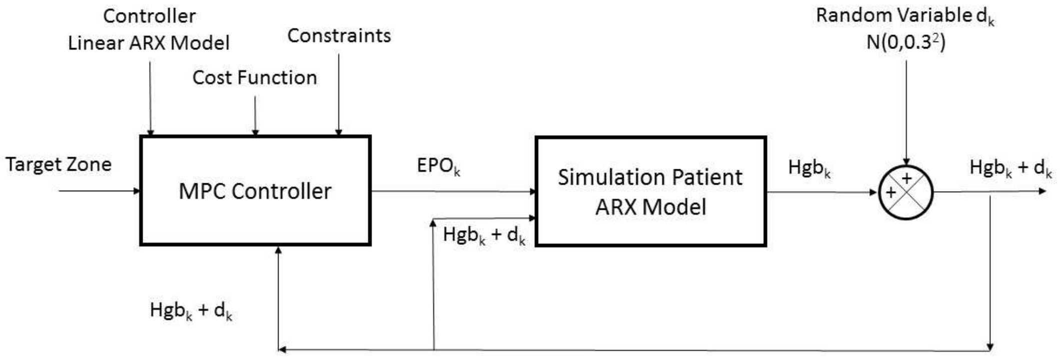

Figure 4.10: Block Diagram of the MPC controller test simulations using an ARX model as the patient simulator

These results are shown in Table 4.7. The additive process noise was drawn from a distribution of $s_k = N(0, 0.3^2)$ and added to the system output after each week of simulation. In practical applications, the hemoglobin value is not expected to change more than 5% between actual hemoglobin measurements (1 week intervals), making this noise distribution near the worst case scenario. Simulations were performed across all 167 patient models for 500 weeks. Due to some of the patient models not being acceptable, the results were filtered. The models were estimated using Matlab's fmincon function and there are no guarantees that a global minimum solution has been found. There are also no guarantees that each patient's data was acceptable to estimate a model. Many of the patients are also healthy enough to not receive epoetin-alfa for many weeks, which could result in a bad model. The results were filtered by removing all the simulations for every patient that scored less than 50% of the points within the zone for at least one of the controllers or the physician's protocol. Filtering with this criteria, the statistics in the table include 132 of the 167 patients. This aids in excluding models that do not behave like actual patients, and can skew the results, especially in the physician protocol statistics. Another item to note, is that the stochastic controllers were given the exact distribution of additive noise, which may not be realistic in actual practice.

Performance Statistic	MPC class.	ZMPC static	ZMPC funnel	ZMPC SCC (7)	ZMPC HCC (7)	ZMPC H-CVaR (1)	ZMPC S-CVaR (1)	ZMPC CVaR (cost)	AMP
Integrated y_k Err.	0.136	0.314	0.186	0.141	0.142	0.164	0.162	0.194	0.486
% of Points in Zone	92.0	82.5	89.1	91.6	91.4	90.5	90.3	89.5	76.1
U_k Total $(\frac{IU}{1000})$	4724	4714	4699	4708	4690	4754	4738	4782	4909
Avg. Weekly U_k	9448.7	9428	9398	9416	9380	9509	9476	9564	9817
Avg. ΔU_k	4684	423	487	3178	2424	4609	7751	8165	344

Table 4.7: Simulation Results for the various ZMPC controllers as compared to the physician's protocol for the additive process noise test scenario

There are many observations that can be concluded within these simulation results. One of the first things to note, is that the average change in the input is extremely conservative for the physician's protocol. This is due to the protocol not allowing the change of inputs very often. Usually the dose is changed, and then not allowed to be changed again for 2-4 weeks. The model based controllers will likely change the dose often as they respond to disturbances and process noise.

The first controller to be discussed is the classical MPC controller. The classical MPC controller is seen to have the highest accuracy in state control. With the tuning parameter, Q, set abnormally high, this result makes sense. The classical controller does however suffer by having very high average drug use, along with very high average Δu_k as compared to the other controllers. The state performance of this controller could be considered close to the upper limit that any of the controllers could achieve within the problem constraints.

The ZMPC controller with static boundaries on the slack variable, δ_k, performs better but quite similar to the Physician Protocol in all categories. It has small improvements in all categories reducing the Integrated Output Error by 35.5% and the total drug use by 4.0%. The percent of points was 8.4% higher and this comes at a cost of increasing the average change in input by only 23.0%. However, this controller remains the most sluggish controller, of all the model based controllers tested, due to the large control zone. Zone MPC typically lags in state performance with regards to setpoint based MPC controllers (B. Grosman *et al.*, 2010), but its benefits come in the form of a more clinically acceptable and safer controller due to the more constant drug doses.

The ZMPC controller with funnel constraints on the slack variable, δ_k, performs much better than the ZMPC controller in terms of state control and total drug use. Adding the funnel constraint offers large improvements over static boundaries. As compared to the physician's protocol, it offers improvements in every category except increasing the average weekly change in dose by only 41.6%, which is still minimal compared to the other controllers. The funnel control zone allows the weak tracking of a setpoint, while also retaining some of the features of the Zone MPC algorithm with the static control zone boundaries.

The two ZMPC controllers using the chance constraints converted to hard constraints assuming Gaussian uncertainty perform similar to each other. These controllers use chance constraints on the upper and lower zone boundary for $k + 2$ to $k + 8$. ZMPC HCC (7) is the hybrid controller that uses classical MPC in the event of infeasibility. The HCC version of the controller becomes infeasible around 2% of the time. ZMPC SCC (7), relaxes the constraints until they are feasible, with these relaxation variables being penalized heavily in the cost function. These controllers also use the same funnel constraints as the ZMPC funnel controller. Both of these controllers offer improvements in state control over the ZMPC funnel controller, with similar total drug use, however they do so at a large increase in the average change in input. As compared to the ZMPC funnel controller, the difference is an increase of 553% and 398% for the HCC and SCC controllers, respectively. The aggressive change in the inputs may be an undesirable feature of these controllers, for a small gain in state performance.

The CVaR constraint controllers offer a similar performance to the other chance constrained MPC controllers. The feasibility of the CVaR constraints is extremely low due to the conservativeness of the CVaR constraints. The zone boundaries of the CVaR constraints tend to overlap very easily. Even with the probability of violation set to 25%, the constraints are not feasible around 8% of the time.

The controller with CVaR in the cost function has good state performance but its average change in u_k is the highest of all the controllers which makes this controller type a poor choice for this application. I speculate that this controller performs poorly due to the tight boundaries in this case. Previous tests of this controller using a larger control zone for a CSTR produced very good results, which is not apparent in these simulations.

4.2.3 Disturbance Rejection

Another necessary test for the controllers is to measure how well they respond to disturbances. Several different major disturbances can be detected within the data. Examples of these disturbances, are slow deterioration in patient health (negative ramp disturbance), acute blood loss (negative step disturbance), and blood transfusions (positive step disturbance). The controllers will be tested under these conditions by overlaying a disturbance vector on top of additive process noise. A disturbance will be introduced approximately every 50 weeks. An example of the nominal case is shown in Figure 4.11. Here there are several step and ramp disturbances added to the system. At weeks 50, 100 ,150 and 200, negative step disturbances are introduced of magnitude -1 (g/dL), -2(g/dL), -3(g/dL) and -4(g/dL). At weeks 250-255, 300-305 and 305-310 there are ramp disturbances introduced at -0.5 (g/dL)/week, -0.75(g/dL)/week and 0.5(g/dL)/week, respectively. At times 350, 400 and 450, there are positive step disturbances introduced of magnitude 2, 3 and 1 (g/dL), respectively.

From weeks 450-500, there exists a negative ramp disturbance of -0.1 (g/dL)/week. It is interesting to note that the physician's protocol can induce an oscillatory behavior in the output. The hemoglobin control of the physician's protocol is not very good and results in a lot of hemoglobin values over the 11.0 g/dL zone target. Hemoglobin values above the upper limit of the target zone are undesirable and result in the use of excess epoetin-alfa, which has economic consequences. The disturbances here are also well spread out in time with almost a year in between the disturbances. Patients may undergo more disturbances within a shorter time limit, which could further impact control. The MPC algorithms are easily able to deal with these acute disturbances and return the hemoglobin to the target zone.

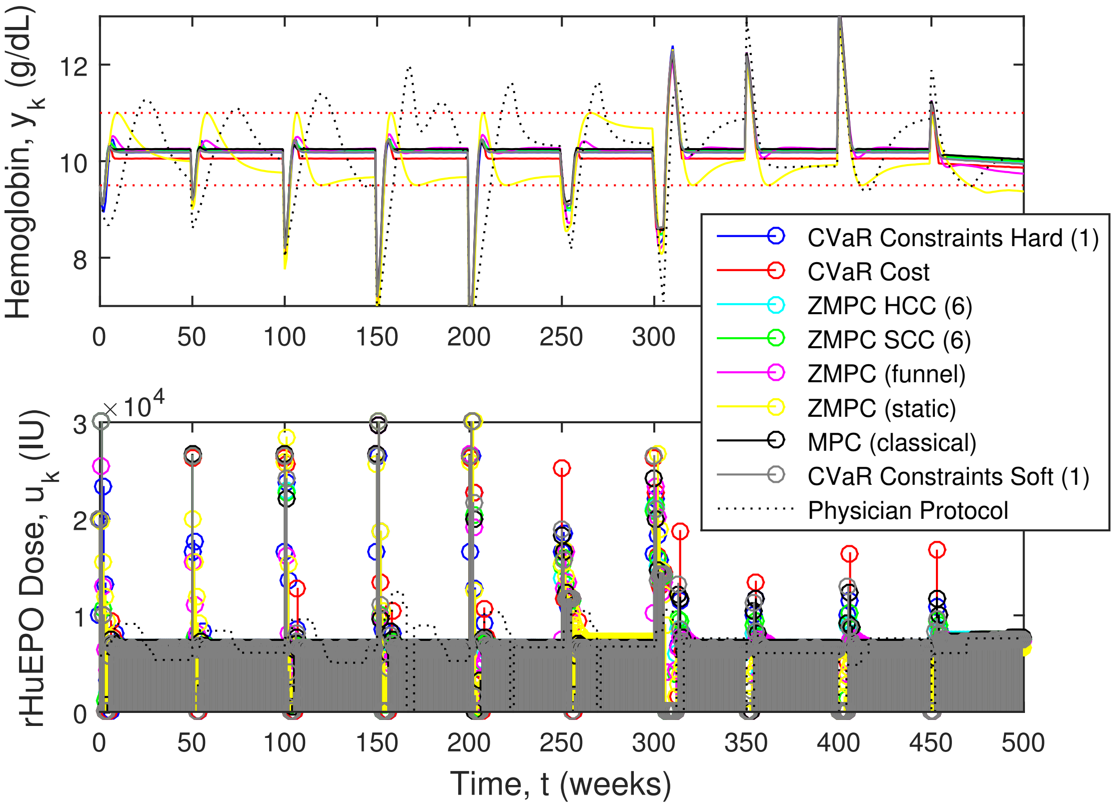

Figure 4.11: Example simulation of the controller response to the designed output disturbance # 1 vector for the nominal case (no process noise)

Applying this identical disturbance to patient number 15, along with an additive process noise of $N(0, 0.25^2)$ results in the controller responses shown in Figure 4.12.

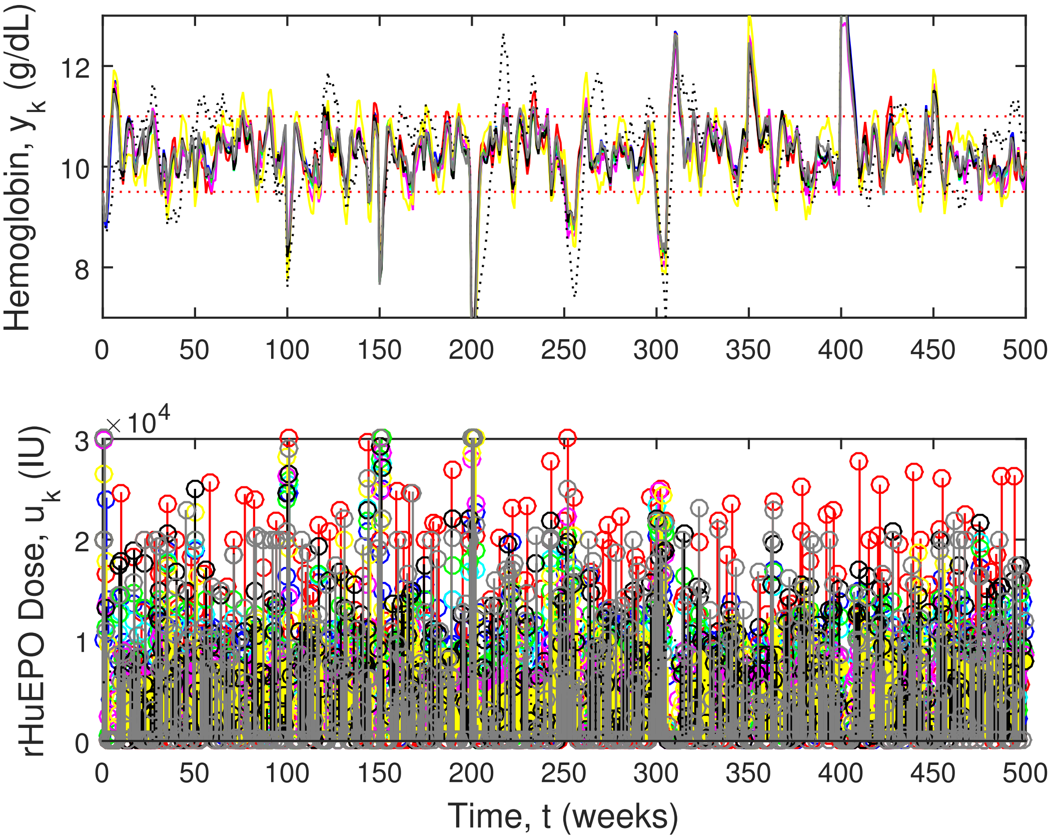

Figure 4.12: Example simulation of the controller response to the designed output disturbance #1 vector along with additive process noise drawn from the distribution of $N(0, 0.25^2)$

If the disturbance vector is instead set as successive negative step disturbances every 10 weeks, it can be seen that the physician's protocol is not able to control the hemoglobin very well again. This particular feature of the current anemia management protocol is one of the biggest detriments as the patients will see many acute disturbances over the course of their lifetime. The physician's protocol is unable to control these situations well, and often the medical professionals are left to guess an appropriate dose to counter these disturbances based on their past experiences. The nominal case is shown in Figure 4.13, while the case with additive process noise is shown in Figure 4.14

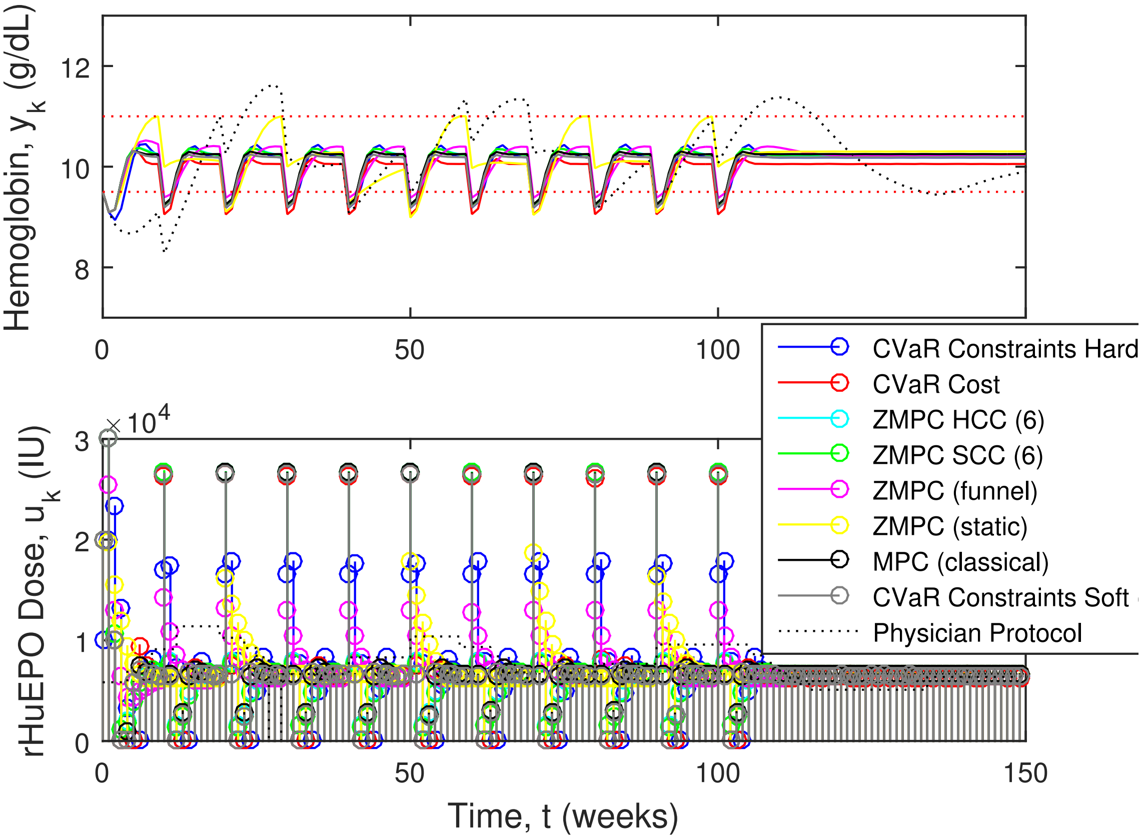

Figure 4.13: Example simulation of the controller responses to successive negative step disturbances for the nominal case (no process noise)

Again, the same disturbance can be applied along with an additive process noise from the distribution $N(0, 0.25^2)$. Figure 4.14 shows the controller responses for patient 15 for this case. The AMP spends a lot more time outside the control zone boundary than the model predictive controllers. The state performance between most of the controllers is very similar.

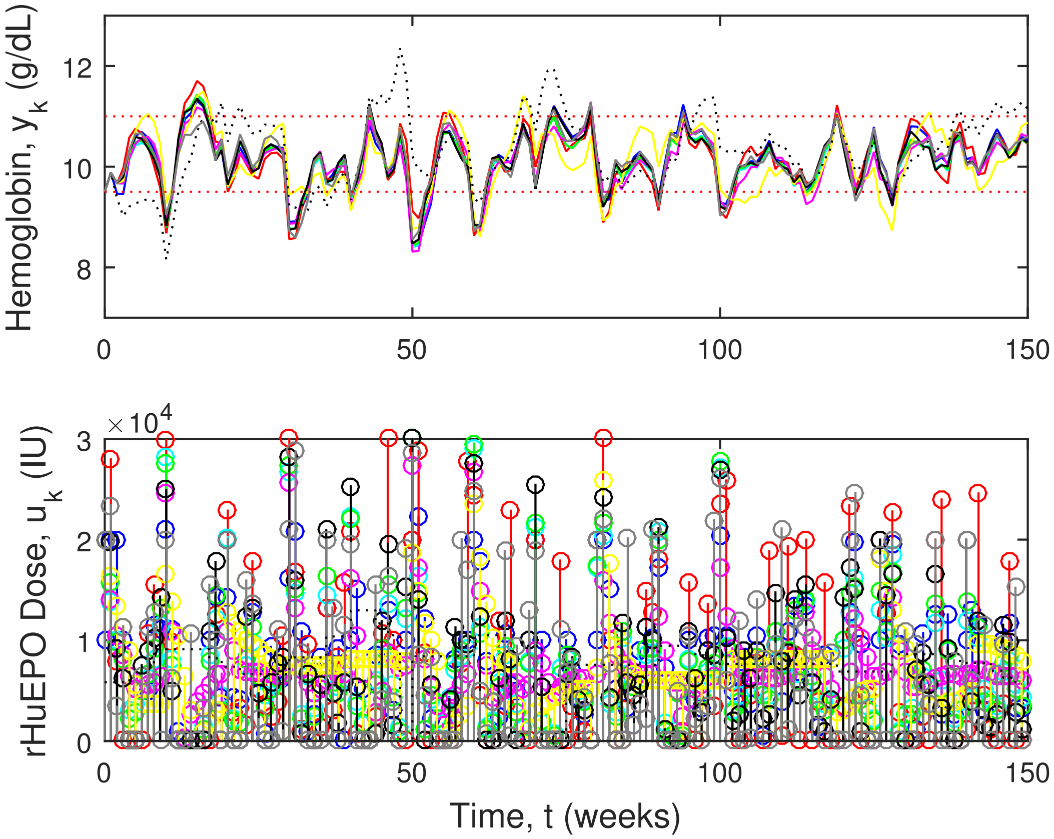

Figure 4.14: Example simulation of the controller responses to successive negative step disturbances along with additive process noise drawn from the distribution of $N(0, 0.25^2)$

Using disturbance vector #1 and an additive process noise with distribution $N(0, 0.25^2)$, simulations were performed for every patient to test the controllers' regulation ability. The results are represented in Table 4.8. Again, the simulations where one of the 9 control methods scored less than 50% of the points within the zone were removed, leaving 117 of the 167 simulations remaining in these statistics.

Performance	MPC	ZMPC	ZMPC	ZMPC	ZMPC	ZMPC	ZMPC	ZMPC	AMP
Statistic	class.	static	funnel	SCC	HCC	H-CVaR	S-CVaR	CVaR	
				(7)	(7)	(1)	(1)	(cost)	
Integrated y_k Err.	0.173	0.381	0.214	0.181	0.182	0.189	0.183	0.203	0.531
% of Points in Zone	89.6	77.6	86.9	89.1	88.9	88.3	88.7	88.5	72.4
U_k Total ($\frac{IU}{1000}$)	5116	5108	5060	5093	5068	5086	5068	5178	5411
Avg. Weekly U_k	10232	10216	10120	10186	10136	10171	10136	10355	10822
Avg. ΔU_k	4407	804	670	2973	2315	4543	7335	8449	473

Table 4.8: Simulation Results for the various ZMPC controllers as compared to the physician's protocol for the designed disturbance test scenario

The controller performance for the disturbance vector simulation results in similar performance values for each of the controllers as compared to the simulations without the disturbance vector. As expected, each of the controllers state management deteriorates slightly due to the acute disturbances. The ZMPC controller with the funnel constraints offers the most desirable solution. It has very good state performance, coupled with a very low average change in u_k. The chance constrained controllers (as tuned) have good state performance, but the rate change terms are far too high to be considered viable in a clinical setting. The Zone MPC (static and funnel) controllers will be studied further in more rigorous simulation tests.

4.3 Controller Simulation Results on PK/PD Patient Simulator

In order to test the controllers with a more realistic scenario, it is proposed to test the controllers' regulation abilities when trying to control the PK/PD model, along with added process , measurement noise and acute disturbances. The following sections outline the design of a realistic patient simulator, justification for the chosen noise distributions and the simulation results on the patient simulator.

A block diagram of the simulation setup is shown in Figure 4.15.

4.3.1 Patient Simulator Design

To begin the control system testing, simulated data was needed initially to acquire a constrained ARX model of the system. As in a clinical setting, an initial few months of data is necessary before a proper model can be identified for the MPC algorithms to be put into use. Initially, the PK/PD models were used along with a designed disturbance, random measurement noise and the physician's protocol control scheme to collect simulated data. A constrained ARX model was subsequently identified from this simulated data. An example of this is shown in Figure 4.16 for both the validation and training data. The data was split evenly into training and validation portions, similar to the clinical data. The bottom subplot, shows the shape of the b_k parameters.

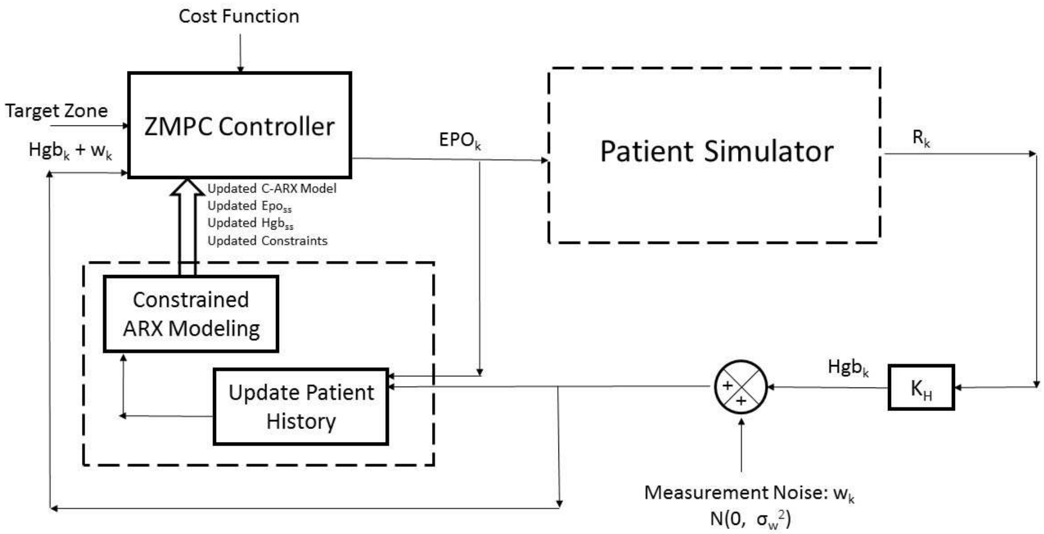

Figure 4.15: Block Diagram of the Simulation Setup for Recursive Zone Model Predictive Control and the Patient Simulator

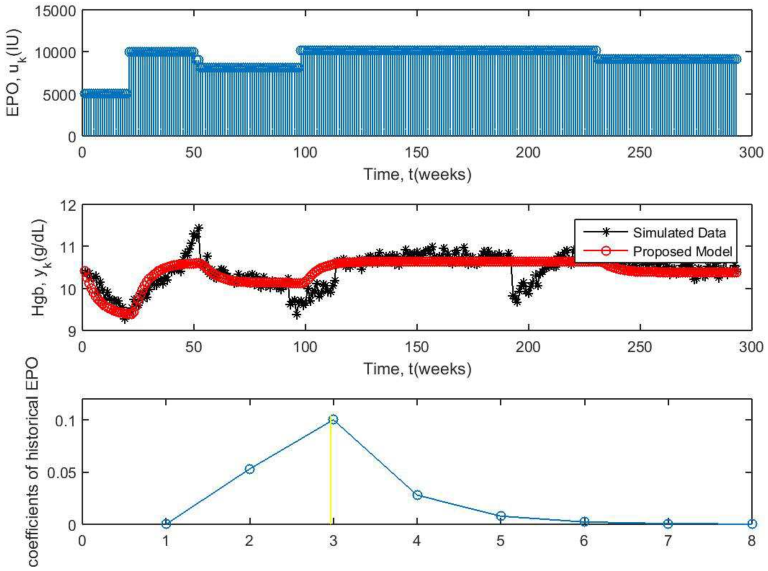

Figure 4.16: Example of a scenario used to attain the C-ARX models from simulated data

Model parameters were estimated for each of the 167 clinical patients and it is these models that serve as the basis for the simulated patients. The actual clinical patients exhibit many varying degrees of behaviour beyond that which the PK/PD model can capture. Most notably, clinical patients may become increasingly dependent on EPO over time. This can be seen in a few clinical patients in Figure 4.17.

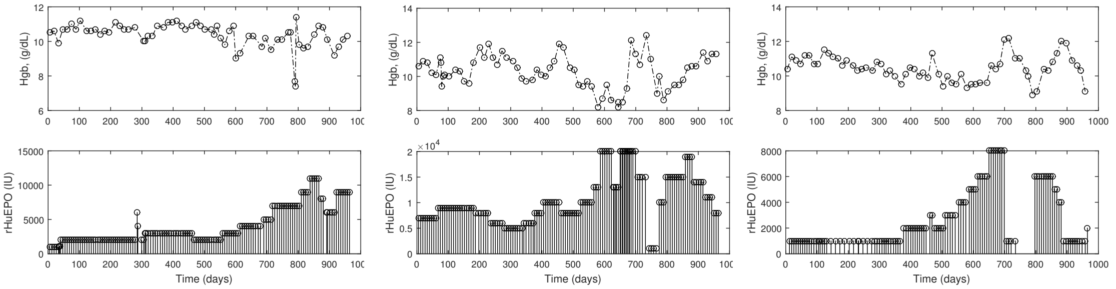

(a) Patient 4 **(b)** Patient 5 **(c)** Patient 6

Figure 4.17: Clinical patients will become continually more dependent on EPO doses if their natural endogenous erythropoietin production deteriorates

Some patients may also become more healthy for short periods of time. This phenomena is depicted in multiple patients in Figure 4.18.

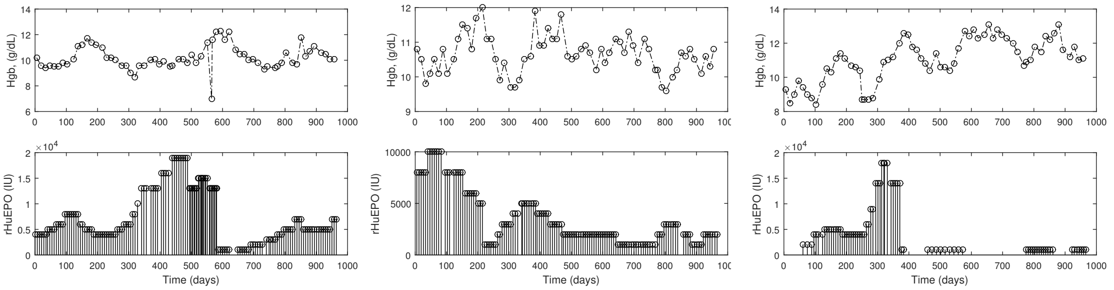

(a) Patient 7 **(b)** Patient 8 **(c)** Patient 9

Figure 4.18: Clinical patients become less dependent on EPO doses as their natural endogenous erythropoietin production increases

Both of these scenarios bring about a time varying nature of the process system. To aid in simulating these conditions, an integrating disturbance with a small negative mean was used. This allows the patients' hemoglobin response to drift slowly away from the original model in either direction, but with a bias to the downside. The accumulation of the disturbance term will impact the steady state input significantly. Another frequent occurrence is acute negative step and ramp disturbances. These can be seen during infections or when significant blood loss occurs. Some acute disturbances can be seen in the clinical patients shown in Figure 4.19. The step disturbances are clearly identifiable. Patient 10 exhibits a negative ramp disturbance around day 800. Patient 12 exhibits a negative ramp disturbance around day 375.

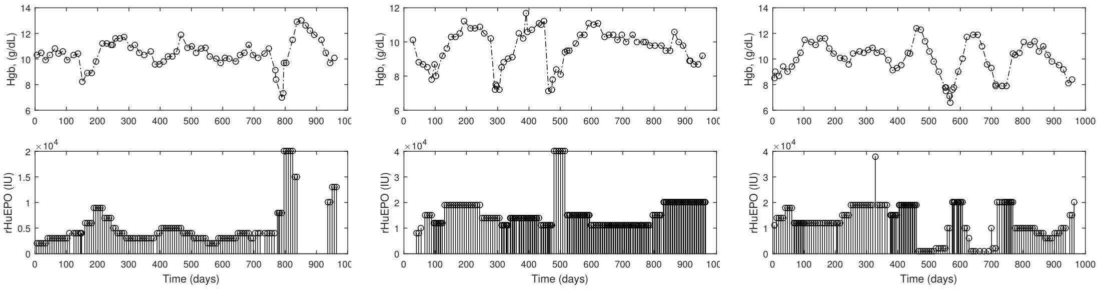

(a) Patient 10 **(b)** Patient 11 **(c)** Patient 12

Figure 4.19: Clinical patients' exhibiting acute disturbances

The occurrence of these types of disturbances is also incorporated into the patient simulator. A negative step or ramp disturbance can be incorporated by modifying the red blood cell population. Low weekly probabilities are given to these types of disturbances making them occur randomly. The RBC population is represented by the 2, 3 and 4th states in the PKPD model. The probability of a step disturbance occurring is set to 1 % each week. This results in approximately one acute step disturbance event per 2 years, per patient. There is a 15 week grace period after each step disturbance where another disturbance cannot occur, to avoid multiple disturbances in very short periods of time. The magnitude of the step disturbance is randomly chosen to reduce the current red blood cell population by multiplying it by a fractional number between 0.73 and 0.98. This disturbance translates to a maximum hemoglobin drop of roughly -3.5 g/dL, which is near the maximum drop observed in the clinical data. The states governing the RBC population can be modified using Equations 4.1, which are derived in the original work on the PKPD model (Y. Chait *et al.*, 2014). The new RBC population is calculated incorporating the step disturbance (A_D). A_D holds a value of 1 unless a disturbance is selected for the current weekly time instance. If a disturbance is selected, A_D is set to a fractional value and R_k is updated. The state x_2 is also updated to reflect changes in the RBC population. States $x_{1,k}$ and E_k remain unchanged.

$$R_{k,new} = A_D R_k \tag{4.1a}$$

$$x_{2,k} = R_{k,new} - \frac{4x_{1,k}}{\mu} \tag{4.1b}$$

Similarly, negative ramp disturbances are also programmed into the simulator. The chance of a negative ramp disturbance is also set to 1% each week. The magnitude of A_D for the ramp disturbance is chosen randomly between 0.7 and 0.95 and then the full magnitude is spread over a duration of time. The time is chosen randomly to be between 4 and 15 weeks. For example, if the total magnitude drop was chosen to be 30% and then the length of the drop was chosen to be 15 weeks, A_D would hold a value of $1 - 0.3/15 = 0.98$ for 15 weeks in a row. There is also a grace period of 10 weeks after the completion of the ramp distubance where no additional ramps or steps can occur.

A simple block diagram of the patient simulator is shown in Figure 4.20, where the integrating process noise is added through the disturbance variable, d_k, and the acute disturbances are added to the model through the use of the variable A_D.

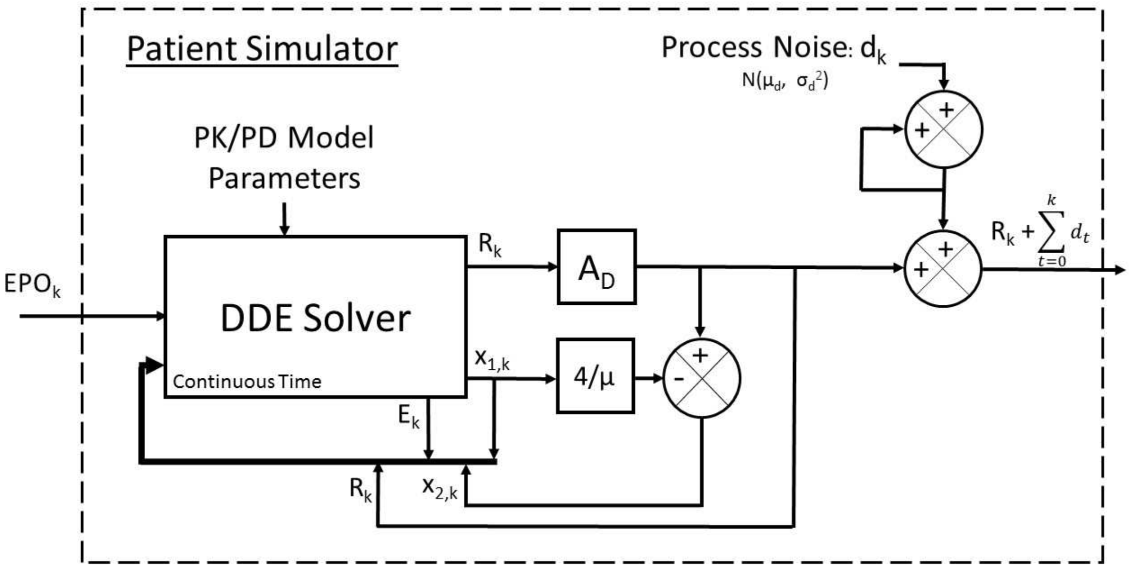

Figure 4.20: Block Diagram of the Patient Simulator

Figure 4.21 shows three simulations where the proprietary AMP is used to control the designed patient simulator. Figure 4.21a shows a negative ramp disturbance similar to that seen in Figure 4.19a and 4.19c. Figures 4.21b and 4.21c have similar time-varying features due to the integrating disturbance accumulating a non-zero sum overtime, similar to Figures 4.17 and 4.18. Figures 4.21b and 4.21c also exhibit a negative step disturbance.

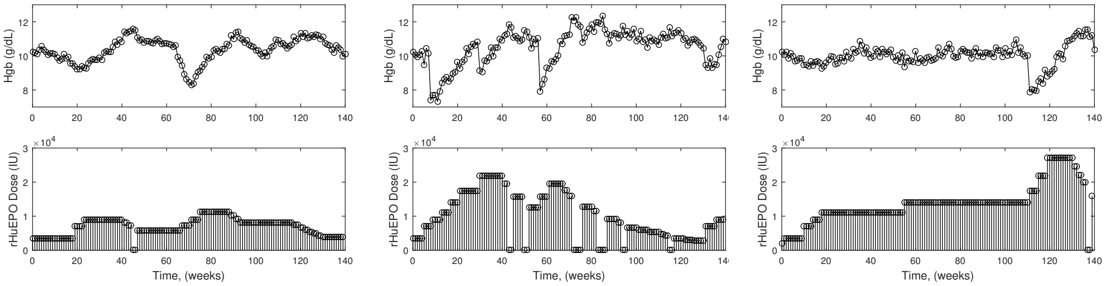

(a) Simulated Patient 1 **(b)** Simulated Patient 2 **(c)** Simulated Patient 3

Figure 4.21: Simulations showcasing the features of the designed patient simulator

4.3.2 Process and Measurement Noise

The patient simulator will use random process noise for the integrating disturbance, as well as a random measurement noise. To determine the appropriate process and measurement noise, a recursive moving window model estimation method was used. This method uses a moving window of 50 points of data for each patient, and estimates a model for these data points. The estimated model is used to predict a single 1-step prediction residual, and then the moving window is advanced by 1 week. This was performed for all patients with a large enough data set, and the residuals were combined to produce a distribution shown in Figure 4.22. The statistics for the residuals are shown in Table 4.9.

Statistic	Value
Mean	0.0053
Standard Deviation	0.264
Mean (absolute)	0.191
90% Confidence Interval	± 0.440
Total No. of Residuals	9335
Clinical Patients used	159
Average Patient Data	126.4 weeks

Table 4.9: 1-Step Residual Statistics

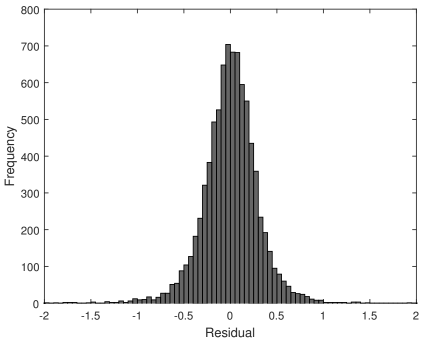

Figure 4.22: 1-Step Residuals for all Patients

The standard deviation of the 1-step residuals is 0.264. With this knowledge, it would be appropriate to have a combined measurement and process noise distribution similar to the error exhibited in the 1-step residuals. CKD patients typically have their blood work drawn and analyzed in a lab. One such commercially available hematology analyzer is Samsung's LABGEO Hemotology Analyzer. This specific device analyzes blood samples automatically using impedance technology for cell counting and photometry for hemoglobin analysis (I. Park *et al.*, 2014). The manufacturer's coefficient of variation (CV) for Hgb measurement for this device is 2.4%. It has been tested in a research study to produce a range of CV values between 0.71 and 1.22 % with a median CV of 0.84 % (I. Park *et al.*, 2014). CV is the ratio of the standard deviation to the mean measurement. For example, a true measurement of 11.0 g/dL would produce a standard deviation for the measurement error of 0.264, according to the manufacturer's specifications.

With both the commercial device and the 1-step residuals in mind, three measurement noise environments for the simulations were chosen to perform the experiments. The first environment uses a higher measurement noise with a distribution of $N(0, 0.20^2)$, while the integrating process noise was drawn from the distribution $N(-0.001, 0.1^2)$. The combined standard deviations of both process and measurement noise add up to a standard deviation of 0.3 g/dL, which should be an adequate high noise test scenario for the modeling and control algorithm. A lower measurement noise environment was also tested using a measurement noise distribution of $N(0, 0.10^2)$, while the integrating process noise was drawn from the distribution $N(-0.001, 0.1^2)$. The lower noise environment will aid in quantifying the effect of measurement noise on the modeling and control algorithms and will represent a more nominal environment. The third noise environment has only measurement noise which is drawn from a distribution of $N(0, 0.20^2)$. All three environments will also be subjected to random step and ramp disturbances on the RBC population.

4.3.3 Simulation Results on PK/PD Simulator

The controllers were compared based on three categories. The first category calculates the integrated output error outside the actual control zone. It captures a summation of the magnitudes of the zone violations and quantifies the state performance. The second category is the average EPO dose given. This category quantifies the cost to treat the patient. The third category quantifies the average change in EPO dose from week to week. This category aids in choosing a controller that has an acceptable level of aggressiveness. The EPO doses are typically given in multiples of 1000 IU. It is more desirable to have a lower average change in weekly drug dose than 1000 IU. The choice of controllers and tuning parameters selected in this section are based on rigorous empirical methods. To justify the use of the parameters and features selected for discussion, a short explanation of the selections is necessary.

The first set of simulations is of different tuning parameters for the classical recursive MPC and is shown in Figure 4.23. The integrated output error is plotted against the average drug dose, while the average change in input statistic is displayed as a number beside each point on the figure. This study was completed using the R-MPC controller with different tuning parameters for Q (10, 30, 50, 80, 120) and R=1. The linear constrained ARX model estimation was completed using a moving window of 50 data points, where each point carries equal weight. The high noise environment was used for these simulations. The simulations were run for 113 simulated patients for 500 weeks each. Parallel to theoretical expectations, as the state tuning parameter Q increases, the controller becomes more aggressive and the state performance improves. These improvements come at the cost of controller aggressiveness and a larger amount of drug use. Q=30 was chosen as the settings for further discussion because it's improvements over Q=10 are noticeable, but the improvements in state performance as the Q becomes higher do not outweigh the disadvantages of the controller aggressiveness and increased drug cost.

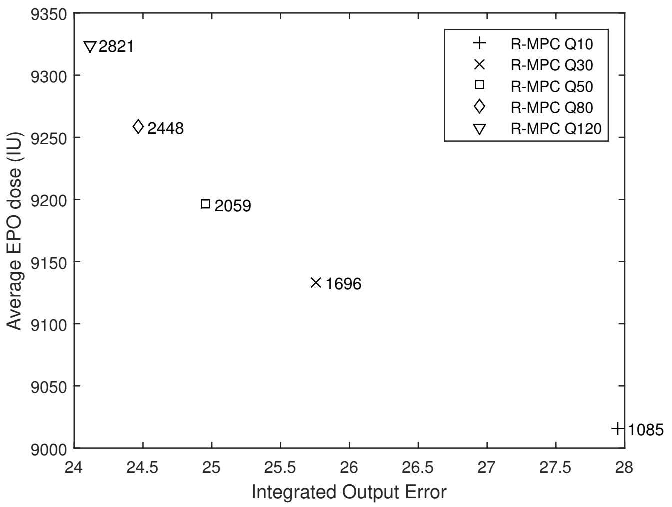

Figure 4.23: Comparison of different classical MPC tuning settings

Another study explored the effect of the window size length used for model estimation. Figure 4.24 shows the effects of changing the window size estimation from 30 to 80, in steps of 10 data points. The simulations were performed on the high noise environment for each of the 113 patients at a simulation length of 500 weeks. Linear C-ARX modeling was used along with Zone MPC with the funnel constraints and a tuning parameter Q fixed at 100 and R=1. The figure shows significant improvements can be made by increasing window length to a value larger than 50. As more points are used in the model estimation phase, the model improves, which matches theoretical expectations. The improvements seen by the controller may be attributed to the design of the patient simulator, as the DDE model remains static. Subsequently, the system gain remains the same and this may contribute to the model accuracy improvement observed with larger window sizes. The controller performance gains start to suffer from diminishing returns as the window size is increased, as can be seen in the figure.

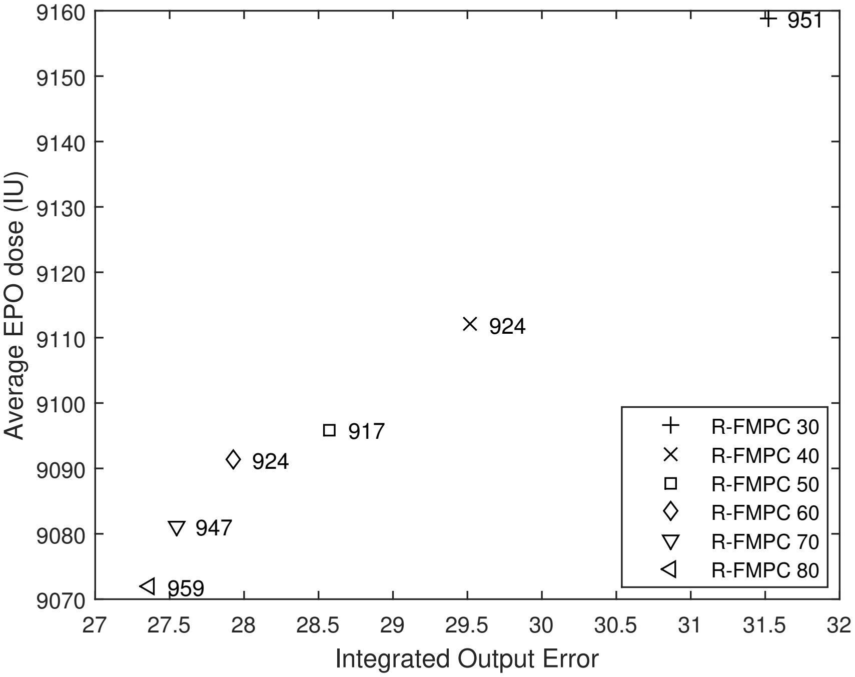

Figure 4.24: Comparison of different window size lengths used for linear constrained ARX model estimation

Different tuning values for the economic term in the cost function were also explored. The state tuning parameter Q was increased to 1000, R was set to 1 and S was varied from 0 to 5, to determine the effect of the economic term. The goal of this study was to reduce the total drug usage, while still having good state performance. Figure 4.25 shows the Recursive Zone MPC with the funnel constraints with the varied economic tuning parameter for all the simulated patient models. The simulations were performed in the high noise environment for a length of 500 weeks per each of the 113 patients.

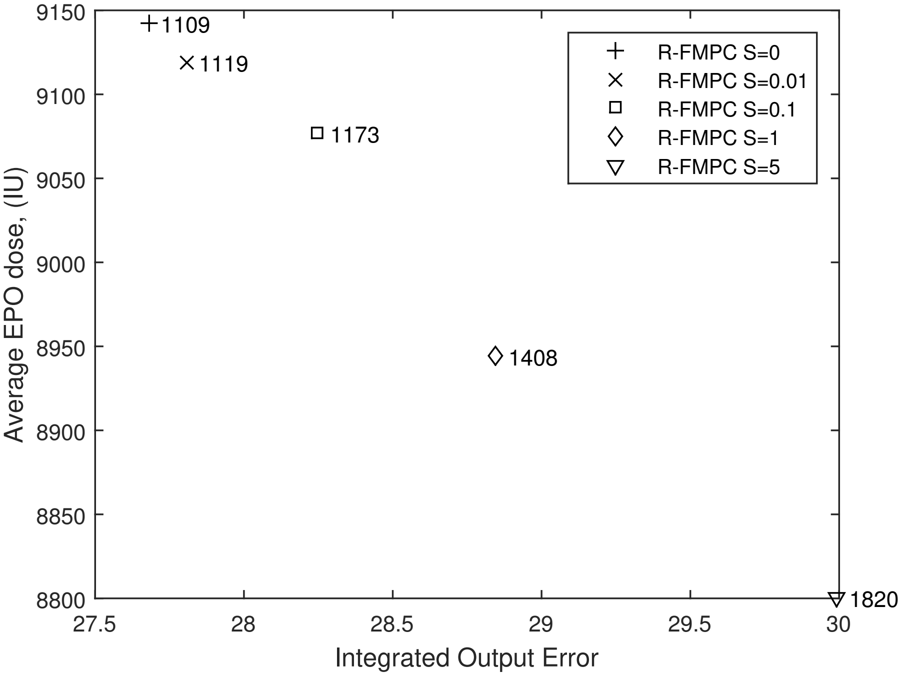

Figure 4.25: Comparison of different tuning parameters for the economic term

The controller behaviour is as expected. As the economic term penalties are increased, the state performance is reduced by up to 8.2%. The maximum average change in drug dose also increased from 1109 to 1820 IU/week, a 64% increase. The maximum drug savings is approximately 3.7% using an economic term tuning parameter of S=5. The effect of the economic term can be seen in Figure 4.26. Here, the economic term produces a bias to the negative side compared with the controller without an economic term. As the economic penalties increase, the offset increases. The economic term is highly sensitive to an incorrect tuning parameter, and makes it difficult to have a one size fits all set of parameters.

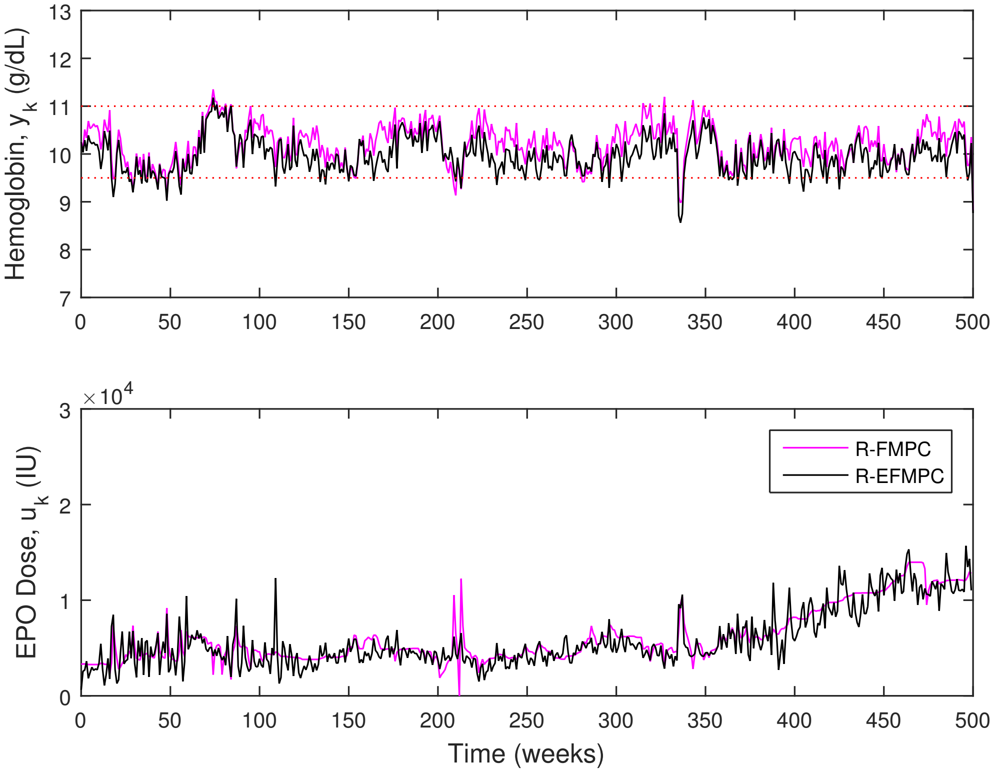

Figure 4.26: Hemoglobin Offset produced by the economic term

Another set of simulations explored the effect of the tuning parameter λ on the weighting matrix in Weighted Recursive Least Squares Regression using the funnel model predictive zone controller. The results are outlined in Figure 4.27. The results show that the state performance increases as λ increases, but so does the total drug dose. Interestingly though, the controller becomes slightly less aggressive as λ increases, as can be seen by the values beside each dot which represent the average change in weekly drug dose (IU). A value of 0.98 will be chosen for λ in the subsequent simulations for testing on the three different noise environments.

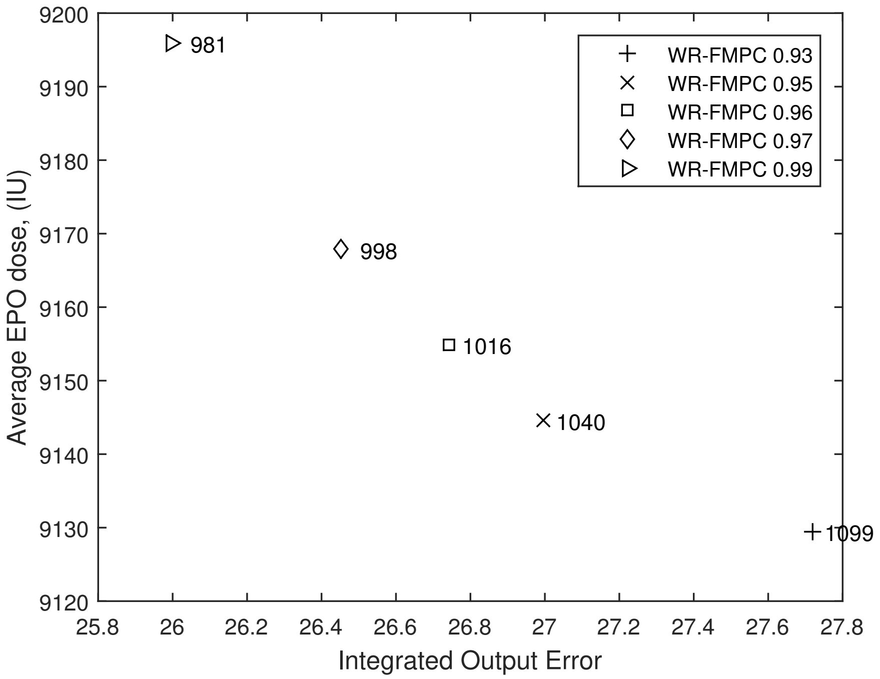

Figure 4.27: Comparison of different weighting matrices for the weighted least squares modeling methods used in tandem with the funnel model predictive controller

The final controllers selected for the simulations on the three different noise environments are shown in Table 4.10 with their tuning settings. The digital PID and current AMP will also be tested.

Controller				Estimation		Control
Identifier	Q	S	R	Window Size	λ	Target (g/dL)
MPC	30	-	1	70	-	10.25
R-MPC	30	-	1	70	-	10.25
R-ZMPC	200	-	1	70	-	9.75 - 10.75
R-FMPC L	100	-	1	70	-	9.75 - 10.75, funnel
R-FMPC NL	100	-	1	70	-	9.75 - 10.75, funnel
WR-FMPC	100	-	1	all	0.98	9.75 - 10.75, funnel
WR-EFMPC	1000	5	1	all	0.98	9.75 - 10.75, funnel

Table 4.10: Tuning parameters for the different model predictive controllers explored

The first noise environment to be explored is the high noise environment. The results of all the simulations for each controller are shown in Figure 4.28. It is easy to see that the classical MPC controller without recursive modeling performs much worse than the classical MPC controller with recursive modeling. The integrated output error is nearly 3 times as large for the controller that does not use recursive modeling. The current AMP also performs very poorly in comparison to the rest of control methods, having an integrated output error value 2 to 3 times larger than the other controllers. The rest of the recursive and weighted recursive controllers perform relatively similar to each other in terms of state performance but some obvious differences can be seen by comparing some of the controllers. When comparing the recursive zone MPC controller with the static boundaries (R-ZMPC) to the linear C-ARX recursive zone MPC controller with the funnel constraints (R-FMPC L), it can be seen that the funnel constraints help to improve the state performance by 12.2%, as well as reduce the total drug usage by 0.7%. This comes at the cost of more frequent EPO dose changes, increasing the average change in EPO by 77.7%. The robustness of the nonlinear C-ARX is not as good as the linear C-ARX method here. The nonlinear C-ARX method (R-FMPC NL) performs worse in state management (-16.1%) and total drug usage (+1.1%) as compared to the linear version (R-FMPC L). The weighted recursive zone MPC controller with the funnel constraints (WR-FMPC) offers a slight improvement in the state management (+7.0%) over the non-weighted version (R-FMPC L), but comes at the cost of slightly increased drug usage (+1.1%) and controller aggressiveness (+5.5%). As expected, the weighted recursive least squares economic zone MPC controller with the funnel constraints (WR-EFMPC) performs slightly worse in state management (-5.1%) than the controller without the economic term (WR-FMPC) but it reduces the total drug usage by approximately 2.7%. Another detriment of the economic term is the large increase in the controller aggressiveness. It increases by 118% and is over the 1000 IU threshold that would be desirable to stay beneath. Last but not least, the PID controller performs worse than most of the MPC controllers in state management, but it also yields a lower total drug usage. This feature of the PID controller is completely attributable to the fact that when an acute disturbance occurs, the PID controller is sluggish to respond on some patients as compared to the MPC controllers, which causes the PID controller to give less dose for longer than the other controllers. The controller settings used for the PID controller are easily able to handle all the patient models and disturbances relatively well, with the least complex solution. The R-FMPC L and WR-FMPC controller both have acceptable levels of controller aggressiveness and perform similar here and would be the most desirable selection based on this noise criteria.

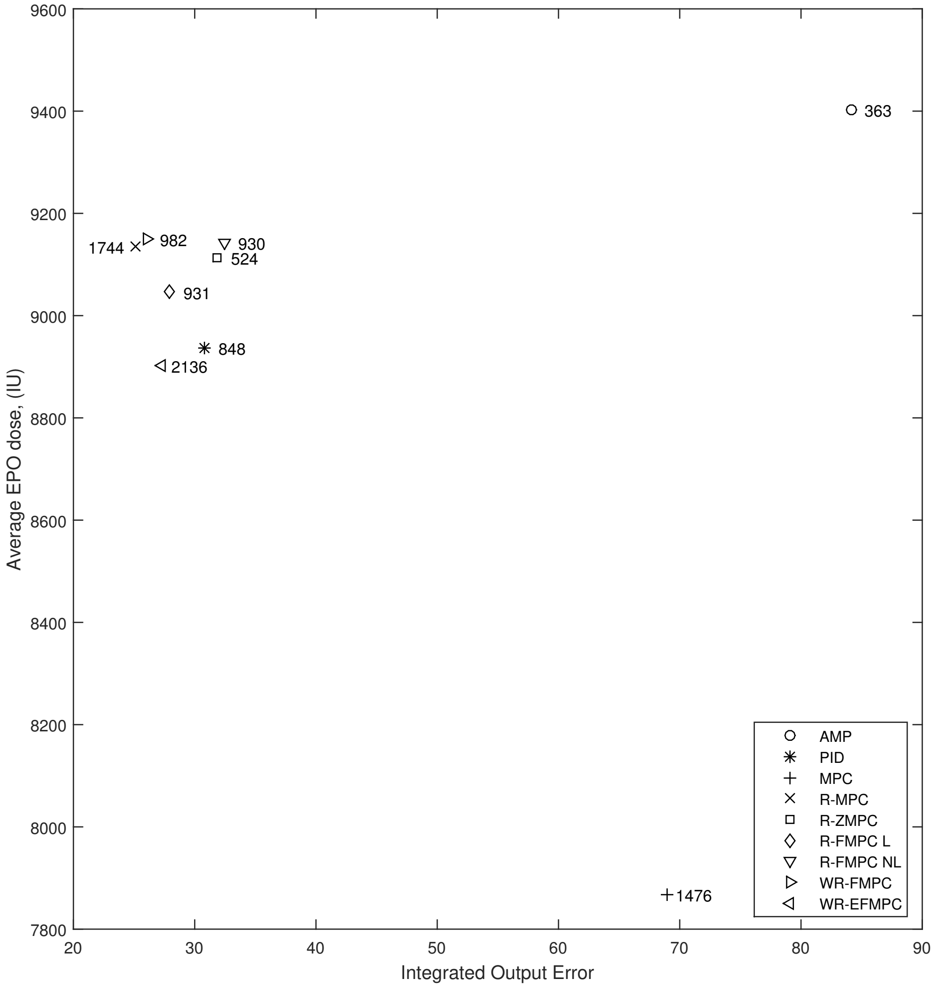

Figure 4.28: Comparison of different anemia management controllers in the high noise environment

The second noise environment to be explored is the low noise environment. The results of the controller simulations are shown in Figure 4.29. The low noise environment impacts the performance of all the controllers, in a relatively equal manor. The location of each point on the figure remains relatively equal to the location on Figure 4.28. The same comparisons can be made here as previously discussed. It should be noted that each controller becomes slightly less aggressive in its control action. The R-MPC and WR-EFMPC controllers still have far too high of input changes to be used safely in a clinical setting. The R-FMPC L and WR-FMPC controller both have acceptable levels of controller aggressiveness and perform similar here and would be the most desirable selection based on this noise criteria. The PID controller performs fairly well, but again its sluggishness on acute disturbances is an undesirable feature.

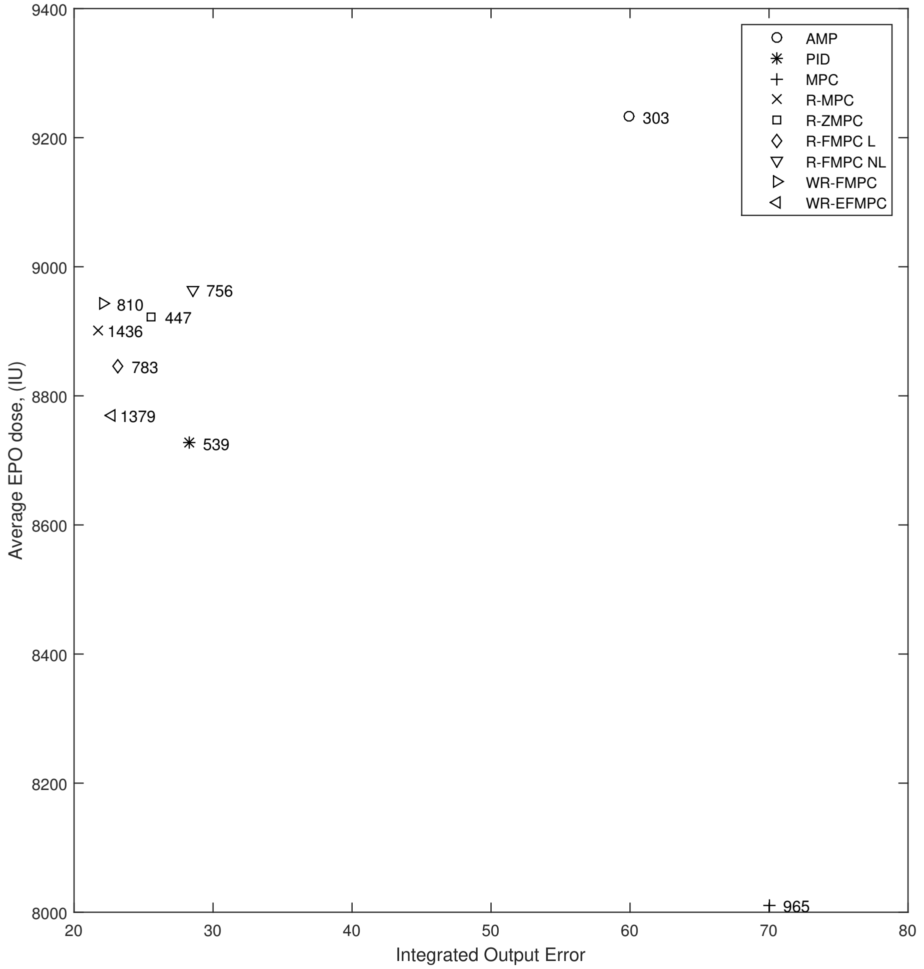

Figure 4.29: Comparison of different anemia management controllers in the low noise environment

The final noise environment was used to perform controller simulations. This environment keeps the high measurement noise but does not use the integrating process noise. This is not likely to occur in a clinical setting, but it is a good exploratory exercise to see the impact that the integrating disturbance has on the controller performance. The controller performance shifts quite a bit in comparison to the other two noise environments. In these simulations, the classical MPC controller without recursive modeling performs much better than previously, as expected. The R-ZMPC controller has a similar state performance location relative to the others, but it comes at the cost of much larger drug usage. This is the result of the hemoglobin settling near the top of the control zone more often than the other controllers. These simulations include only negative acute disturbances, which will cause the R-ZMPC controller to settle near the top boundary more often as the controller forces the Hgb upwards after the disturbance. The R-FMPC NL controller still performs worse as compared to the linear version, which solidifies the linear modeling method as the method of choice to obtain a C-ARX model. The aggressiveness of the WR-EFMPC and R-MPC controller are still quite high, and taking into consideration the previous results, these controllers are not recommended for use.

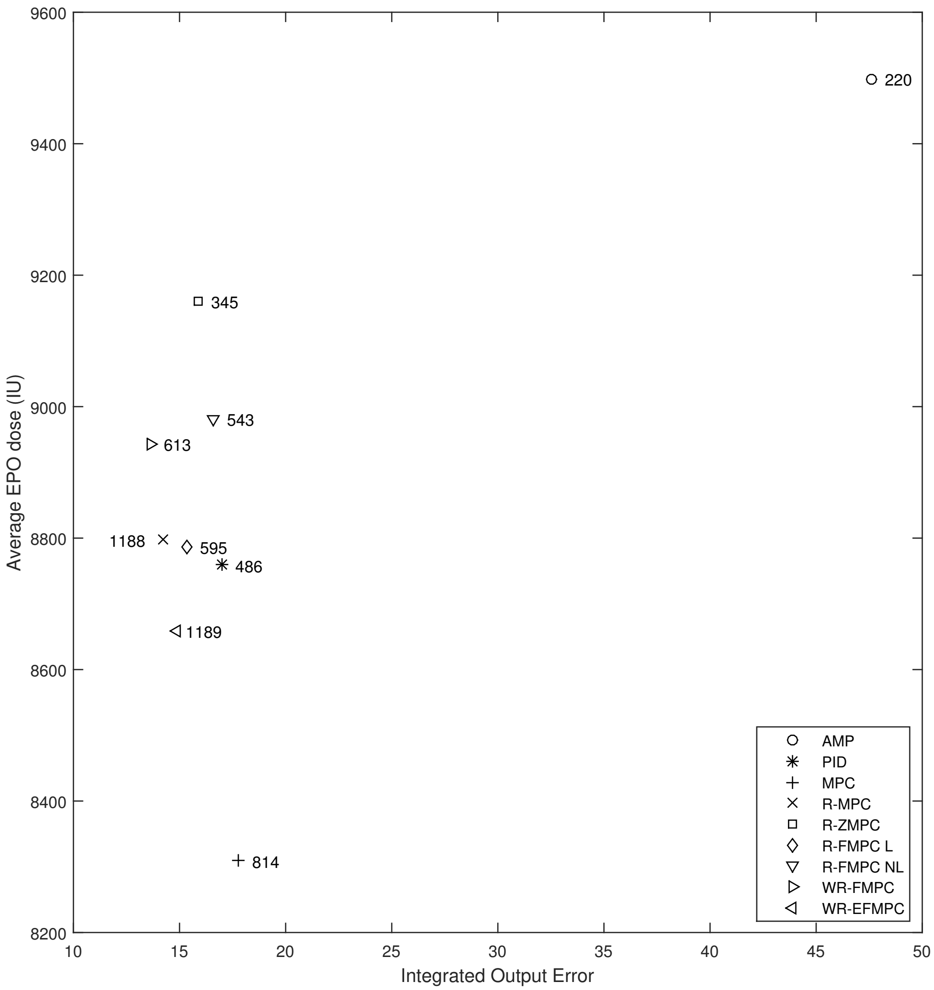

Figure 4.30: Comparison of different anemia management controllers in the noise environment without the integrating disturbance

Several of the simulations, with a partial showing of the controllers, will be used to illustrate abnormalities that are common with some of the controller methods. The first two figures are shown in Figure 4.31. In figure (a), the AMP causes a lot of oscillations in the hemoglobin. In figure (b), the current AMP is unable to provide proper doses for this patient, which would necessitate the divergence from the current AMP leaving the physician to choose doses for the patient blindly. In both cases, the WR-FMPC controller is able to control the hemoglobin value well.

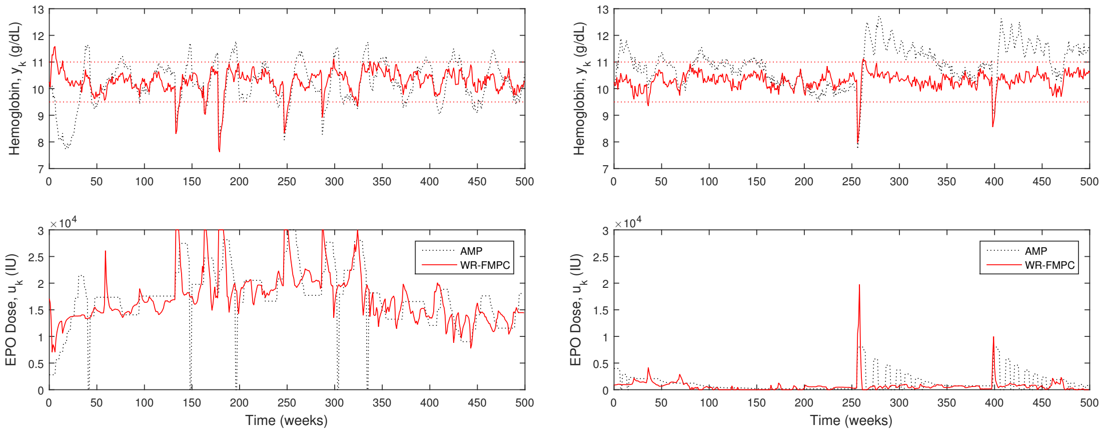

(a) AMP induced Hgb Oscillation

(b) Divergence from AMP necessary

Figure 4.31: Simulation Results where the current AMP fails to control the patient Hgb adequately

Figure 4.32a shows the importance of the recursive modeling algorithm. A comparison of classical MPC and R-MPC shows that without recursive modeling, the MPC controller cannot account for changing patient health. Figure 4.32b shows the tendency of the R-ZMPC controller to settle near the upper boundary in these simulation tests. Due to the fact that all the acute disturbances are negative, the R-ZMPC controller will often guide the hgb to the upper part of the control zone, which will use more drug than necessary to maintain the hgb in the desired range. Less commonly, the reverse also happens, where the hgb settles near the bottom. It is not fair to judge the R-ZMPC controller by its increased drug usage because of the different control zone shape, but it highlights the fact that the hgb values will often be near the boundaries of the zone, and small disturbances and noise can push the state outside of the control zone more easily.

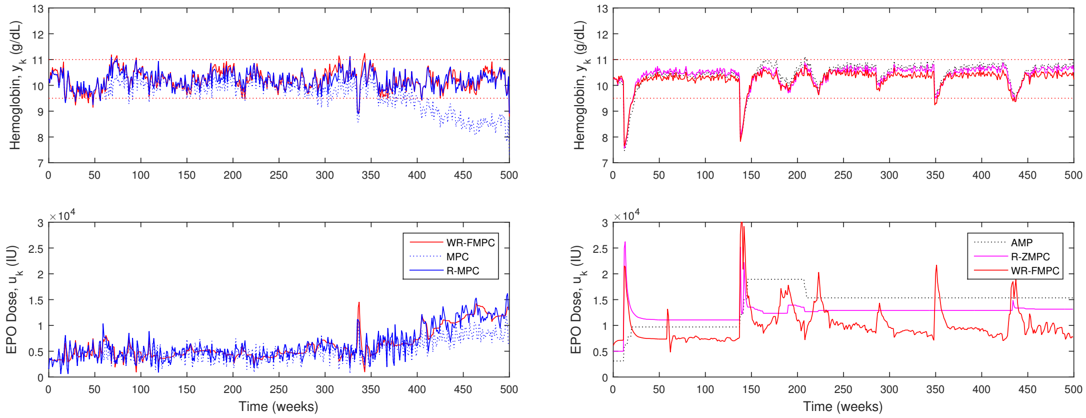

(a) MPC fails without recursive modeling **(b)** Zone MPC using excessive EPO

Figure 4.32: Simulation Results showing the importance of recursive modeling, and a case where R-ZMPC uses much more drug dose than necessary

Figure 4.33 shows two cases which magnify the problem with the digital PID controller, while showing the WR-FMPC controllers ability to handle the situations well. Figure 4.33a shows the sluggishness of the PID controller during acute disturbances. The PID controller is late to respond to a step disturbance, and overshoots the target zone around the 375 week mark. The PID controller could be tuned individually to better manage this patient, but it will be difficult to manage each patient individually. The WR-FMPC algorithm is a one-size-fits-all algorithm with identical tuning settings for each patient.

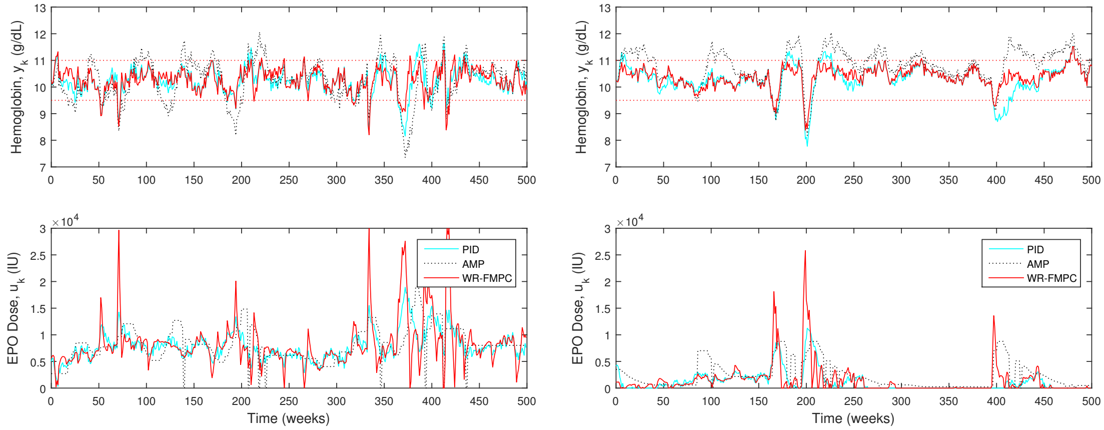

(a) PID performs sluggishly **(b)** MPC handles modeling without a dose

Figure 4.33: Simulation Results showing some of the failures of the PID controller

Figure 4.33b shows a case where no EPO dose is given for almost two years. The WR-FMPC controller is still able to counter the acute disturbance at the 400 week mark, due to the constrained modeling technique. The PID controller performs very poorly here due to integral wind-up. The sluggishness of the PID controller can also been seen again in this figure in the 175 to 225 week mark, where the PID responds slowly to the disturbances and overshoots the target zone both times.

Figure 4.34 shows two cases where the patient health changes significantly over the course of the simulation due to the integrating disturbance. The zone MPC controllers with the funnel constraints are able to control both of these situations well.

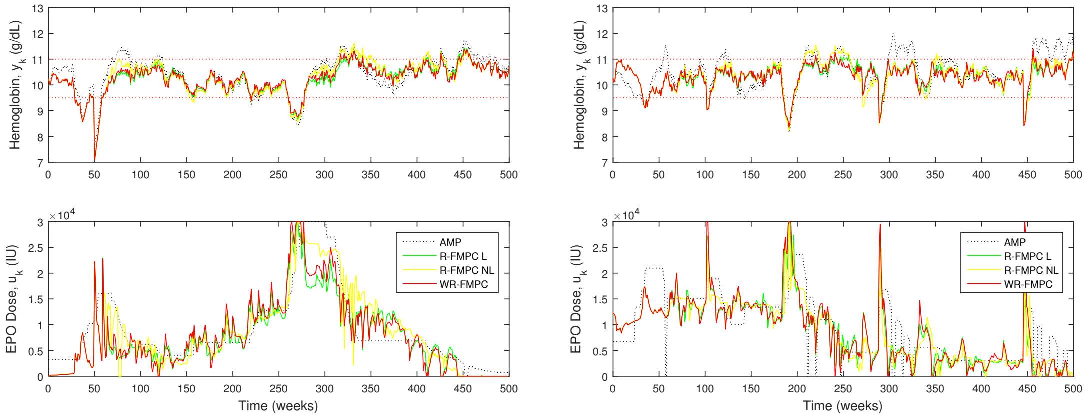

(a) Patient health changes drastically

(b) Patient health improves over time

Figure 4.34: Simulation Results showing some patients that have a decaying/improving health over time

Figure 4.35 shows the difficulties in obtaining a one-size-fits-all set of tuning parameters for the patients for economic MPC (WR-EFMPC). Utilizing the economic term can offer improvements in drug savings, but the controller is difficult to tune for the whole set of patients and results in reduced ability to manage the state effectively. The state management should not be sacrificed to reduce the cost of ESA treatment. Figure 4.35a shows a case where the economic controller is very aggressive, while Figure 4.35b shows a case with the same tuning settings where the controller is not very aggressive. Both simulations show that the economic term usually just causes a slight offset between WR-EFMPC and WR-FMPC.

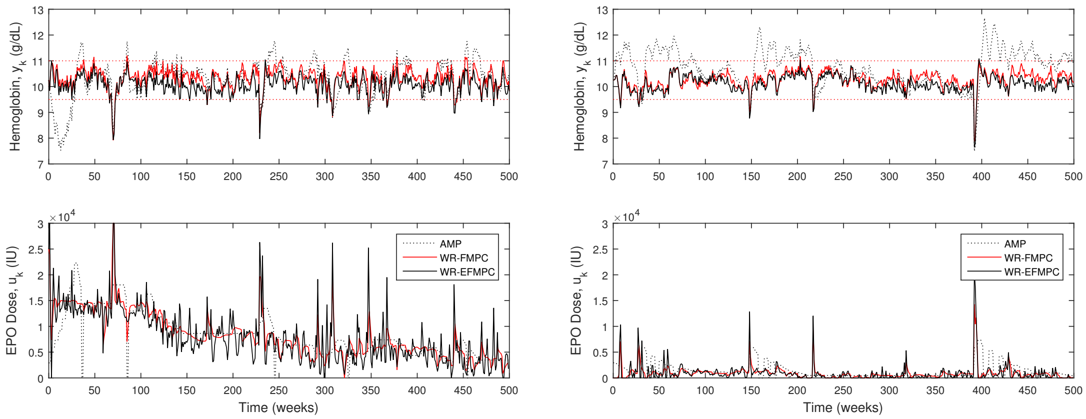

(a) Aggressiveness is high for this patient **(b)** Aggressiveness is low for this patient

Figure 4.35: Simulation Results showing the difficulty for obtaining a one-size-fits-all set of tuning parameters for economic R-FMPC

Figure 4.36a shows the reduced performance that the nonlinear C-ARX method provides during control. The reduced performance might be attributed to the robustness of the fmincon function and its ability to find a proper model at each time point. If no model is obtained, the previous model is used. The linear QP version of the C-ARX method is far more robust than the NLP version, and it rarely ever fails to find a minimum solution. The nonlinear method is not recommended for use in the clinical setting. The controller decision comes down to a choice between the linear weighted and non-weighted recursive zone MPC controllers with the funnel constraints (WR-FMPC and R-FMPC). Figure 4.36b shows there is minimal difference between the weighted and non-weighted versions of R-FMPC. These results align with the modeling results, as little difference is also seen between the two modeling methods. As the state management lags slightly in the non-weighted version for all three noise environments, the linear weighted recursive zone model predictive control using the funnel constraints (WR-FMPC) is recommended for use.

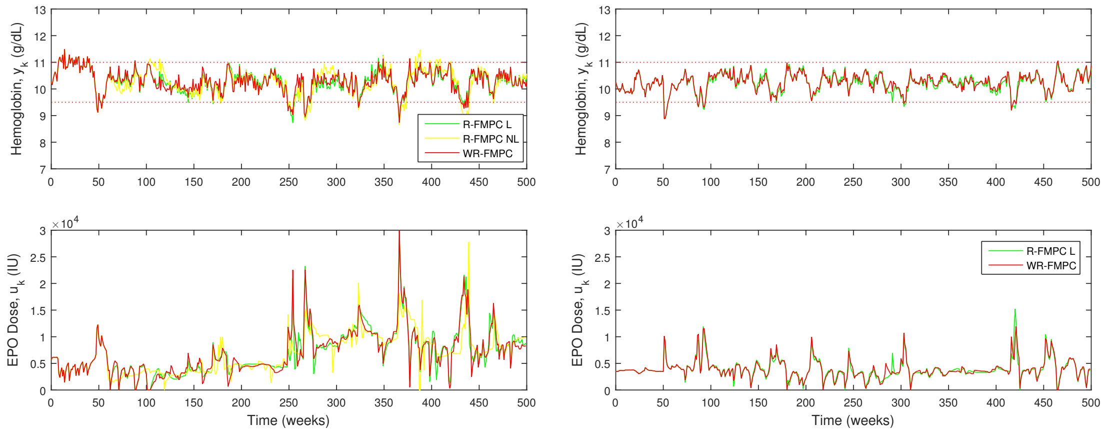

(a) Nonlinear modeling performs poorly **(b)** Minimal difference exhibited

Figure 4.36: Simulation Results showing the minimal difference between weighted and non-weighted R-FMPC and the poor performance of the nonlinear C-ARX method for recursive model estimation

4.4 Conclusion

In the simulations performed using the C-ARX models as the simulation patient, the ZMPC controller with the funnel constraints had comparable state management to that of the highest performing controllers utilizing chance constraint formulations. The exception was that the ZMPC (funnel) controller also had a lower total drug usage, as well as a far lower average rate of change as compared to the Chance Constrained controllers. Using the funnel constraint allows the tuning parameters to be set to a one-size-fits-all configuration where the controller aggressively changes the input only if the state exists outside of the zone, while remaining almost stationary, if within the zone. Due to the large number of clinical patients, this tuning robustness is a highly sought after feature of Zone MPC.

Due to the time-varying nature of the clinical patients and frequent disturbances on the system, it is not enough to implement a controller without a method for updating the model. The simulation results using the PKPD model as the patient simulator, along with the integrating process noise and random acute disturbances, tested the controllers in the most rigorous of simulation tests. The integrating process noise offers unique challenges to overcome because it is possible to have an accumulation of the disturbance over time. The controller must be able to properly account for this added disturbance. Due to modeling inaccuracies and modeling error using a linear model on a nonlinear system, the process models used in the controller may produce large offset and non-optimal solutions as the hemoglobin extends beyond the models valid range. Recursively estimating a constrained ARX model at each sampling time produces a highly robust controller to the time-varying nature of the process model. It is important to restrict the model parameters to a particular structure to ensure each model attained will be appropriate for use. Without restricting the structure, it is difficult to know whether the optimal modeling solution will produce a model of the system that will validate well. Without the constraints, the attained model may also be unstable, which does not match theoretical expectations.

Many different types of controllers were tested through the use of computer simulations. Observing the simulation results, it is recommended to implement a Weighted Recursive Zone Model Predictive Controller utilizing the funnel control zone (WR-FMPC), using a longer window size in the length of 70+ weeks. It is recommended that the weighting in weighted least squares be a value of λ=0.98 or greater. The data should also be filtered to remove some effects of the measurement noise. The recommended filter is an EWMA filter as presented with a filter value α=0.75. The funnel shape should be tuned according to the equations presented using a value of p=0.6. The controller should have the cost function tuning weights set at Q=100 and R=1. The prediction horizon should be set to N=8.

Chapter 5

Future Work

5.1 Introduction

This chapter outlines the future areas of research that have been identified to date.

5.1.1 Patient Simulator

Significant improvements can be made to the patient simulator. The current simulator relies on a PKPD model estimated from data, random integrating and measurement noise and step and ramp disturbances. A wiser choice would be to build the patient simulator solely based on measurement noise and time-varying parameters in the PKPD model. The disturbances and changes in patient health could then be explained by biological mechanisms, rather than random noise. One of the current uncertainties in the controller performance assessment on the current patient simulator design is that the PKPD model never changes. Therefore, the system gain remains static. In actuality, the system gain would be time-varying and dependent on ever-changing model parameters. The current simulator design may give misleading controller performance results as a result of the static gain.

An efficient patient simulator is needed that is able to more accurately reflect the behaviour of an actual patient. It may be necessary to have government approval of the patient simulator to allow the controller performance simulation results to act as an acceptable pre-clinical trial. This order of events would be similar to what exists for Type 1 Diabetes. The UVA PADOVA Type 1 Diabetes Simulator exists as an FDA approved simulator in the USA (C. Man *et al.*, 2014), and is sufficient to test controllers on for pre-clinical trials.

5.1.2 Process Model Improvement

The foundation of any model predictive controller is the system model. A great deal of time has been spent perfecting the constrained ARX modeling method but the model structure may be able to be improved. A more complex model involving more hemoglobin measurements or a disturbance model may offer an improved model. Using additional inputs or outputs such as iron doses, iron levels or white blood cell counts may offer modeling improvements. Different model types, such as a neural network may also provide improved modeling results, resulting in better controller performance.

5.1.3 Advanced Model Predictive Controllers using Parameter Uncertainty

The stochastic controllers in this work included only additive process noise as the uncertainty. A more appropriate controller would include parameter uncertainty in the controller formulation. It is possible that the inclusion of parameter uncertainty or different forms of robust optimization may offer improved control results.

5.1.4 Self-tuning PID

The Digital PID controller presented in this thesis was designed empirically using many simulations performed on several different patient models. Its performance was not perfected as opposed to that of the model predictive controllers. Given the good performance seen by the PID controller on most models, a self-tuning PID controller may be able to overcome the issues seen on a small fraction of the patients, as well as improve the performance in general.

Bibliography

A. Bemporady, L. Pugliay and T. Gabbriellin (2011). A stochastic model predictive control approach to dynamic option hedging with transaction costs. In: *American Control Conference*. O'Farrell Street, San Francisco, CA, USA. pp. 3862–3867.

A. Gaweda, A. Jacobs, G. Aronoff and M. Brier (2008). Model predictive control of erythropoietin administration in the anemia of esrd. *Am J Kidney Dis* **51**, 71–79.

A. Gaweda, A. Jacobs, G. Aronoff, S. Rai and M. Brier (2014). Individualized anemia management reduces hemoglobin variability in hemodialysis patients. *Journal of the American Society of Nephrology* **25**, 159–166.

A. Gaweda, M. Brier, A. Jacobs, G. Aronoff, B. Nathanson and M. Germain (2010). Determining optimum hemoglobin sampling for anemia management from every-treatment data. *Clinical Journal of the American Society of Nephrology* **5**, 1939–1945.

A. Levey, R. Atkins and J. Coresh (2007). Chronic kidney disease as a global public health problem: approaches and initiatives - a position statement from kidney disease improving global outcomes. *Kidney International* **72**, 247–259.

A. Parisio, M. Molinari, D. Varagnolo and K. Johansson (2013). A scenario-based predictive control approach to building hvac management systems. *IEEE International Conference on Automation Science* pp. 428–435.

A. Singh, L. Szczech, K. Tang, H. Barnhart, S. Sapp, M. Wolfson and D. Reddan (2006). Correction of anemia with epoetin alfa in chronic kidney disease. *New England Journal of Medicine* **355**, 2085–2098.

B. Grosman, E. Dassau, H. Zisser, L. Jovanovic and F. Doyle (2010). Zone model predictive control: A strategy to minimize hyper- and hypoglycemic events. *Journal of Diabetes Science and Technology* **4**, 961–975.

C. Man, F. Micheletto, D. Lv, M. Breton, B. Kovatchev and C. Cobelli (2014). The uva/padova type 1 diabetes simulator: New features. *Journal of Diabetes and Technology* **8**, 26–34.

Christopher, P. (2000). Designing efficient software for solving delay differential equations. *Journal of Computational and Applied Mathematics* **125**, 287–295.

D. Seborg, T. Edgar, D. Mellichamp and F. Doyle (2011). *Process Dynamics and Control*. John Wiley and Sons Inc.

Elliot, S. (2008). Erythropoiesis-stimulating agents and other methods to enhance oxygen transport. *British Journal of Pharmacology* **154**, 529–541.

F. Allgower, R. Findeisen and Z. Nagy (2004). Nonlinear model predictive control: From theory to application. *Journal of the Chinese Institute of Chemical Engineers* **35**, 299–315.

G. Pannocchia, J. Rawlings (2003). Disturbance models for offset-free model-predictive control. *Journal of the American Institute of Chemical Engineering* **49**, 426–437.

I. Park, S. Ahn, Y. Kim, S. Kang and S. Cho (2014). Performance evaluation of samsung labgeo hc10 hematology analyzer. *Archives of Pathology & Laboratory Medicine*.

J. Garriga, M. Soroush (2010). Model predictive control tuning methods: A review. *Ind. Eng. Chem. Res* **49**, 3505–3515.

J. Grosso, C. Ocamp-Martinex, V. Puig and B. Joseph (2014). Chance-constrained model predictive control for drinking waternetworks. *Journal of Process Control* **24**, 504–516.

J. Rawlings, K. Muske (1993). Model predictive control with linear models. *AIChE Journal* **39**, 262–287.

J. Ren, J. McAllister, Z. Li, J. Liu and U. Simonsmeier (2017). Modeling of hemoglobin response to erythropoietin therapy through contrained optimization. In: *Proceedings of The 6th International Symposium on Advanced Control of Industrial Processes*. Taipei, Taiwan.

K. Turksoy, L. Quinn, E. Littlejohn and A. Cinar (2014). Multivariable adaptive identification and control for artificial pancreas systems. *IEEE Transactions on Biomedical Engineering* **61**, 883–891.

L. Shampine, S. Thompson (2001). Solving ddes in matlab. *Applied Numerical Mathematics* **37**, 441–458.

M. Brier, A. Gaweda, A. Dailey, A. Jacobs and G. Aronoff (2010). Randomized trial of model predictive control for improved anemia management. *Clinical Journal of the American Society of Nephrology* **5**, 814–820.

M. Rosner, W. Bolton (2008). The mortality risk associated with higher hemoglobin: Is therapy to blame?. *Kidney International* **74**, 782–791.

National Kidney Foundation, NKF (2017). Global facts: About kidney disease. *https://www.kidney.org, accessed June 2017.*

O'Dwyer, A. (2006). *Handobok of PI and PID Controller Tuning Rules*. Imperial College Press.

P. Bogacki, L. Shampine (1989). A 3(2) pair of runge - kutta formulas. *Applied Mathematics* **4**, 321–325.

P. Damien, H. Lanham, M. Parthasarathy and N. Shah (2016). Assessing key cost drivers associated with caring for chronic kidney disease patients. *BioMed Central Health Services Research*.

R. Gondhalekar, E. Dassau, H. Zisser and F. Doyle III (2013). Periodic-zone model predictive control for diurnal closed-loop operation of an artificial pancreas. *Journal of Diabetes Science and Technology* **7**, 1446–1460.

R. Rockafellar, S. Uryasev (2000). Optimization of conditional value-at-risk. *Journal of Risk* **2**, 21–42.

Rawlings, J. (2000). Tutorial overview of model predictive control. *IEEE Control Systems* pp. 38–52.

S. Trevitt, S. Simpson and A. Wood (2016). Articial pancreas device systems for the closed-loop control of type 1 diabetes: What systems are in development?. *Journal of Diabetes Science and Technology* **10**, 714–723.

Shampine, L. (2005). Error estimation and control for odes. *Journal of Scientific Computing* **25**, 3–16.

Singh, A. (2007). The target hemoglobin level in patients on dialysis. *Dialysis and Transplantation* **36**, 1–3.

T. Knab, G. Clermont and R. Parker (2015). Zone model predictive control and moving horizon estimation for the regulation of blood glucose in critical care patients. In: *Proceedings of The 9th International Symposium on Advanced Control of Chemical Processes, The International Federation of Automatic Control*. Whistler, British Columbia, Canada.

T. Soderstrom, P. Stoica (1989). *System Identification*. Prentice Halll.

V. Batora, M. Tarnik, J. Murgas, S. Schmidt, K. Norgaard, N. Poulsen, H. Madsen, D. Boiroux and J. Jorgensen (2015). The contribution of glucagon in an artificial pancreas for people with type 1 diabetes. In: *Proceedings of the American Control Conference*. Chicago, Illinois, USA. pp. 5097–5102.

V. Bobal, J. Bohm, J. Fessl and J. Machacek (2005). *Digital Self Tuning Controllers*. Springer-Verlag London Ltd.

V. Jha, G. Garcia-Garcia and K. Iseki (2013). Chronic kidney disease: Global dimension and perspectives. *Lancet* **382**, 260–272.

W. Couser, G. Remuzz, S. Mendis and M. Tonelli (2011). The contribution of chronic kidney disease to the global burden of major noncommunicable diseases. *Kidney International* **80**, 1258–1270.

Y. Chait, J. Horowitz, B. Nichols, R. Shrestha and M. Germain C. Hollot (2014). Control-relevant erythropoiesis modeling in end-stage renal disease. *IEEE Transactions on Biomedical Engineering* **61**, 658–664.

Z. Jing, Y. Wei-jie, Z. Nan, Z. Yi and W. Ling (2012). Hemoglobin targets for chronic kidney disease patients with anemia: A systematic review and meta-analysis. *Journal of American Institue of Chemical Engineers* **7**, 1–9.